CREST LEVEL ASSESSMENT OF
COASTAL STRUCTURES BY
FULL-SCALE MONITORING,
NEURAL NETWORK PREDICTION
AND HAZARD ANALYSIS
ON PERMISSIBLE WAVE OVERTOPPING

CLASH

EVK3-2001-00058

R E P O R T

Workpackage 3

Report on full scale measurements Zeebrugge 2nd full winter season

October 2004

Ir. Geeraerts Jimmy
Ir. Boone Cathy

UNIVERSITEIT
GENT

Ghent University

INDEX

LIST OF FIGURES

LIST OF TABLES

FULL SCALE MEASUREMENTS ON THE ZEEBRUGGE BREAKWATER

1 INTRODUCTION

The present report describes the full scale measurements at the Zeebrugge breakwater within the framework of Workpackage 3: "Full Scale Measurements" of the CLASH-project. First a general description of the field site is given. Afterwards, two types of full scale measurements are described: on the one hand the wave overtopping measurements and on the other hand the measurements to identify hazards resulting from wave overtopping. Finally, results obtained until now (September 2003) are presented.

2 FIELD SITE

The Zeebrugge field site is situated on the eastern part of the Belgian Coast (Fig. 1) at the outer Zeebrugge harbour (Fig.2). The outer harbour is protected by two rubble mound breakwaters. The slope of the breakwater is ca. 1:1.5 (1:1.4 where the measurements take place) and is protected by 25 tons grooved cubes which are somewhat flattened (Height/Width = 0.85). The core consists of quarry run (2-300 kg) and 1-3 ton rocks form a filter layer (Fig. 5). On the landward side, a filter construction is placed between the core and the sandfill.

The tidal range varies 4.61 m between Z+0.19 and Z+4.80 (mean spring tide) and Z+0.90 and Z+3.88 (mean neap tide) (Z + 0.00 = *MLLWS* + 0.08). The design conditions are: significant wave height H_s = 6.20 m, maximum peak period T_p = 10 s, water level Z + 6.76. The breakwater is 20 m high, with the crest level at Z + 12.40 (theoretical design level).
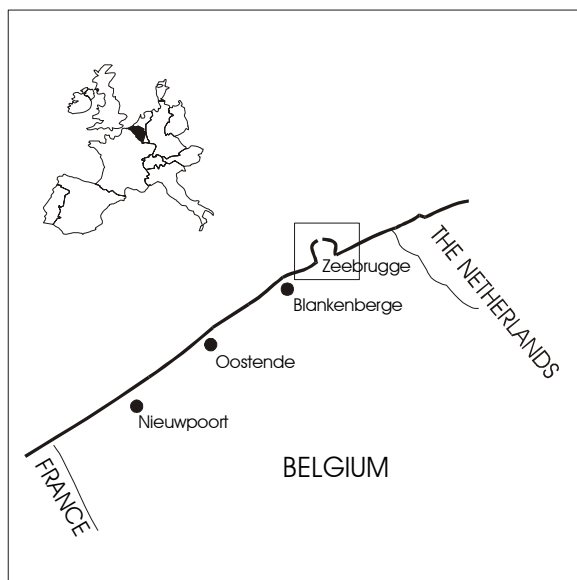
Fig. 1: *Location of Zeebrugge harbour at the Belgian North Sea Coast*
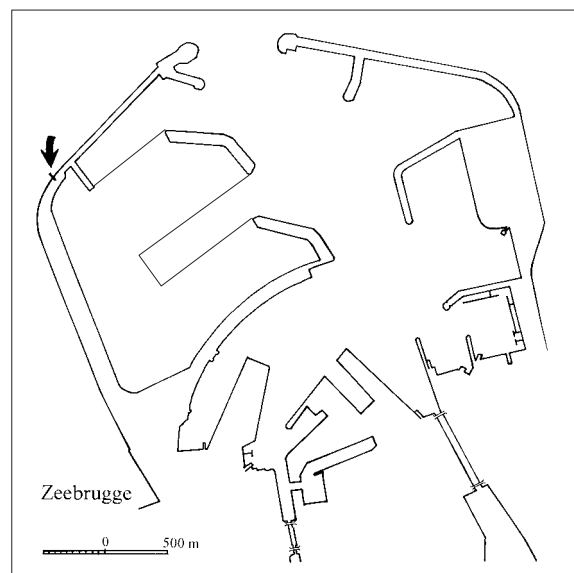
Fig. 2: *Location of the field site at Zeebrugge harbour*

3   FULL SCALE MEASUREMENTS

Full scale measurements are carried out on the northern part of the western breakwater of the outer harbour (Troch et al. (1998)). Two cross-sections of the breakwater, with an interspace of approximately 140 m, are instrumented. Fig. 3 shows a plan view with both instrumented cross-sections indicated. Bathymetric surveys in front of both instrumented cross-sections have been carried out in 1999. Results were confirmed during the surveys of 2002. Fig. 4 gives bathymetry for both cross-sections. Bottom elevation is referred to "Z"-level as defined above. The foreshore is characterized by an erosion pit in front of the breakwater and a flat slope more seaward.

**Overtopping Tank
+ Wave Detectors**
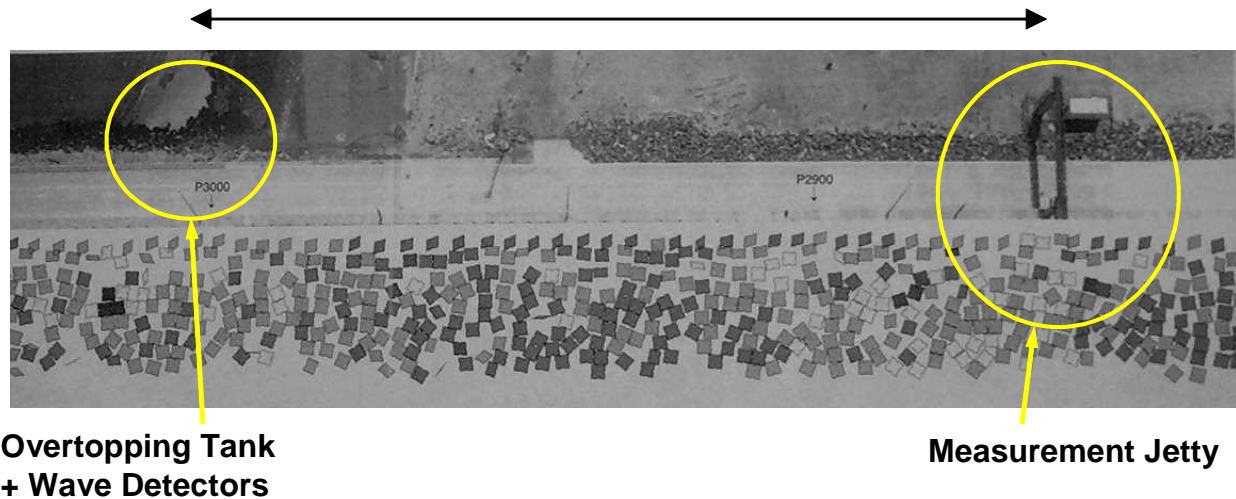
Measurement Jetty

Fig. 3:   *Plan view with indication of both instrumented cross-sections*
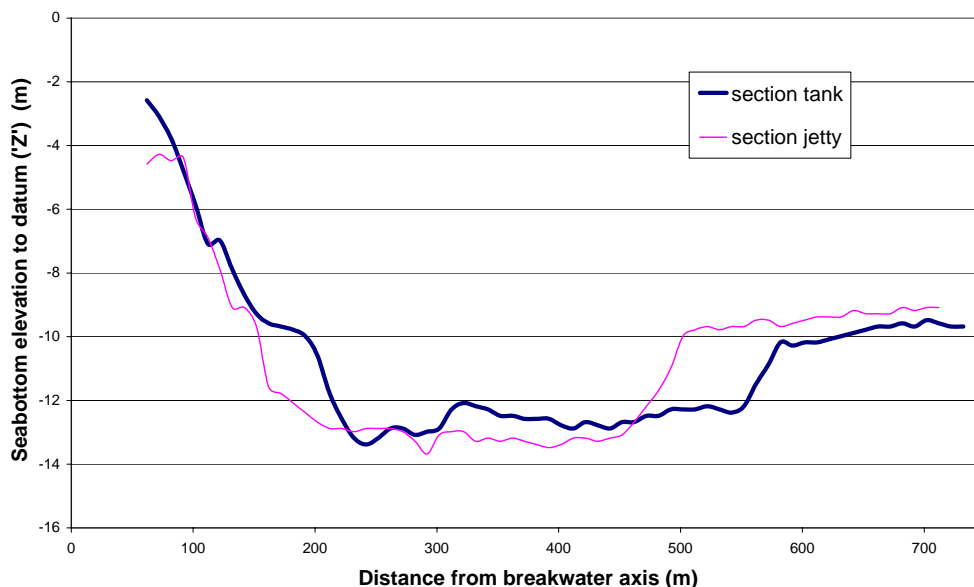
Fig. 4:   *Bathymetry for two instrumented cross-sections*

3.1 CROSS SECTION 1 : MEASUREMENT JETTY – WAVE CONDITIONS

In the first cross-section a measurement jetty of 60 m length is constructed on top of the breakwater (Fig. 5 and 6). It is supported by a steel tube pile (Ø = 1.80 m) at the breakwater toe and by concrete columns on top of the breakwater. Instruments placed in this cross-section are listed in table 1. Only instruments directly used within CLASH are mentioned. These instruments are described here after.
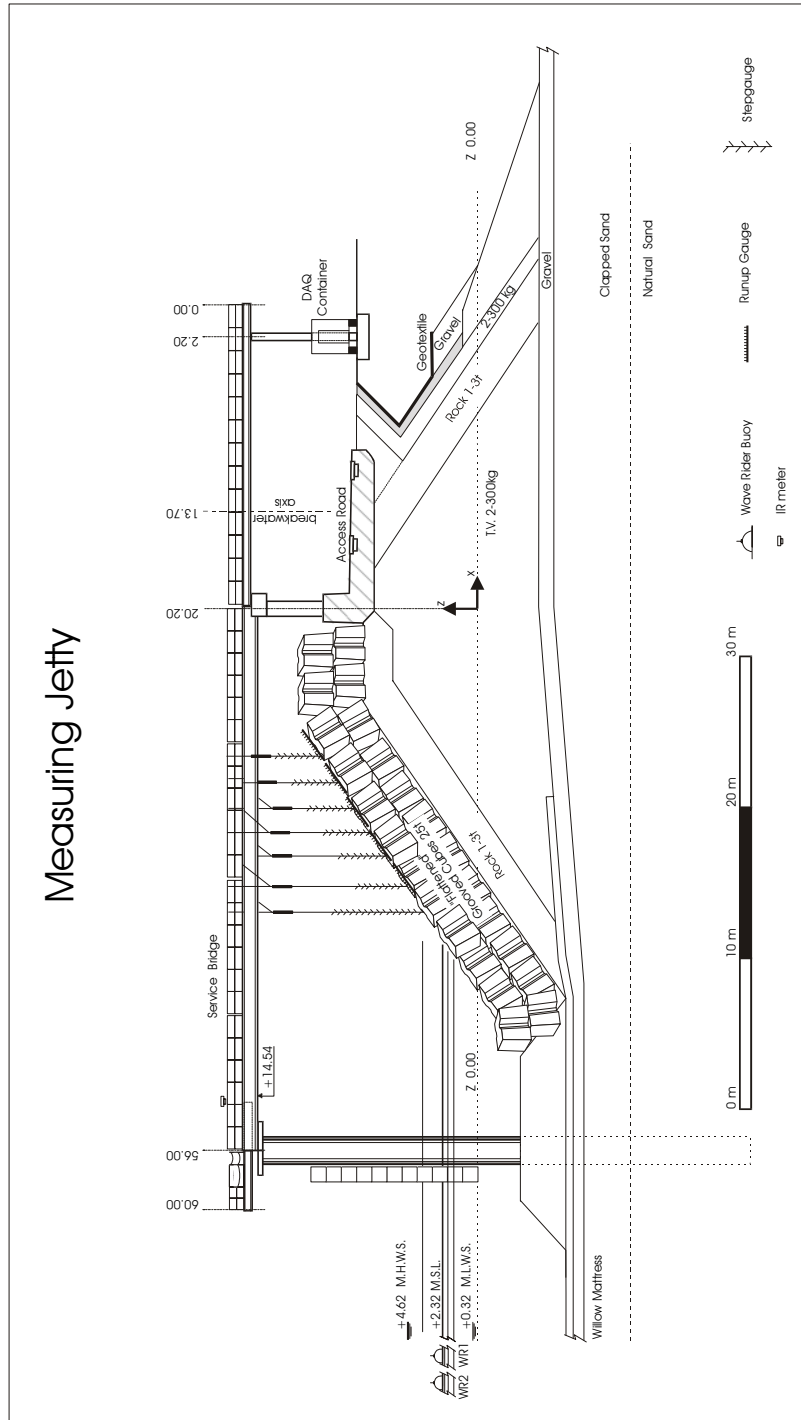
Fig. 5: *Zeebrugge breakwater: Cross-section with measurement jetty and location of the instruments*

Fig. 6: *Zeebrugge breakwater: Global view on measurement jetty*

Table 1:   *Instruments in measurement jetty cross-section*

Location	Sensor	Distance to axis of breakwater [m]	Elevation sensor to datum ('Z') [m] (1)	Variables measured
1	Directional Waverider Buoy	215	-	Water Surface elevation (waves)
2	Waverider Buoy	150	-	Water Surface elevation (waves)
3	Anemometer	28	+17.2	Wind velocity and direction
4	Infra-red sensor	26.7	+17.2	Water Surface elevation
5	Radar	27.2	+17.2	Water Surface elevation

(1) Z0.00 = MSL – 2.36 = MLLWS + 0.08

DIRECTIONAL WAVERIDER BUOY

The complete wave measuring system consists of a Directional waverider buoy, a Wavedirection RECeiver (WAREC) and a personal computer with WAREC-pc software for data display and data storage.

The directional waverider (Datawell) is a spherical, 0.9 m diameter, buoy which measures wave height and wave direction. The direction measurement is based on the translational principle which means that horizontal motions instead of wave slopes are measured. As a consequence the measurement is independent on buoy roll motions. A single point vertical mooring ensures sufficient symmetrical horizontal buoy response also for small motions at low frequencies. The buoy is standard provided with sea surface temperature measurement.

On-board data reduction computes energy density, main direction, directional spread and the normalised second harmonic of the directional distribution. The frequency resolution is 0.005 Hz from 0.025 to 0.1 HZ and 0.01 Hz from 0.1 to 0.59 Hz. Sampling frequency is 3.84 Hz.

The waverider processes 8 sets of 256 translational data samples per half hour to get a wave/direction spectrum. The receiver sorts the incoming data, in a way that the complete spectral data will become available with the highest reliability. Spectral data of both, the most recently calculated spectrum and the previous spectrum (one half hour earlier) are available.

Communication with the WAREC is via a serial RS232 interface. The data of both spectra are available on command. There is also a command to obtain the real time translational data (heave, translation, north, translation west) with a rate of 1.28 Hz.

NON-DIRECTIONAL WAVERIDER

The (non-directional) Waverider buoy (Datawell) is approximately spherical with diameter about 0.9m. The accelerometer inside is passively stabilised in the vertical plane for storm and swell frequencies (0.035 HZ – 0.55 Hz). By integrating twice the measured acceleration, these waveriders transmit a voltage signal between – 1 and + 1 V, proportional to the wave height, to Datawell Digital Waverider Receivers. In order to be compatible with the acquisition card, this signal is transformed to 0 – 10 V range with an AD7B30-08-2 module from Analog Devices. Due to the strong tidal currents in front of the breakwater, the buoys move notably. The resolution of the waverider buoys is 0.01 m with an accuracy of 1.5%.

INFRA-RED WAVE HEIGHT METER

The infra-red wave height sensor (IR-meter, THORN EMI, UK) measures the water level at the toe of the breakwater. The IR-meter is placed on top of the measurement jetty (Fig. 3). The water level is determined by measuring the time used by an infra-red light pulse to travel between the IR-meter and the water surface and back. As the velocity of the infra-red beam is known, the distance between the IR-meter and the water surface can be computed. The stationary accuracy of the IR-meter is 0.03 m, while the dynamical accuracy is ca. 0.05 m.

WAVE GUIDE RADAR

The Enraf WaveGuide is a radar gauge for level, tide and wave measurement. It has four programmable level alarms and also provides diagnostic information. This information can be displayed on the internal display, the Portable Enraf Terminal (PET) as well as on remote systems. The MPU board provides a 4-20 mA analog level output and can be used to adapt the WaveGuide for control applications or analog recorders.

The radar level gauge (Fig. 6) is a device that uses high frequency (10 GHz) electromagnetic waves to determine the distance from the radar antenna to the water surface. The electromagnetic wave is reflected by the water surface. The phase difference between the transmitted and the received signal is measured. The corresponding travelled distance can

then be calculated from this phase relation. This measurement principle is known as synthesised pulse radar (SPR).

The microwave signal is generated in the Antenna Unit (Fig. 7, nr. 2). After generation, this signal is led, via the mounting device (Fig. 7, nr. 3), to the antenna (Fig. 7, nr. 4). The radar antenna shapes the beam and emits the signal. The microwave signal reflected from the water surface is then received by the same radar antenna. The digital electronics in the Antenna Unit measures both the transmitted and reflected signal. After processing, the digital data is transmitted to the Control Unit (Fig. 7, nr. 1). In the Control Unit the measured distance is converted into level data and made available for remote communication. Fig. 8 gives a view on the installed radar at the measurement jetty.
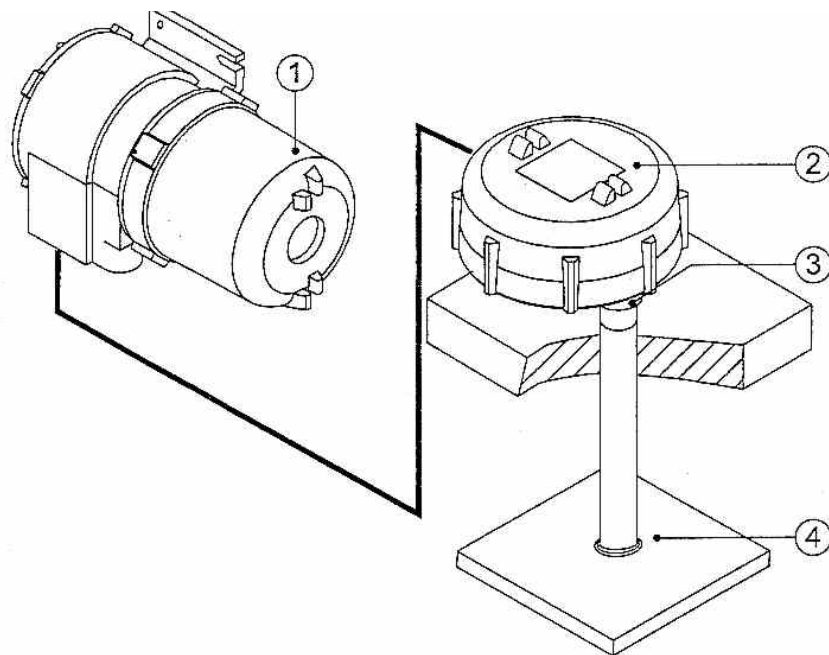
Fig. 7: *WaveGuide Radar configuration*

Fig. 8: *Installed Wave Guide Radar at the measurement site*

COMBINED WIND SENSOR

Combined wind speed and direction measurements are carried out by a VAISALA (WMS301) compact sized wind sensor. This instrument combines wind speed and direction sensors integrated in one unit. The rotating cup anemometer at the top of the unit provides linear response to wind speed. The vane attached to the body of the unit provides fast response to wind direction. The accuracy of the anemometer is ca. 0.3 m/s for wind speeds smaller than 10 m/s). The error is smaller than 2% for wind speeds above 10 m/s. The accuracy of the vane is better than ca. 3°.

Fig. 9 shows the infra-red wave height meter and the combined wind sensor on top of the measurement jetty.

Fig. 9: *Infra-red wave height meter and combined wind sensor at the measurement jetty*

3.2 CROSS – SECTION 2 : OVERTOPPING MEASUREMENTS

Fig. 5 shows the cross section in which wave overtopping measurements are carried out. The instruments to measure the wave overtopping are: an overtopping tank and wave detectors. The wave overtopping measurements are supported by means of 2 video cameras. Measurement instruments in this cross-section are described here.

WAVE OVERTOPPING TANK

Wave overtopping (i.e. the amount of green water washed over the crest of the breakwater) is measured by means of pressure measurements in a concrete construction. The volume of the overtopping tank which collects the overtopping water is about 28 m^3 (Fig. 10). The overtopping tank is placed just behind the crest of the breakwater (Fig. 11). To ensure a continuous measurement of wave overtopping, a compound weir is placed in the northern side wall of the overtopping tank (Fig. 10, 13, 14 and 15). The weir controls the outflow of the water.
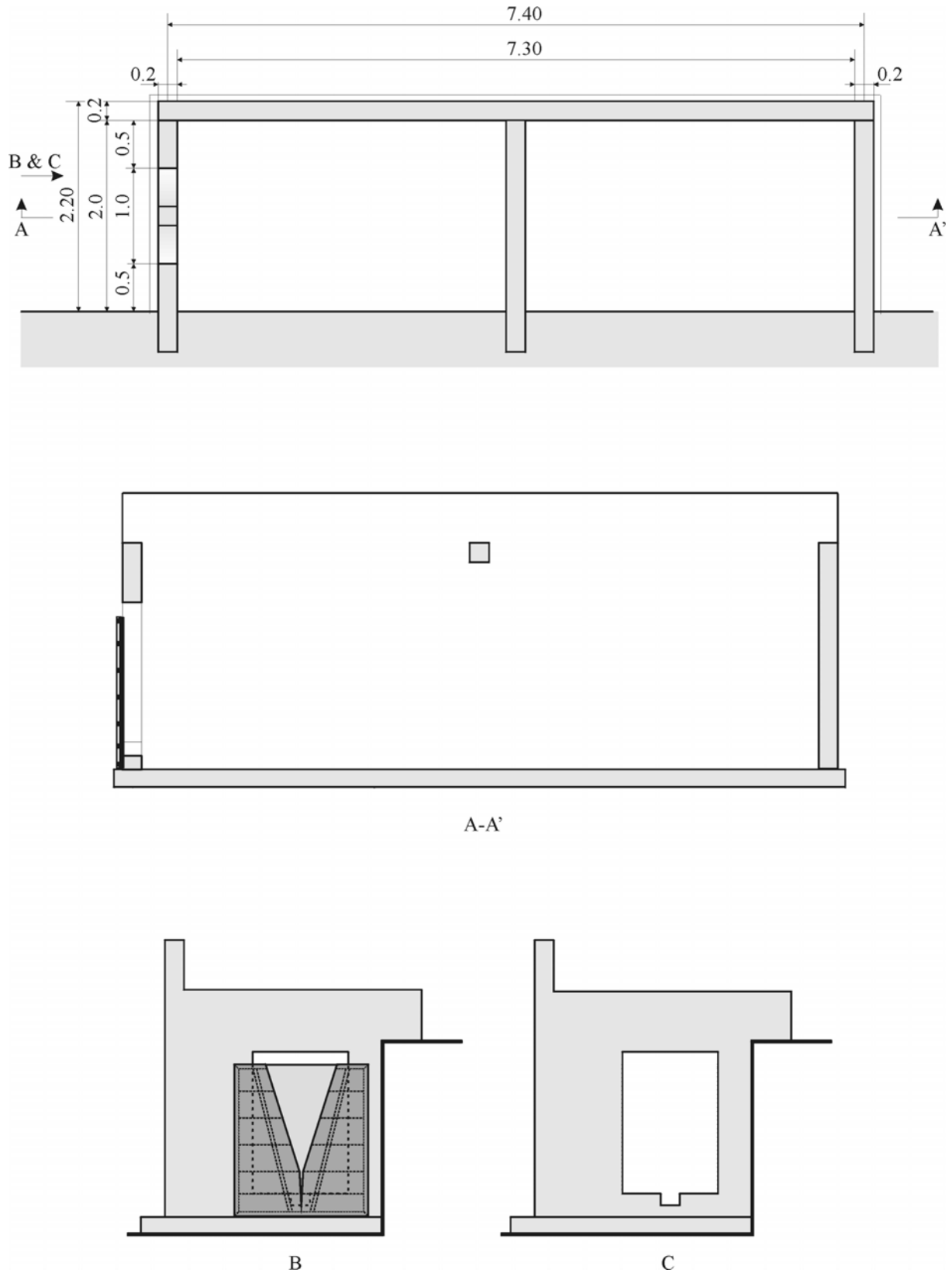
Fig. 10: *Overtopping tank (dimensions in m)*

Fig. 11: *Overtopping tank (general view)*

Fig. 12: *Overtopping tank (situation)*

Fig. 13: *Compound weir (seen from inside the overtopping tank)*

Fig. 14: *Compound weir (seen from outside the overtopping tank.*
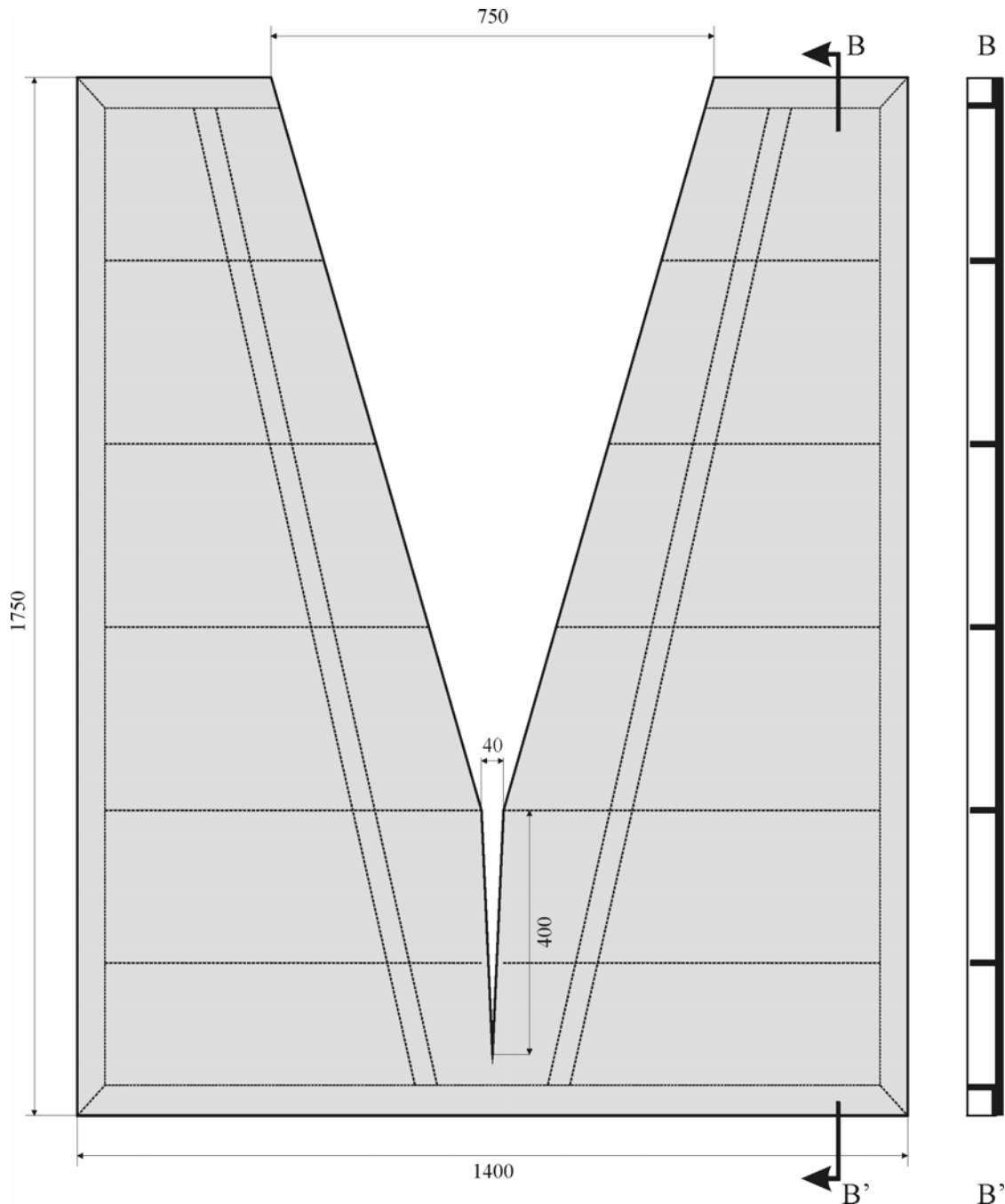
Fig. 15: *Compound weir*

The water height in the overtopping tank is measured by two pressure sensors at the bottom of the overtopping tank. Signals of these sensors are sampled at $f_s = 10$ Hz. These pressure sensors are connected to both ends of a tube (Fig. 16). Five tubes (Fig. 17) are also connected to this tube. The other ends of these five tubes are equally distributed over the bottom of the tank. Water level in the tank is measured by means of these five tubes.
Many factors make the water surface not quiescent: standing waves, rainfall, wind blowing over the water surface,... which makes that the static water pressure measured at the different ends of the tubes is not completely the same. Through these five tubes an "average" water level in the tank is measured by the two pressure sensors.
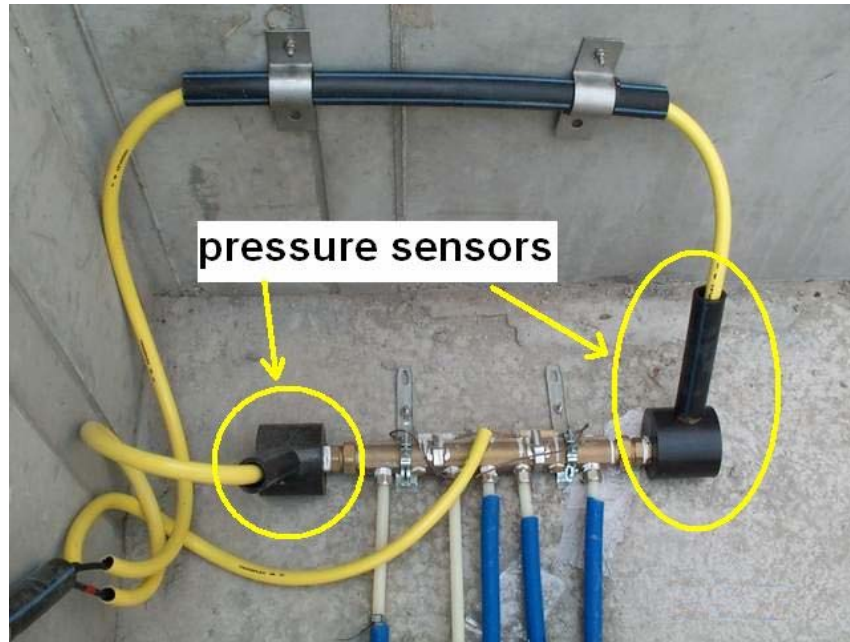
Fig. 16: *The five tubes are connected to another tube which has a pressure sensor on both ends*

Fig. 17: *Five tubes placed at the bottom of the tank allow to measure the pressure at five different places*

The compound weir has been calibrated in the Hydraulics Laboratory of Ghent University. The lower part of the weir at full scale and the upper part on a 1:2 scale model.

The calibration formula of the compound weir reads:

$$Q_1 = a.h^{\frac{3}{2}} \qquad\qquad 0 \le h \le 0.60 \text{ m} \qquad\qquad (1)$$

$$Q_2 = a.h^{\frac{3}{2}} + b.h^{\frac{5}{2}} \qquad\qquad h \ge 0.60 \text{ m} \qquad\qquad (2)$$

The coefficients in (1) and (2) are respectively $a = 0.0805$ and $a = -0.1691$ and $b = 0.3533$.

The outflow discharge in function of the water height in the overtopping tank is shown in Fig. 18.
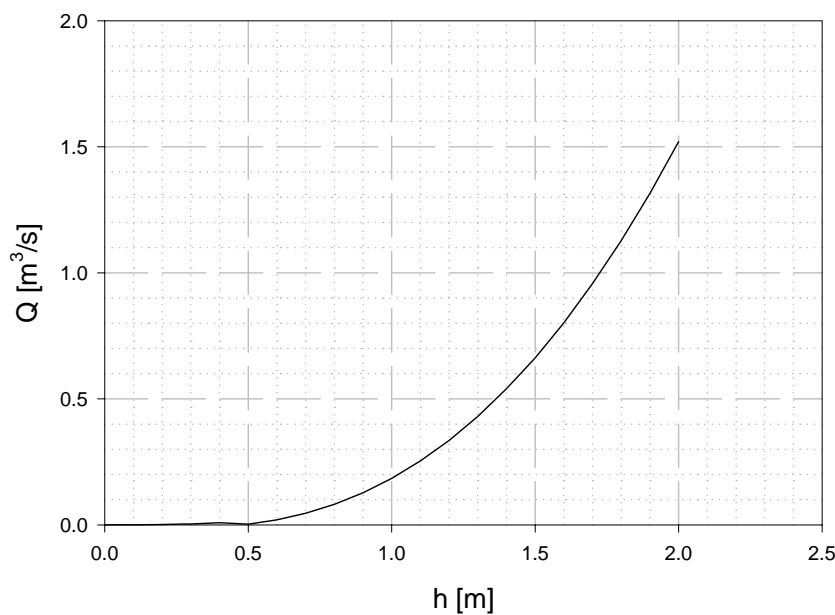
Fig. 18: *Calibration formula of the compound weir*

The weir has been calibrated at full scale at the field site as well. This calibration was done on August 11-12, 1999. The calibration was done by filling up the overtopping tank completely. The weir was closed up with a paddle (Fig. 19(a)). The paddle was released and the water could pour out freely (Fig. 19(b)). The water height in the overtopping tank has been measured.

(a)   (b)
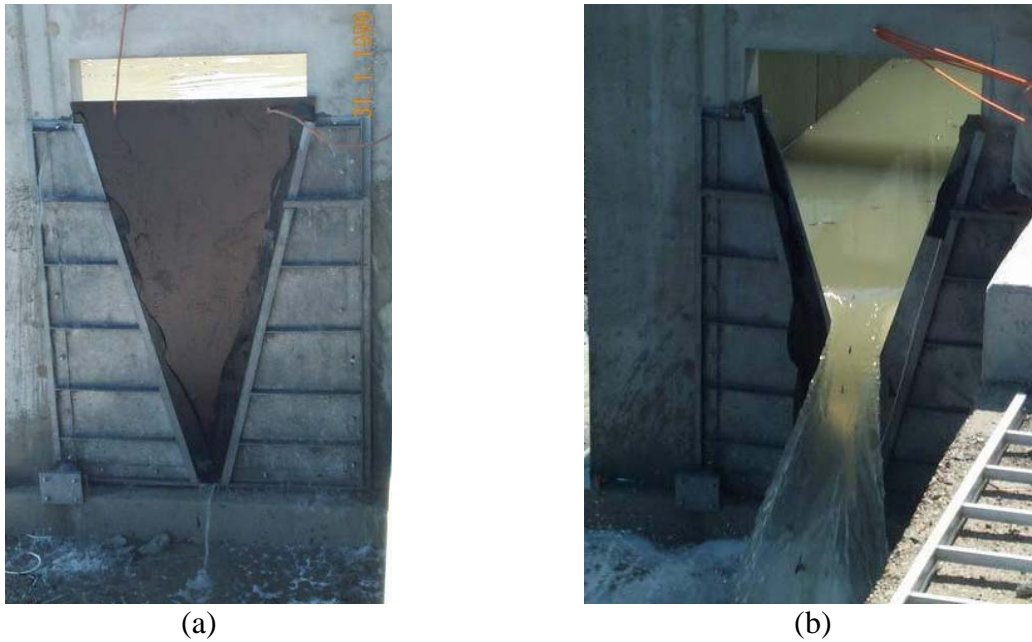
Fig. 19: *Compound weir is closed up (a) with a wooden paddle which is released (b) to empty the filled up overtopping tank*
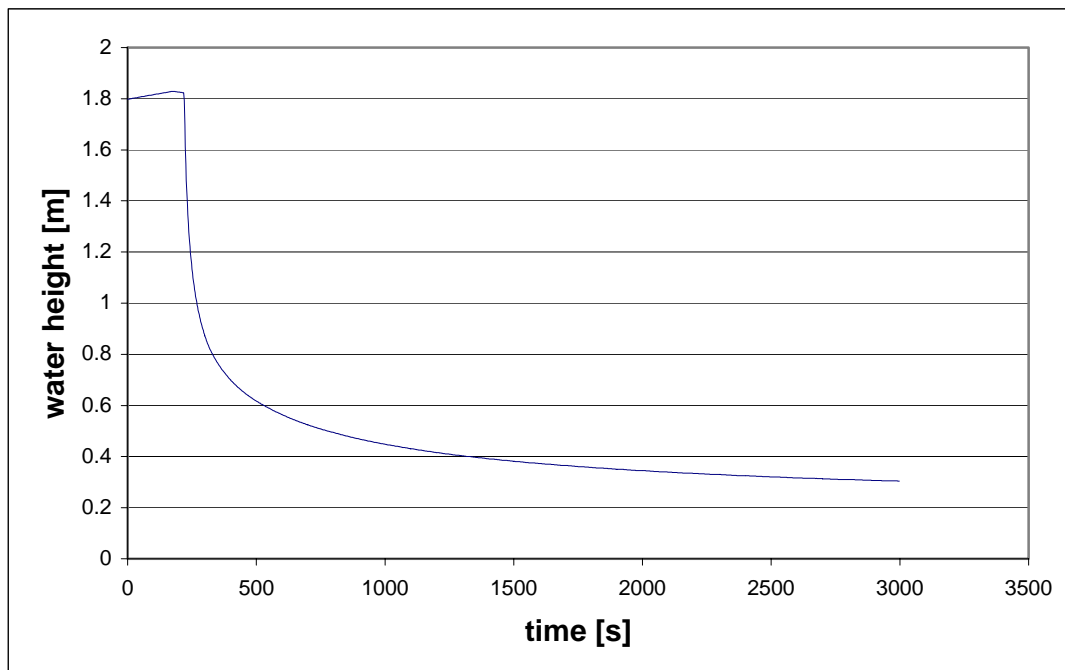
Fig. 20: *Registration of the water height in the overtopping tank while emptying the overtopping tank.*

Out of the measurements shown in figure 20, the discharge *Q* in function of the water height *h* has been derived, by using the general formula (continuity equation):

$$Q = A \frac{dh}{dt} \qquad (3)$$

or with a discrete time interval: $Q = A \dfrac{\Delta h}{\Delta t}$. The surface of the overtopping tank A equals 14.8 m^2 on average. Δt was taken 2 seconds.

The following results (Fig. 21) are obtained. The fitted line through the laboratory calibration data is also shown in Fig. 21. It is seen that the discharges at full scale are a little bit higher than the discharges measured in laboratory circumstances.
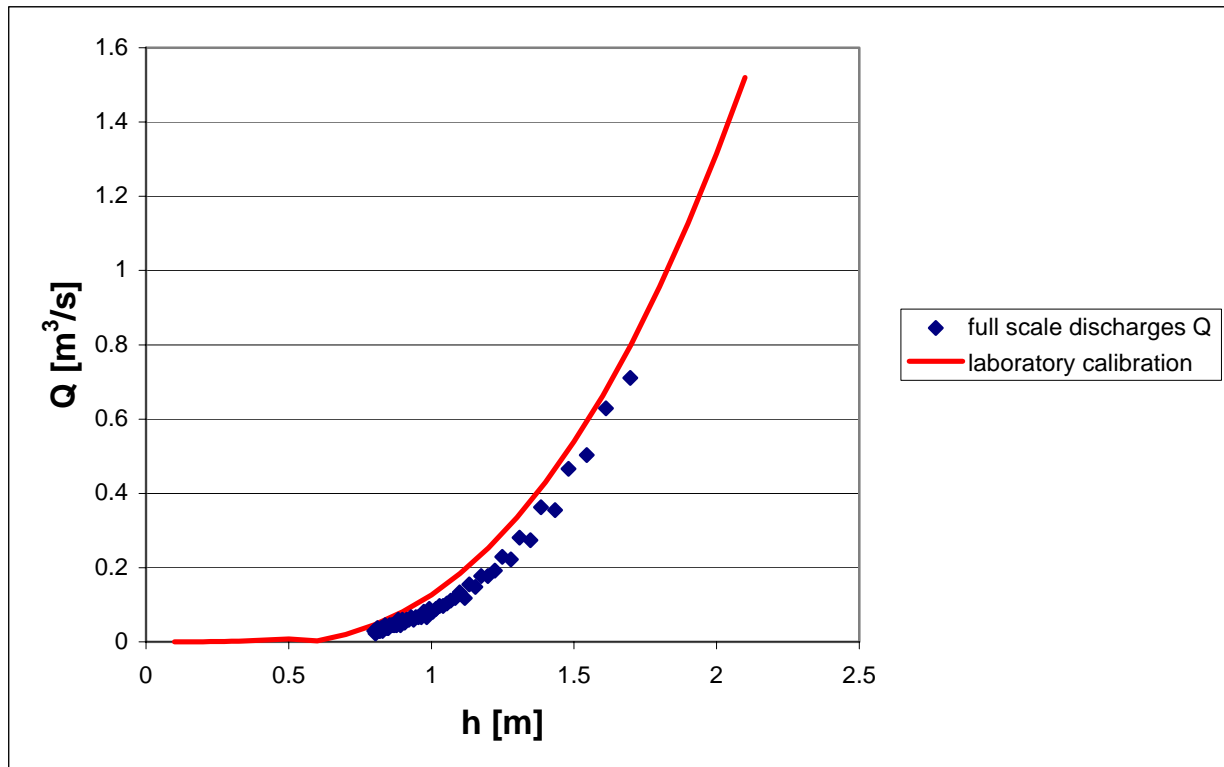
Fig. 21: *Comparison of laboratory calibration of compound weir and full scale discharge measurements*

WAVE DETECTORS

On and near the crest armour units six wave detectors have been installed (Fig. 22 and Fig. 23). These measure the number of overtopping waves. By considering the measurements together one gets an idea about the extent of an overtopping event.

A wave detector consists of two electrodes which get short-circuited electrically when an overtopping wave hits the electrodes.
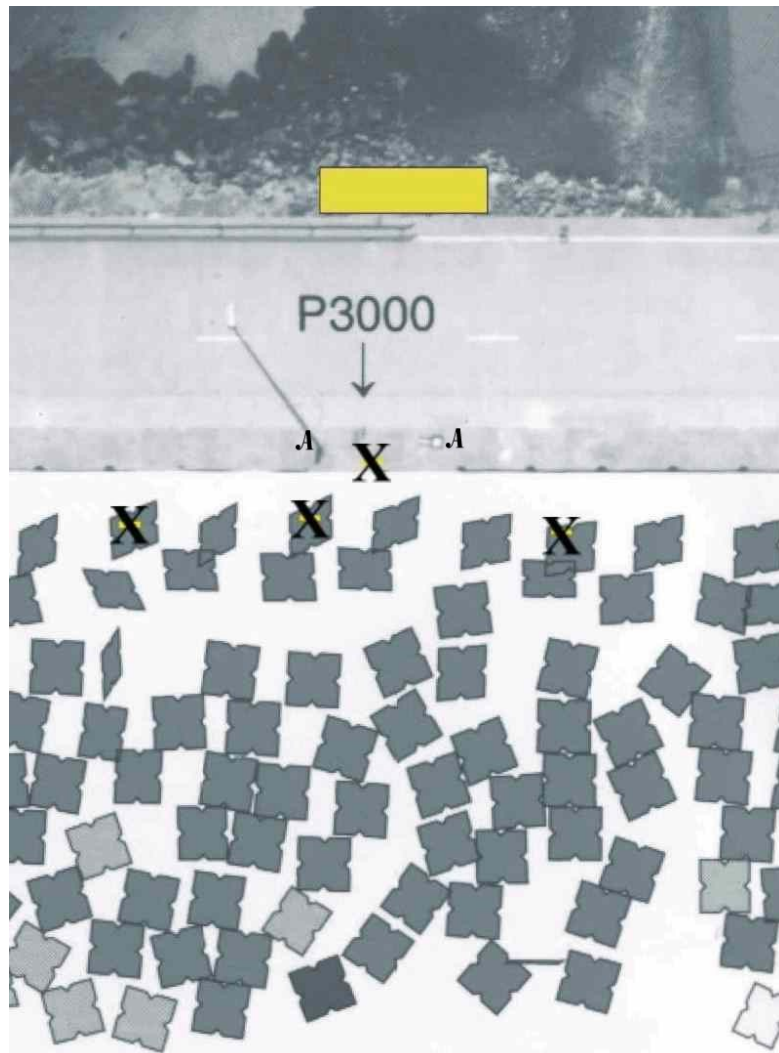
Fig. 22: *Position of wave detectors (indicated by black crosses); **A** = additional detectors placed on crestwall within CLASH ; rectangular box = overtopping tank*

Fig. 23: *Wave detectors (WD); detail (WD3) and situation (4 of the 6 detectors)*

As an example how the measurements are be interpreted, Fig. 22 shows data from the wave overtopping tank pressure sensor (PR) and the wave detector (WD) gathered during a storm event. It is seen that every time one or multiple wave detectors detect an overtopping wave, an increase in the water height in the overtopping tank has been noticed in the corresponding pressure measurement graphs.
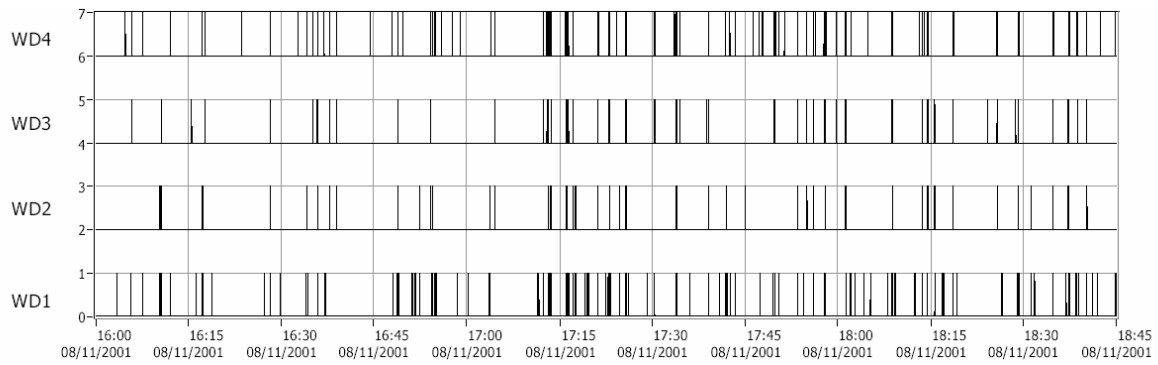
(a)
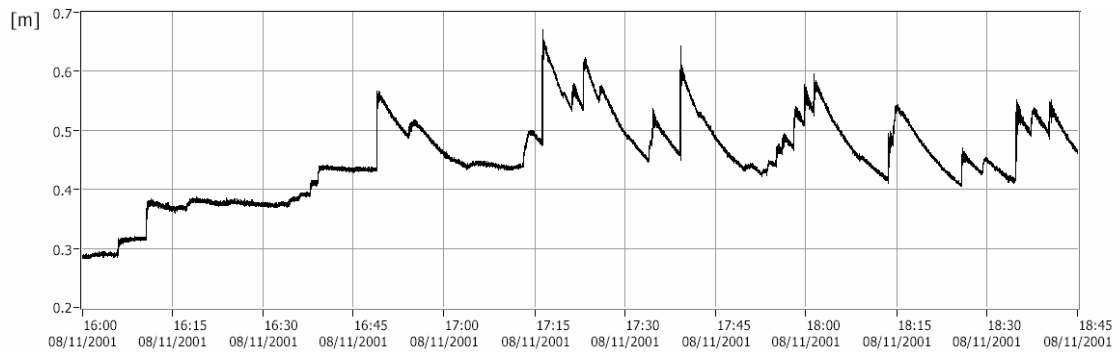
(b)
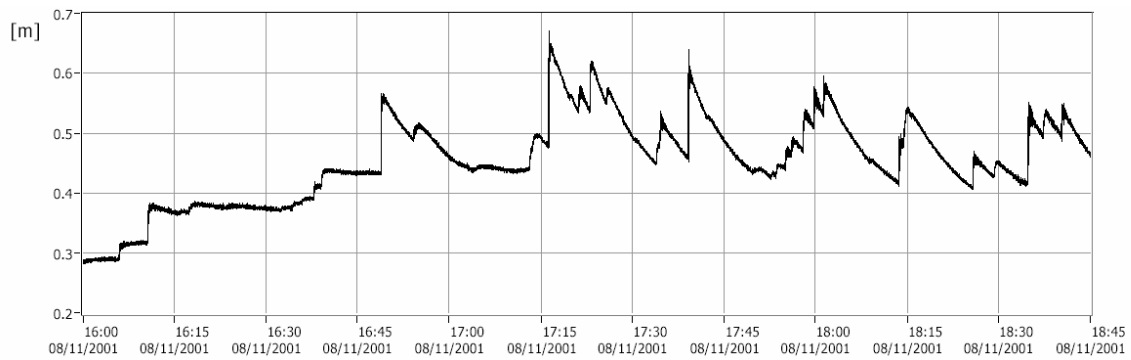
(c)

Fig. 24: *Measurement data of (a) wave detectors (WD), (b) overtopping tank pressure sensor 1 and (c) overtopping tank pressure sensor 2 during a storm event*

METHODOLOGY FOR CALCULATION OF OVERTOPPING DISCHARGES

Three different methods to calculate the overtopping discharges have been used:

A. Method 1, using the continuity equation

From the continuity equation the inflow discharge $Q_{in}(t)$ is calculated as:

$$Q_{in}(t) = Q_{out}(h(t)) + A\frac{dh}{dt} \tag{4}$$

The instantaneous inflow discharge $Q_{in}(t)$ is composed of two terms, Q_{out} and $A\frac{dh}{dt}$. Both terms are derived from the water depth $h(t)$ inside the overtopping tank. Fig. 25(a) shows $h(t)$ for a storm event as a typical saw tooth-type signal, with a steep increase of $h(t)$ during an overtopping event when water enters the overtopping tank, and a mild decrease of $h(t)$ after the overtopping event when water flows out of the tank through the weir.

The first term $Q_{out}(h(t))$ in the RHS of equation (4), i.e. the outflow discharge over the weir, is calculated according to the calibrated discharge relationship eq. (1) and (2) (par. 3.2)

$$Q_{out}(h(t)) \quad = \quad c_1\,h(t)^{5/2} \ \text{ for } h \leq h_t$$

$$= \quad c_2\,h(t)^{3/2} + c_3\,h(t)^{5/2} \ \text{ for } h > h_t \tag{5}$$

where $h_t = 0.60$ m, and $c_1 = 0.0805$, $c_2 = -0.1691$ and $c_3 = 0.3533$. The resulting time series of $Q_{out}(t)$ for storm 3 is shown in Fig. 25(b) and exhibits a saw tooth-type shape similar to the water depth $h(t)$.

The second term $A\frac{dh}{dt}$ in the RHS of equation (2), i.e. the time rate of change of the volume inside the overtopping tank, is calculated using the constant surface area $A = 14.80$ m² and the time-derivative of $h(t)$. The function $A\frac{dh}{dt}$ is also shown in Fig. 25(b). Positive values of $A\frac{dh}{dt}$ correspond to increasing water depths, and negative values to decreasing water depths. The peaks in the function $A\frac{dh}{dt}$ occur during wave overtopping events when water enters the tank, and therefore these peaks are visual detectors of the (number of) overtopping waves.

Adding both time series $Q_{out}(t)$ and $A\frac{dh}{dt}$ from Fig. 25(b) yields the instantaneous inflow discharge $Q_{in}(t)$, and is presented in Fig. 25(c). As the second term $A\frac{dh}{dt}$ is an order of magnitude larger than the first term $Q_{out}(t)$, the function $Q_{in}(t)$ has the typical shape of

$A\dfrac{dh}{dt}$, with positive peaks at overtopping events, and (nearly) zero values in between when there is no inflow in the tank.

The average overtopping rate q, per unit crest width, from here on referred to as q_{ceq} from method 1, is finally calculated from $Q_{in}(t)$, using:

$$q_{ceq} = \frac{1}{b}\frac{1}{T_0}\int_0^{T_0} Q_{in}(t)dt \qquad (6)$$

where $b = 7.40$ m is the tank width parallel to the crest, and T_0 is the duration of the analysed wave record.
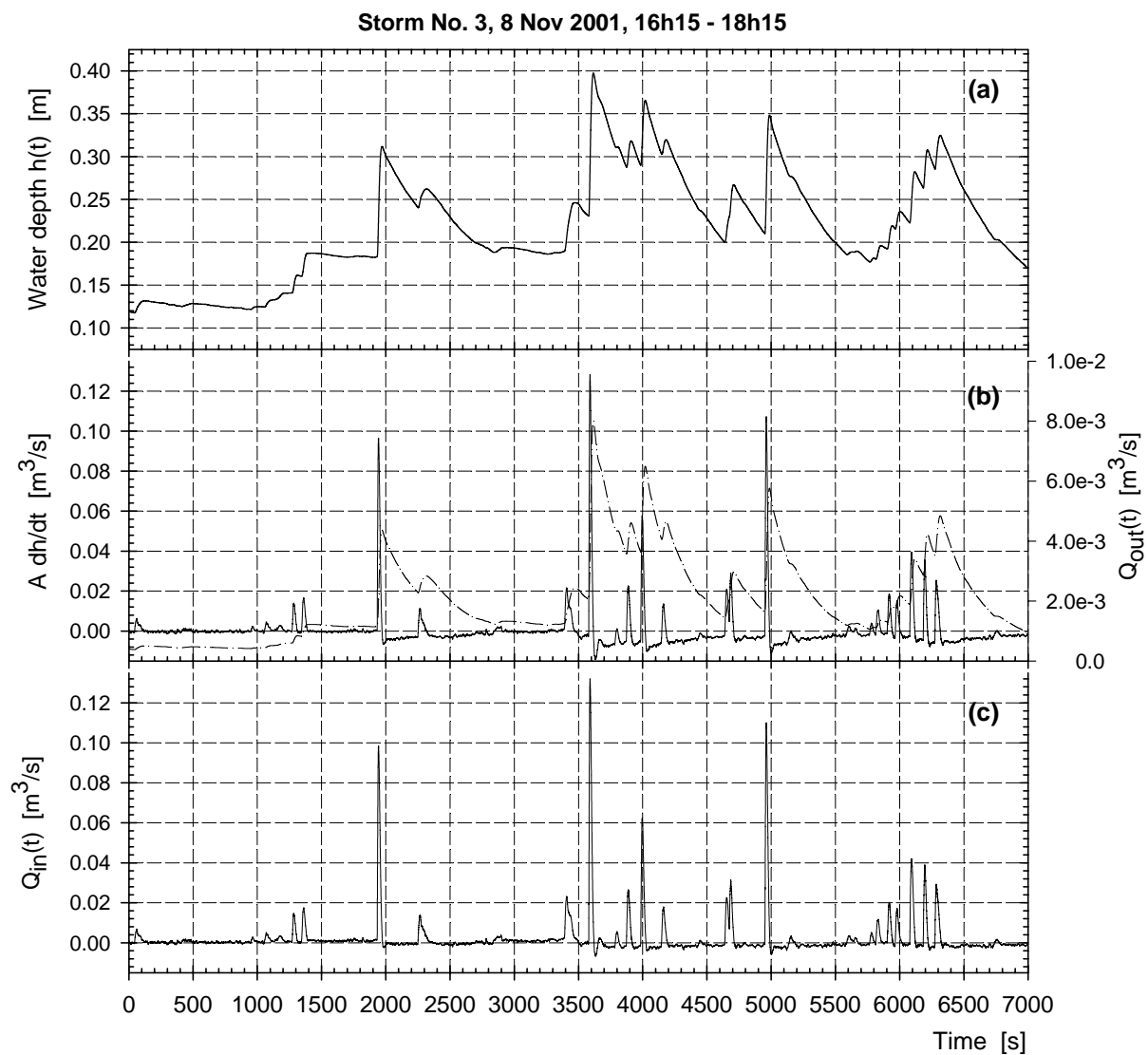
Fig. 25: *Calculation of overtopping discharge using continuity equation*

B. Method 2, using individual overtopping volumes

The noise remaining in the water depth signal $h(t)$ after low pass filtering is still producing scatter in the time derivative $A\dfrac{dh}{dt}$ in between the peaks. The values of $Q_{in}(t)$ scattered around zero in between the overtopping events may affect adversely the time-averaged overtopping rate q_{ceq} calculated from the whole duration using eq. (6). Therefore a modified calculation of the average overtopping rate q is proposed, using the peaks of the overtopping events only from the function $Q_{in}(t)$ and neglecting the scatter around zero. For a single peak of an overtopping event, the individual volume V_i (per m crest width) of the overtopping wave with number i is calculated from:

$$V_i = \frac{1}{b}\int_{t_0}^{t_1} Q_{in}(t)dt \qquad (7)$$

where t_0 and t_1 denote the start and end time of the single overtopping event. It was found that typically $t_1 - t_0 \approx 60\,\text{s}$. The average overtopping rate q_{Vi} using this second method is calculated using:

$$q_{Vi} = \frac{1}{T_0}\sum_{i=1}^{N_{ov}} V_i \qquad (8)$$

where N_{ov} is the number of overtopping events during the storm with duration T_0.

C. Method 3, using water depth jumps

The previous two methods use the calculated instantaneous inflow discharge $Q_{in}(t)$, based on Q_{out} and $A\dfrac{dh}{dt}$, and depend on the accuracy of determination of $Q_{out}(t)$. A third simplified method uses the water depth $h(t)$ directly to calculate the increase in volume inside the tank. The positive jumps Δh_i in the water depth signal $h(t)$ are detected (using a threshold value $\Delta h_{min} = 3.5$ mm related to the pressure sensor's accuracy) and added as individual volumes contributing to the total volume V inside the tank:

$$V = A\sum_{i=1}^{N_{ov}} \Delta h_i \qquad (9)$$

The average overtopping rate $q_{\Delta h}$ calculated using this third method is:

$$q_{\Delta h} = \frac{1}{b}\frac{1}{T_0} V \qquad (10)$$

During an overtopping event inducing a positive jump Δh_i, with a duration of 60 s on average, water is already flowing over the weir out of the tank, and a correction to the individual volumes $A\Delta h_i$ inside the tank has to be added.

The correction ΔV_i for a single overtopping event i is:

$$\Delta V_i = \int_{t_0}^{t_1} Q_{out}(t)dt \tag{11}$$

yielding a total correction volume V_{cor} for the whole duration T_0:

$$V_{cor} = \sum_{i=1}^{N_{ov}} \Delta V_i \tag{12}$$

modifying the total volume V inside the tank (eq. 9) to:

$$V = A\sum_{i=1}^{N_{ov}} \Delta h_i + \sum_{i=1}^{N_{ov}} \Delta V_i \tag{13}$$

and the average overtopping rate $q_{\Delta h}$ (eq. 10) is extended to:

$$q_{\Delta h} = \frac{1}{b}\frac{1}{T_0}\left(V + V_{cor}\right) \tag{14}$$

3.3 MEASUREMENTS TO IDENTIFY HAZARDS FROM WAVE OVERTOPPING

Different instruments to identify and measure hazards resulting from wave overtopping have been installed at the Zeebrugge field site during the first year of CLASH. Within this framework wave forces on instrumented dummies, an instrumented pipeline and a vertical wall are measured. Moreover, an investigation for the breaking of window glass is carried out.

A. Forces on instrumented dummies

Three dummies have been installed and instrumented. Two of them are placed on the crest wall directly behind the armour units. The third (smaller) one is placed at the landward side of the access road on top of the breakwater's crest.

The dummies are a rough schematization of human beings. They are instrumented to get information about the magnitude of forces exerted by overtopping waves on people walking or standing on top of a breakwater.

Fig. 26 shows the design drawing of the dummies. It concerns an aluminium rectangular body (1.70 m * 0.50 m) mounted on a steel frame. Forces are measured by means of three S-shaped load cells (indicated by the rectangles in Fig. 26). Design force has been estimated using the work by Pedersen (1996). Signals from the force transducers are sampled at $f_s = 100$ Hz.

Fig. 27 and 29 give a view at the installed dummies at the breakwater, while Fig. 28 gives a detail of a mounted S-shaped sensor. Fig. 30 shows two S-shaped load cells (Tedea – Huntleigh). These load cells are suited for use in both tension and compression. Capacity for the sensors of the dummies is –1000 kg to +1000 kg. Total error is 0.05 % of the applied force.
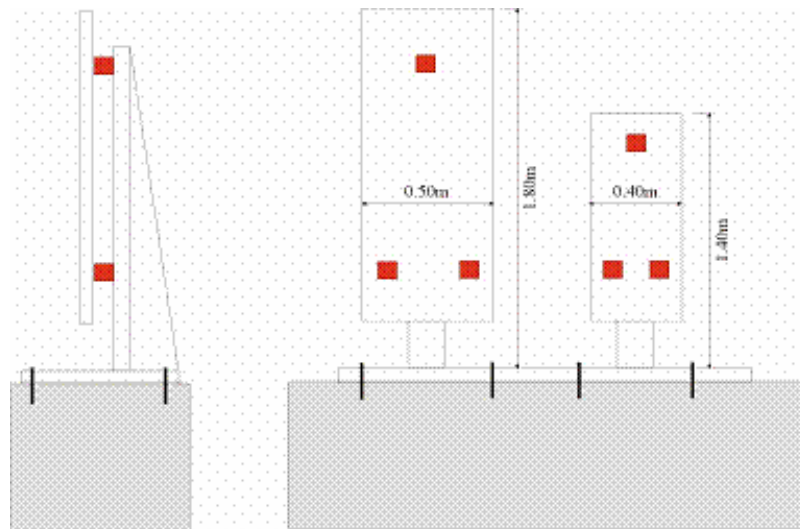
Fig. 26: *Principle drawing of the instrumented dummies; squares symbolize force transducers*

Fig. 27: *Installed dummy on landward side of access road* **Fig. 28:** *Detail of mounted load cell*

Fig. 29: *Global view on the installed dummies at the breakwater's crest*
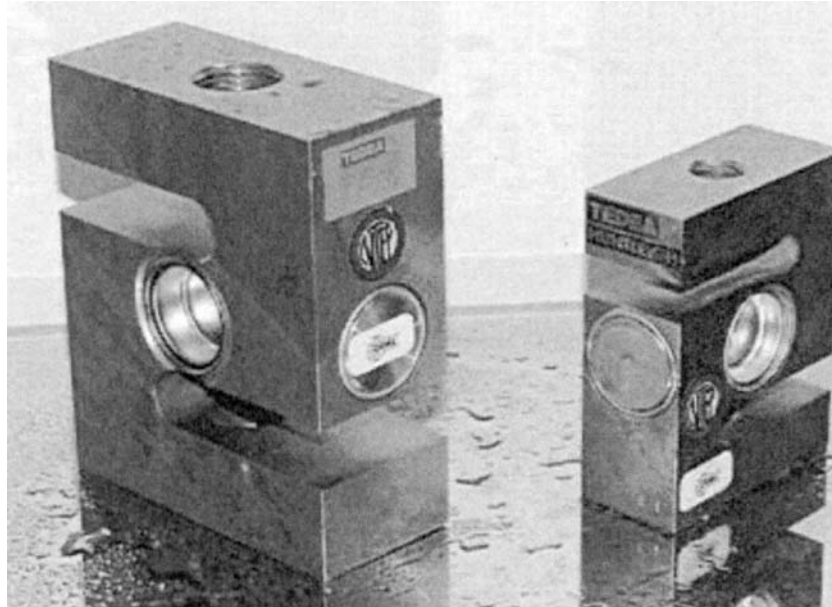
Fig. 30: *Tedea Huntleigh S-shaped load cells*

B. Forces on an instrumented pipeline

In many harbours pipelines to transport oil or gas are installed on top of a breakwater. To gain information about overtopping wave forces on such pipelines, an instrumented "pipeline" (Fig. 31 and 32) has been installed. In fact it concerns a steel dredging hose with length = 6.00 m, diameter D = 0.65 m and a wall thickness t = 0.01 m. Horizontal and vertical force components on the pipeline are measured by means S-type load cells as presented above. Capacity of the load cells for this application is from – 2000 kg to + 2000 kg. Total error is 0.03% of the applied load in this case.
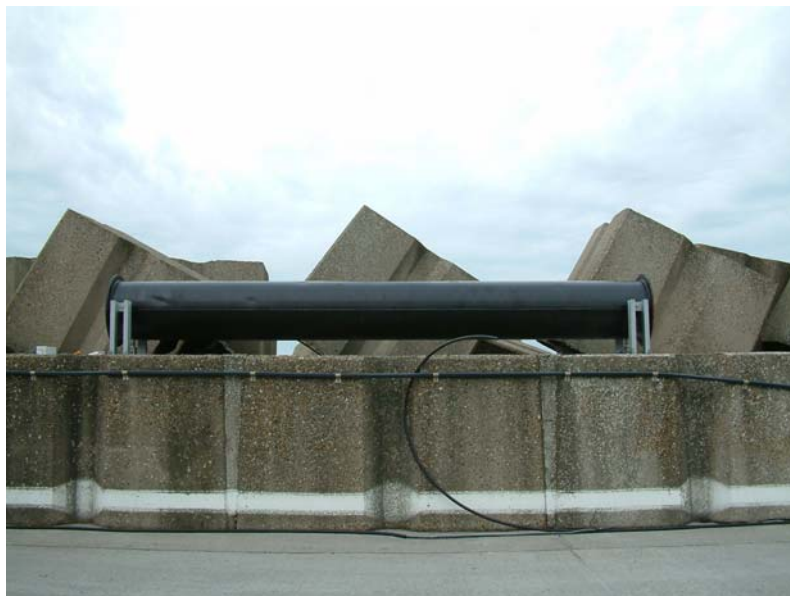
Fig. 31: *Instrumented pipeline: front view*

Fig. 32: *Instrumented pipeline : situation*

C. Forces on a vertical wall

These measurements are carried out by measuring the force on an aluminium plate, with the same dimensions as the body plate of the dummies (1.70 m * 0.50 m), mounted to the concrete column supporting the measurement jetty (see Fig. 33). This column serves as vertical wall. Forces are measured by three S-shaped load cells, with the same positioning and capacity as for the dummies. Fig. 34 shows a detail of the mounted body plate with indication of a mounted load cell. Moreover, pressures are measured by five flush-mounted pressure sensors positioned along a vertical line in the centre of the aluminium plate. Fig. 35 gives a detail indicating the position of two of these pressure sensors.
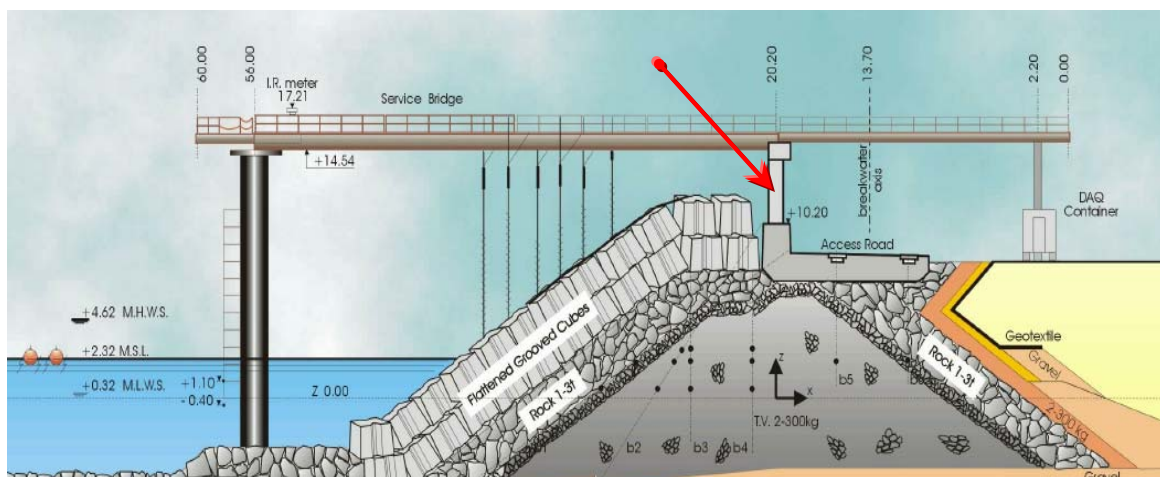
Fig. 33: *Position of the vertical wall at the breakwater's crest (indicated by the arrow)*

Fig. 34: *Measurements of forces on a vertical wall: detail with the circle indicating mounted S-shaped load cell*
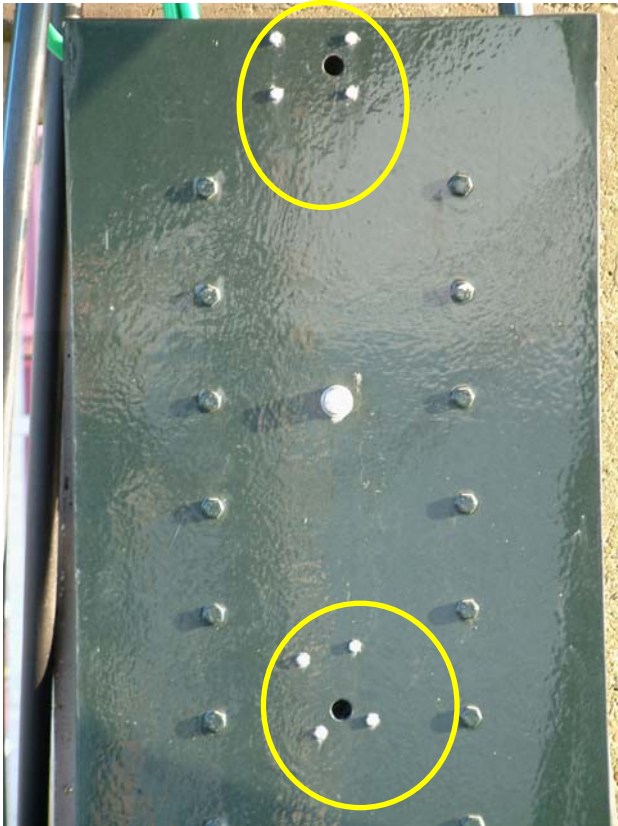
Fig. 35: *Measurements of forces on a vertical wall: details with circles indicating positions of flush mounted pressure sensors*

D. Velocities of overtopping waves

Since November 2003, velocity meters are installed at two locations between the armour units near the crest wall. One is located near the pipeline (Fig. 37); the other is situated in front of the large dummy nearest to the measurement jetty (Fig. 36).
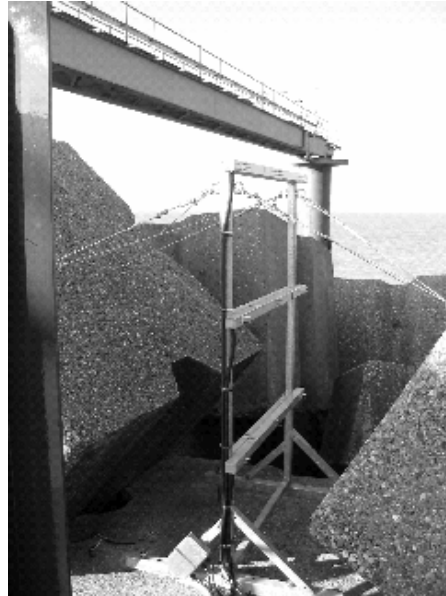
Fig. 36: *Velocity meter in front of the dummy nearest to the measurement jetty*

Fig. 37: *Velocity meter in front of the pipeline*

Each velocity meter consists of 2 (near pipeline) or 3 (near dummy) units that are horizontally installed on a metal frame. The one near the dummy consists of 3 units as the dummy is much higher than the pipeline. Each unit contains 3 pairs of electrodes which detect the presence of water at this location. An overview and numbering of the electrodes is given in Fig. 38.

The first time a pair of electrodes become wet, a counter starts running and the local DAQ system is activated. For each next pair of electrodes that become wet, the time and the number of the electrode are saved. After 4 seconds of running, the system stops measuring and calculates the velocities between each couple of electrodes. The system is then activated again when a pair of electrodes becomes wet.

Fig. 39 show the velocities that are calculated from 2 units (corresponds to the small velocity meter). In this way, the small velocity meter is able to determine 8 velocities, while the large velocity meter is able to determinate 13 velocities.

(a) Velocity meter near the dummy   **(b)** Velocity meter near the pipeline
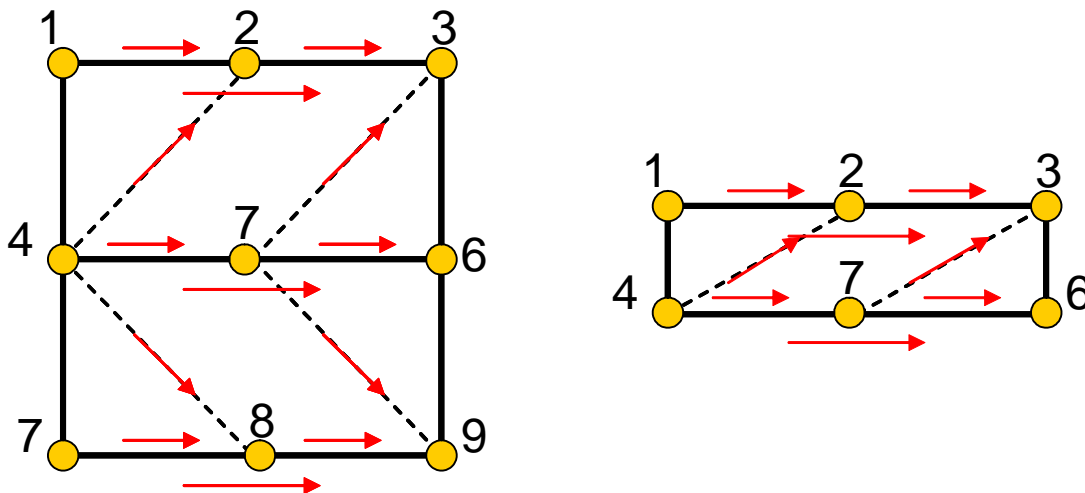
Fig. 38: *Principle of the velocity meters*
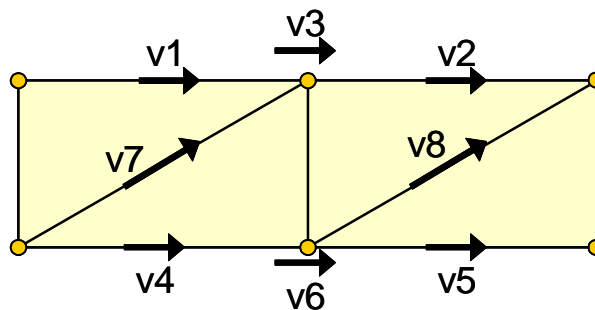
Fig. 39: *Velocities calculated with the small velocity meter*

E. Investigation for breaking of window glass

To investigate the breaking of window glass due to overtopping waves, three windows (2.00 m * 1.00 m) with different glass thickness, i.e. 3 mm, 5mm and 8mm have been installed at the Zeebrugge field site. A broken glass detection system allows to find out when (due to which event) one (or more) of the glass windows has been broken. Fig. 40 (a) and (b) show a view on the installed windows.

(a)   **(b)**

Fig. 40: *Investigation for the breaking of window glass: global view on the instrumentation*

4 RESULTS FROM FULL SCALE MEASUREMENTS

4.1 RESULTS FROM WAVE OVERTOPPING MEASUREMENTS

Wave overtopping has been measured at the Zeebrugge breakwater during nine storms. An overview is given in Table 2.

Table 2: *Storms measured in Zeebrugge*

Storm No.	Date	Time	Duration (s)
1	6 November 1999	11h30 – 13h30	7200
2	6-7 November 1999	23h45 – 01h45	7200
3	8 November 2001	16h15 – 18h15	7200
4	26 February 2002	12h30 – 14h30	7200
5a	27 October 2002	17h00 – 18h00	3600
5b	27 October 2002	18h00 – 19h00	3600
5c	27 October 2002	19h00 – 20h15	4500
6	29 January 2003	10h00 – 12h00	7200
7	7 October 2003	12h00 – 14h00	7200
8	22 December 2003	00h00 – 02h00	7200
9	8 February 2004	14h45 – 16h45	7200

The time spans indicated are the time spans during which the *SWL* is almost constant (around the moment in time of high water t_{HW}) and during which wave overtopping occurred. For the October '02 storm, water level varied, so the time series was split up in three different subseries with their own respective almost constant water level.

Table 3 summarizes the wave characteristics for the different storms. Wave data in this table are based on information gathered from the non-directional wave rider buoy closest to the breakwater. For storms from the winter season 2003 – 2004 on (i.e. from storm 7) data from the directional waverider buoy is available (see further).

The wave overtopping data analysis results have been summarised in Table 4. The mean overtopping discharge per m structure width *q,* calculated according the three different methods as presented above, is given there, together with the number of overtopping events.

Table 3:   *Wave characteristics, surf similarity parameter and water level for the storms.*

Storm No.	H_{m0} (m)	H_s (m)	$T_{m-1,0}$ (s)	T_p (s)	T_m (s)	ξ_0 (-)	SWL (m Z)
1	3.04	2.89	6.88	7.34	5.70	3.52	5.28
2	2.60	2.44	6.93	9.3	5.36	3.88	5.11
3	3.47	3.31	8.41	10.28	6.35	4.05	5.01
4	2.63	2.52	6.49	7.91	5.32	3.68	4.21
5a	3.74	3.61	7.50	8.57	6.21	3.46	4.40
5b	3.86	3.71	7.64	8.57	6.35	3.47	4.60
5c	3.71	3.55	7.98	8.57	6.45	3.70	4.35
6	3.16	3.03	7.28	7.91	5.94	3.66	4.71
7	3.23	3.08	7.00	7.91	5.84	3.47	4.77
8	3.03	2.88	7.33	8.57	5.85	3.76	5.26
9	3.59	3.41	7.37	8.57	6.14	3.47	5.32

Table 4:   *Average overtopping rates for all storms, calculated using the 3 methods based on the continuity equation, the individual overtopping volumes and the water depth jumps, respectively with N_{ov} the number of overtopping events.*

Storm No.	q_{ceq} (l/sm)	q_{Vi} (l/sm)	$q_{\Delta h}$ (l/sm)	N_{ov} (-)	N_{ov} / hour (-)
1	3.161E-02	5.709E-02	4.677E-02	10	5
2	2.299E-02	2.211E-02	1.842E-02	3	1.5
3	2.825E-01	3.310E-01	3.588E-01	29	14.5
4	3.919E-03	1.010E-02	9.031E-03	1	0.5
5a	4.037E-01	5.158E-01	4.404E-01	19	19
5b	5.919E-01	8.585E-01	5.963E-01	30	30
5c	6.296E-01	7.036E-01	6.780E-01	31	24.8
6	8.479E-02	9.620E-02	8.646E-02	9	4.5
7	6.410E-02	8.920E-02	7.280E-02	9	4.5
8	2.900E-02	6.680E-02	5.590E-02	2	1
9	2.200E-01	5.910E-01	5.630E-01	16	8

For all storms, water depth signals h(t) in the tank together with the field spectra are given hereafter (Fig. 41 to 62).
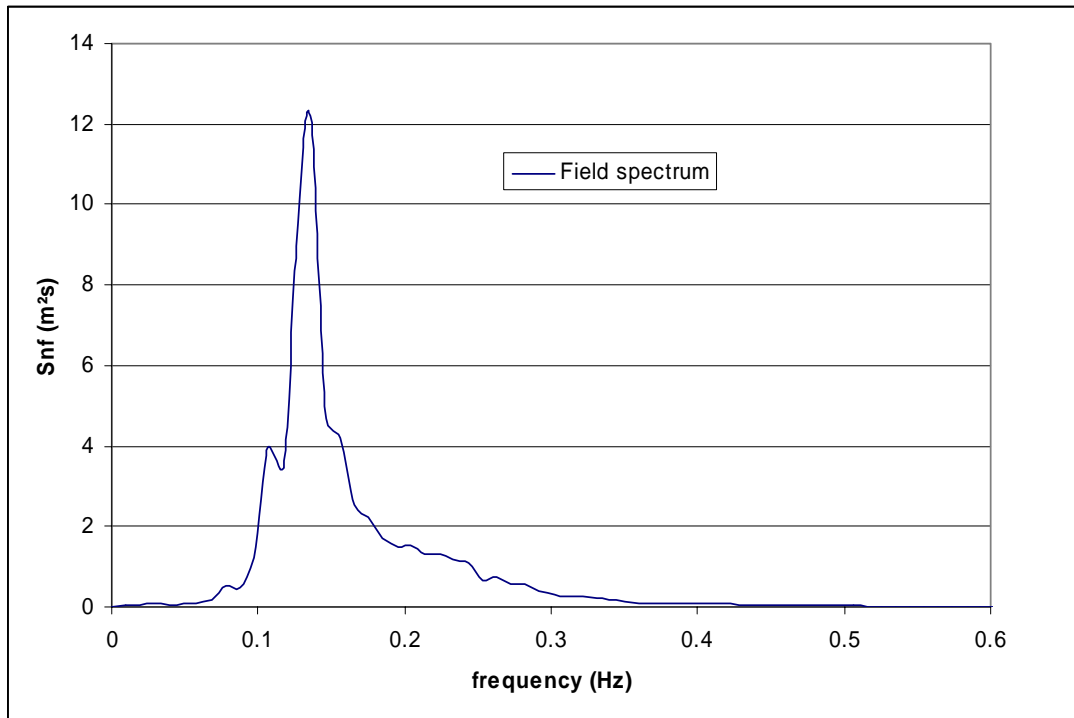
Fig. 41: *Field Spectrum for storm 1 of Nov. 6, 1999 (11.30 – 13.30)*
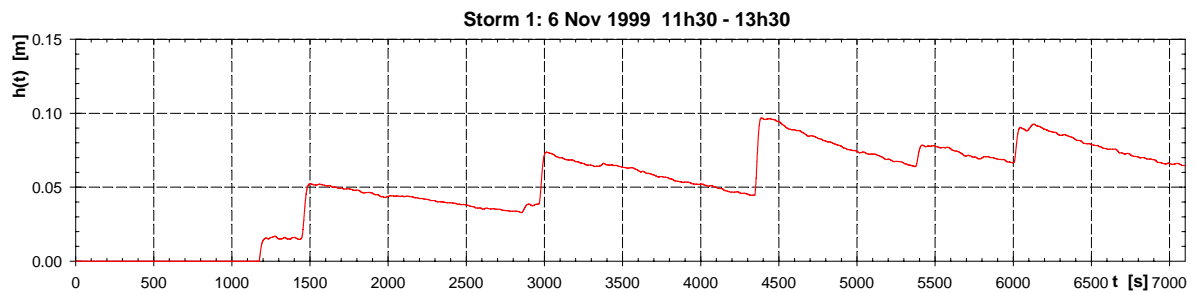
Fig. 42: *H(t) in the overtopping tank for storm 1 of Nov. 6, 1999 (11.30 – 13.30)*
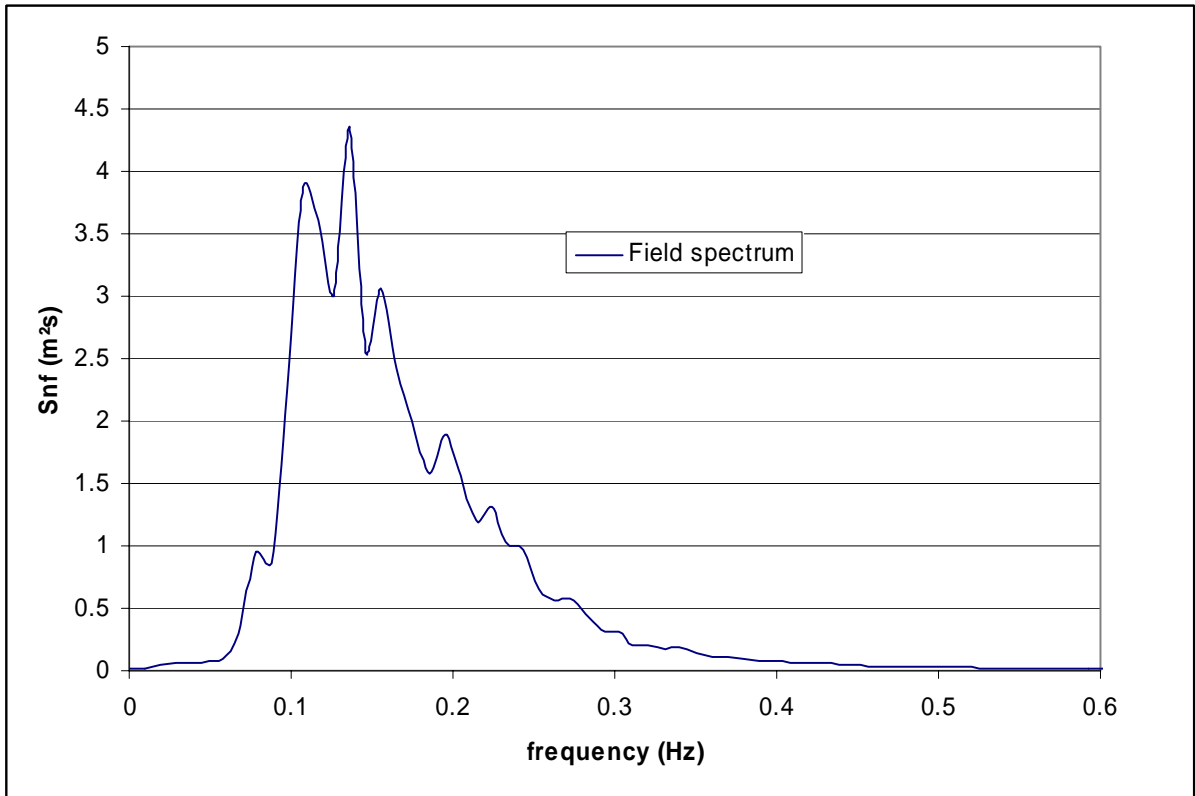
Fig. 43: *Field Spectrum for storm 2 of Nov. 6 - 7,1999 (23.45 – 01.45)*
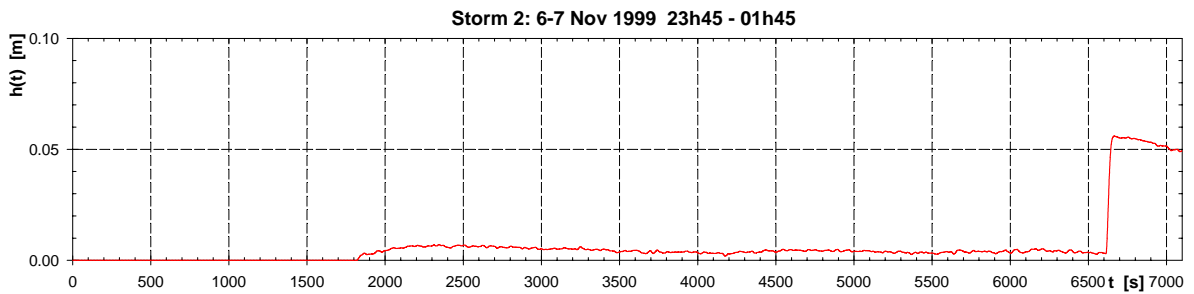
Fig. 44: *H(t) in the wavetank for storm 2 of Nov. 6 – 7,1999 (23.45 – 01.45)*
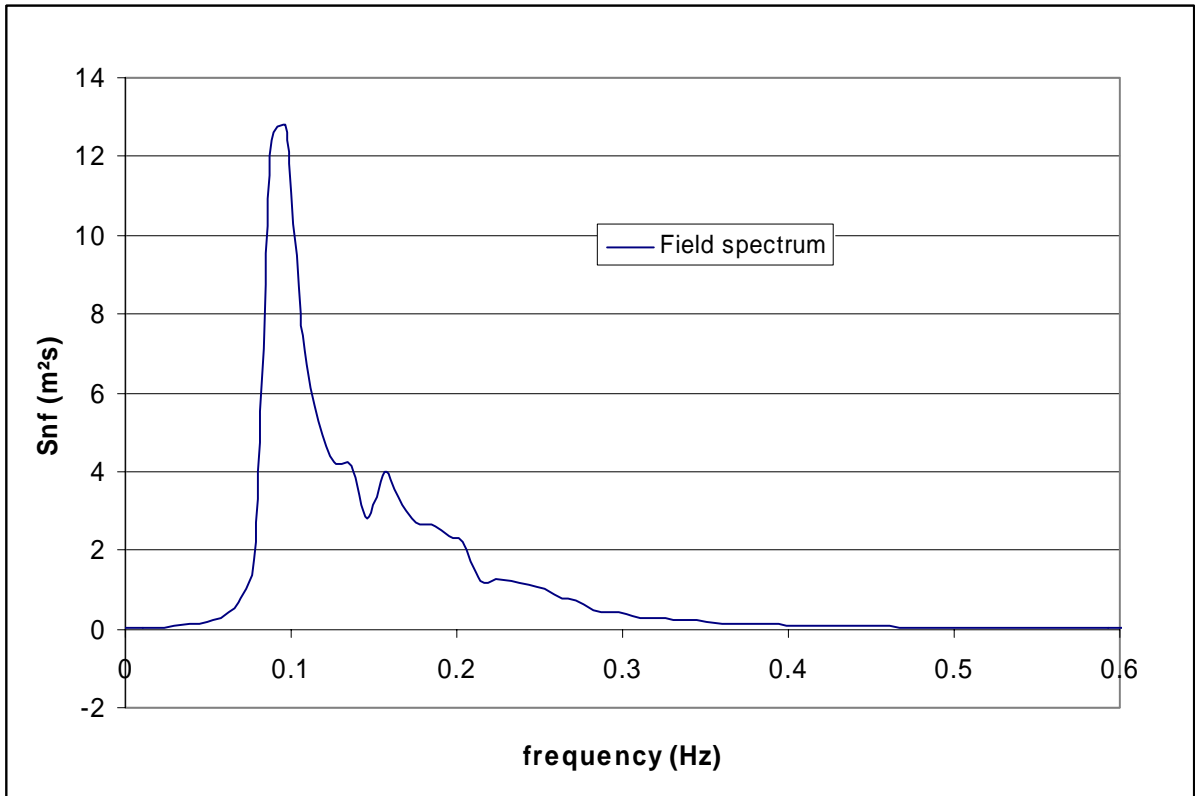
Fig. 45: *Field Spectrum for storm 3 of Nov. 8, 2001 (16.15 – 18.15)*
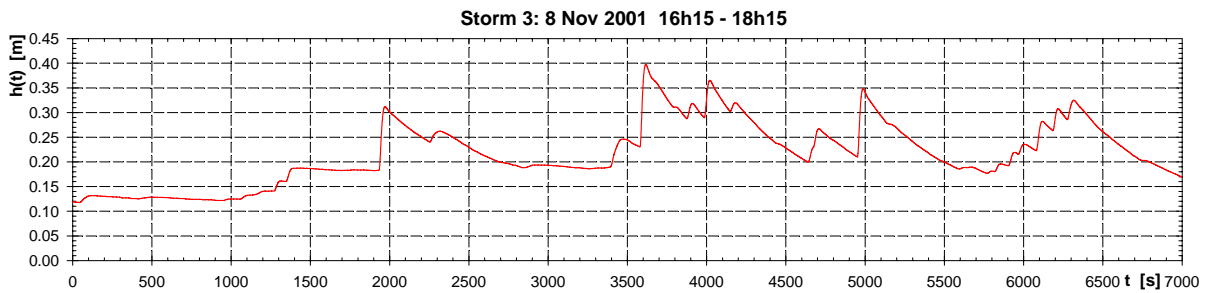
Fig. 46: *H(t) in the overtopping tank for storm 3 of Nov. 8, 2001 (16.15 – 18.15)*
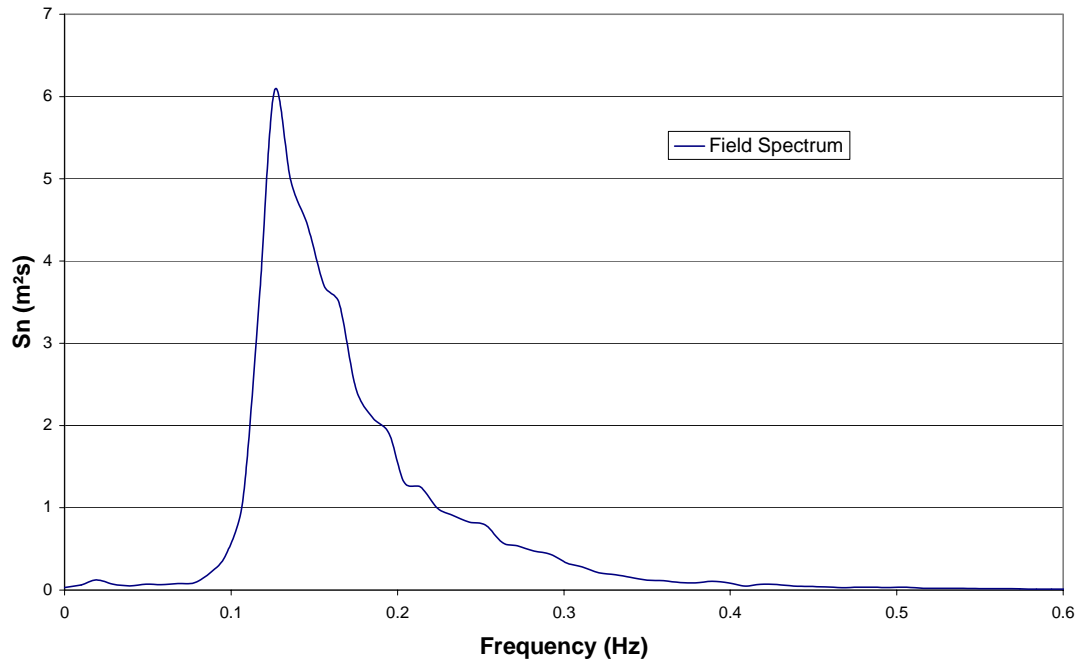
Fig. 47: *Field Spectrum for storm 4 of Feb. 26, 2002 (13.30 – 14.00)*
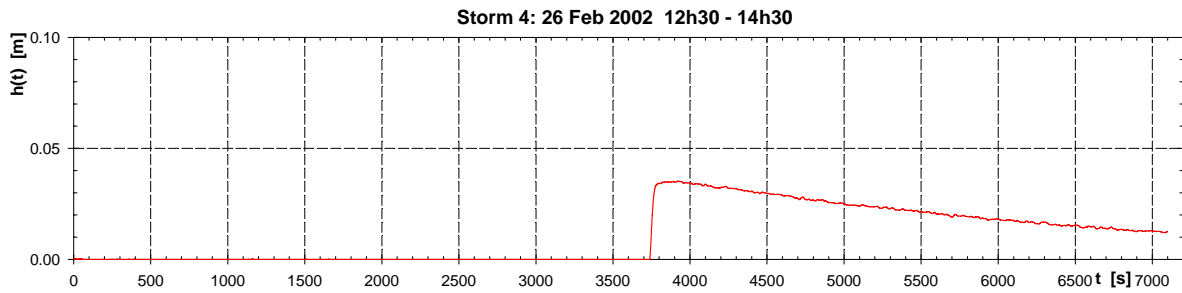
Fig. 48: *H(t) in the overtopping tank for storm 4 of Feb. 26, 2002 (12.30 – 14.30)*
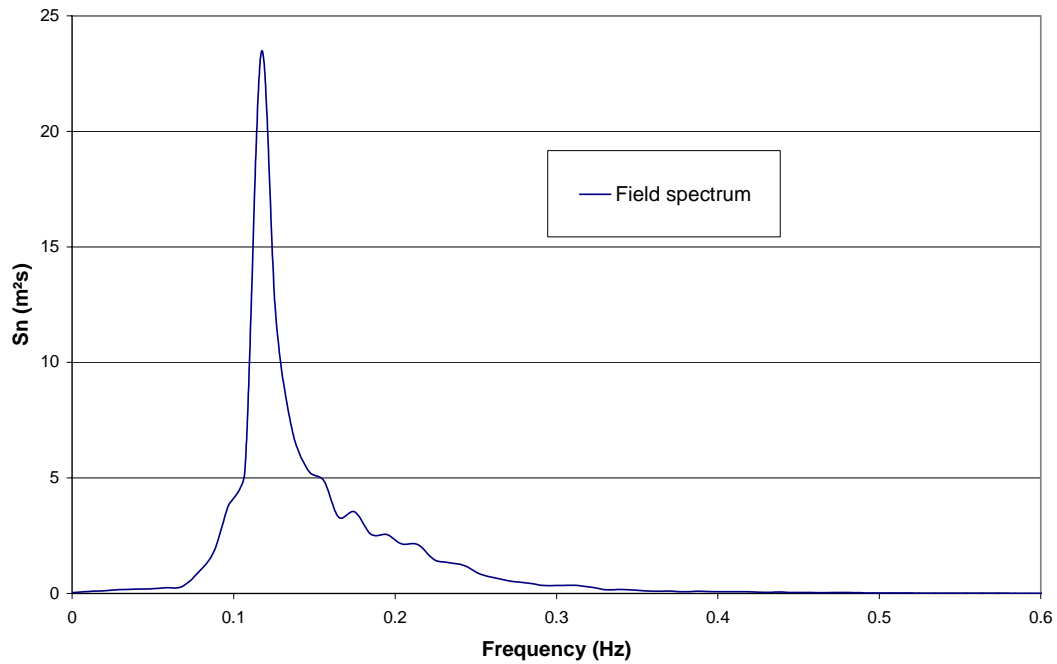
Fig. 49: *Field Spectrum for storm 5a of Oct. 27, 2002 (17.00 – 18.00)*
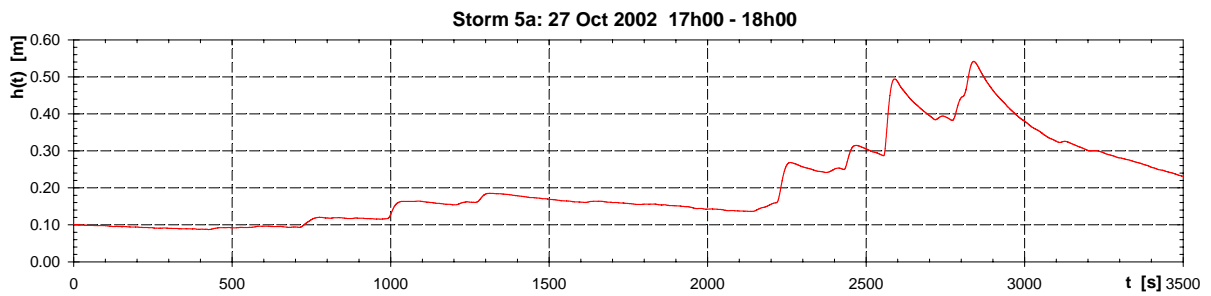
Fig. 50: *H(t) in the overtopping tank for storm 5a of Oct. 27, 2002 (17.00 – 18.00)*
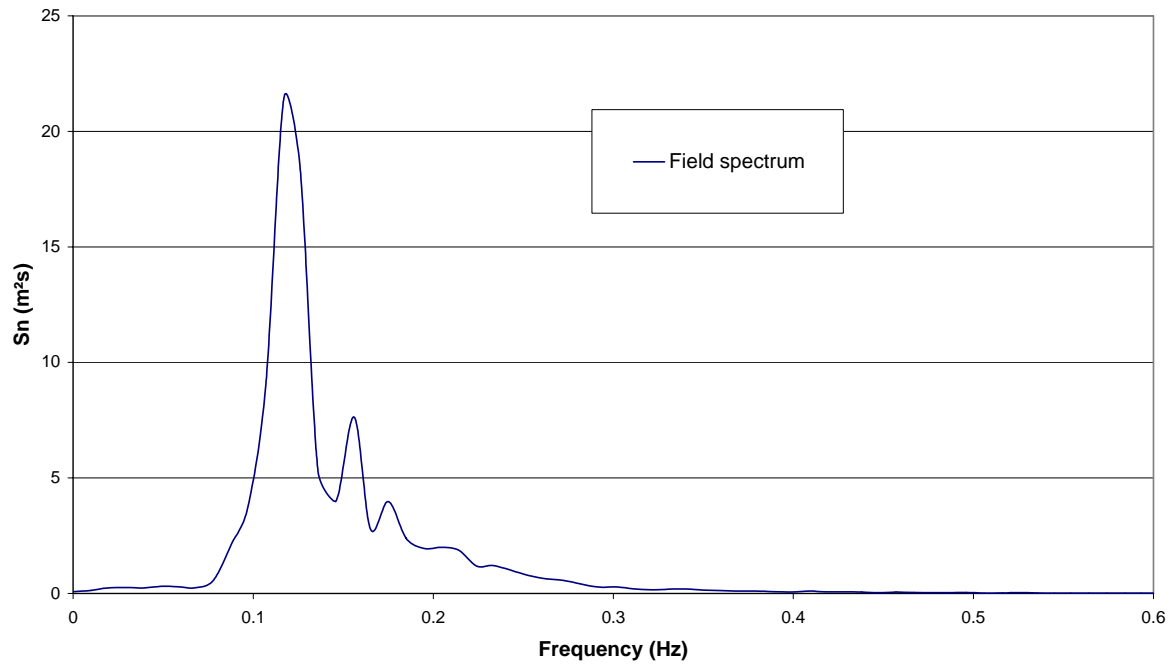
Fig. 51: *Field Spectrum for storm 5b of Oct. 26, 2002 (18.00 – 19.00)*
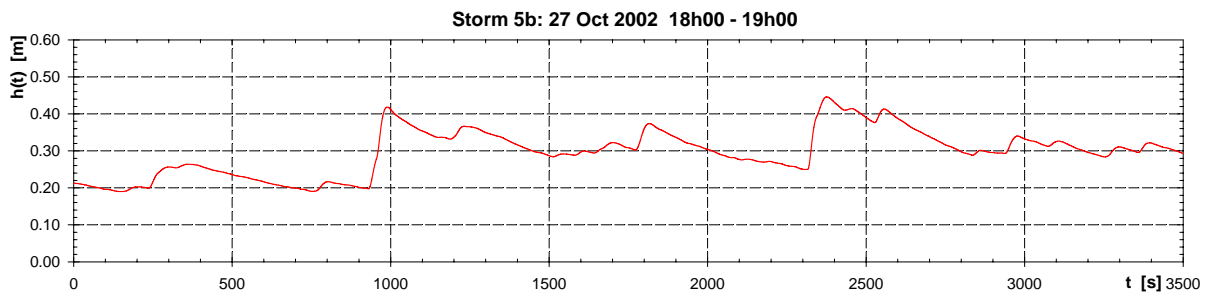
Fig. 52: *H(t) in the overtopping tank for storm 5b of Oct. 26, 2002 (18.00 – 19.00)*
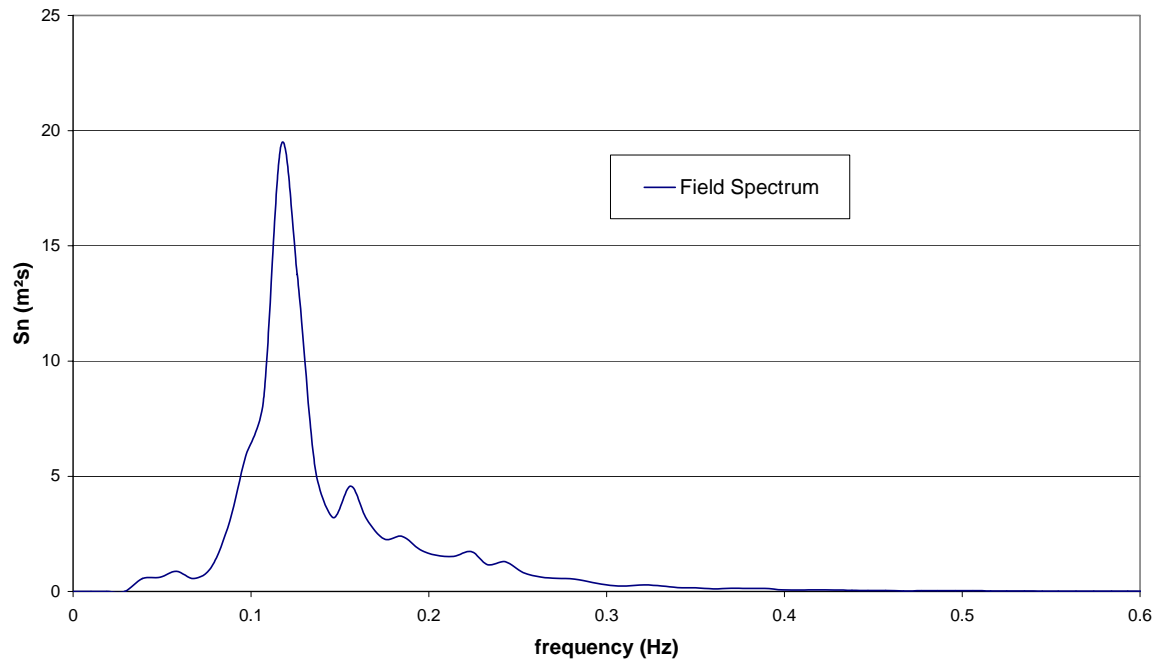
Fig. 53: *Field Spectrum for storm 5c of Oct. 27, 2002 (19.00 – 20.15)*
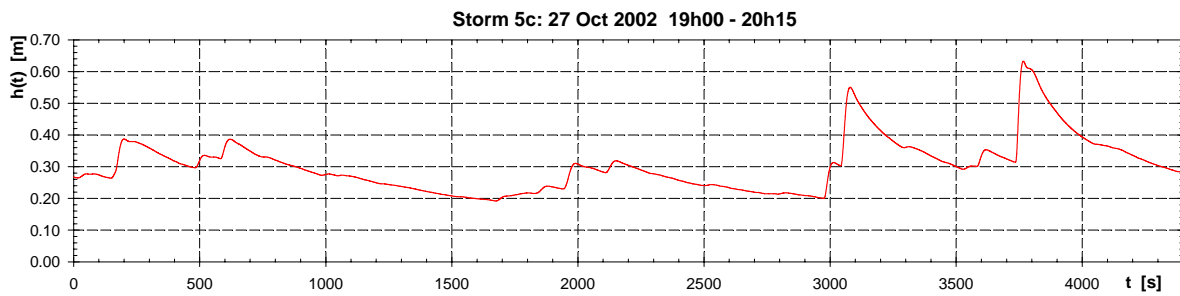
Fig. 54: *H(t) in the overtopping tank for storm 5c of Oct. 27, 2002 (19.00 – 20.15)*
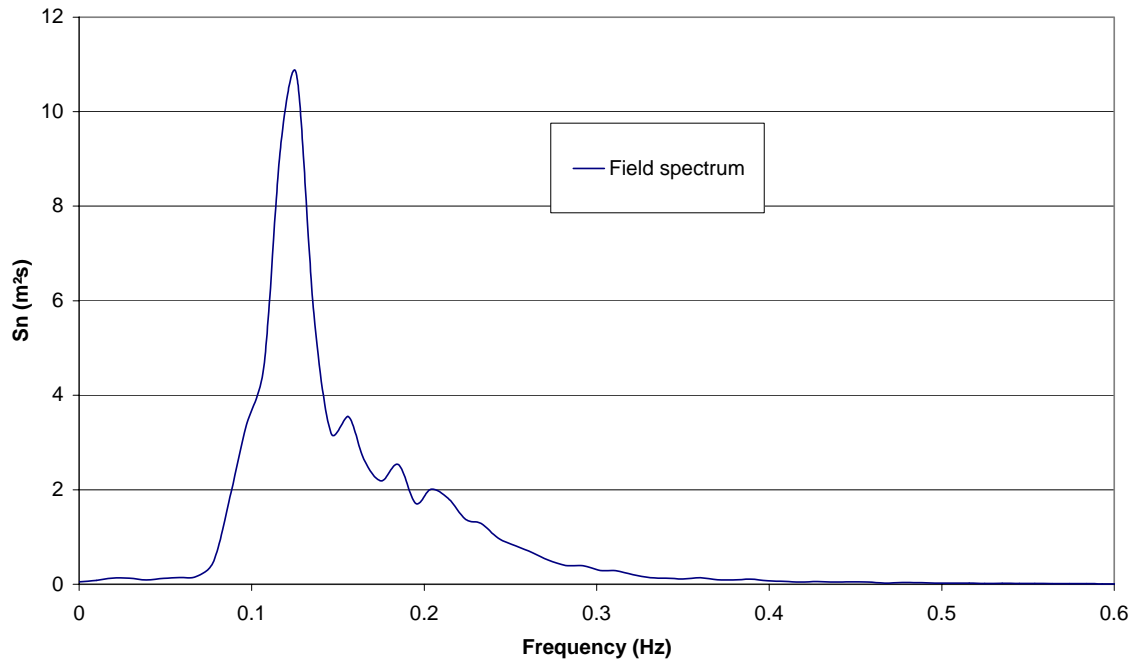
Fig. 55: *Field Spectrum for storm 6 of Jan. 29, 2003 (10.00 – 12.00)*
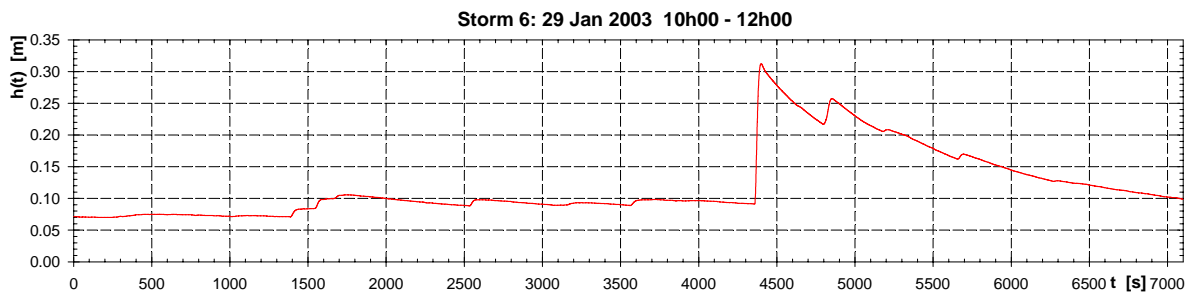
Fig. 56: *H(t) in the overtopping tank for storm 6 of Jan. 29, 2003 (10.00 – 12.00)*
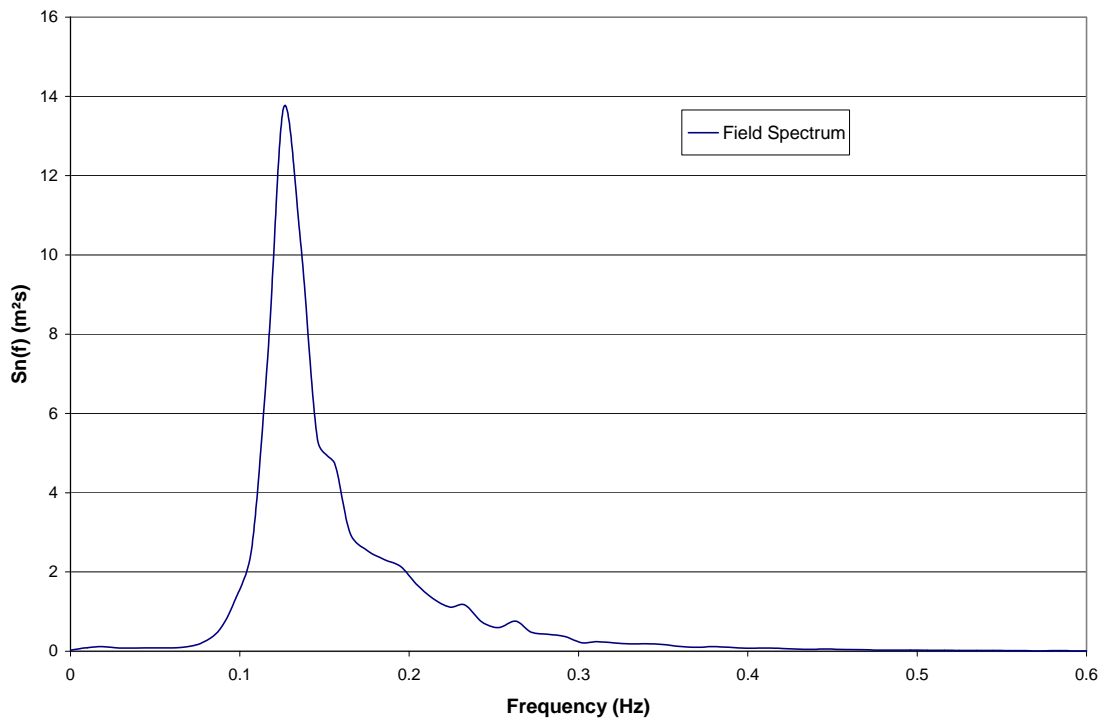
Fig. 57: *Field Spectrum for storm 7 of Oct 7, 2003 (12.00 – 14.00)*
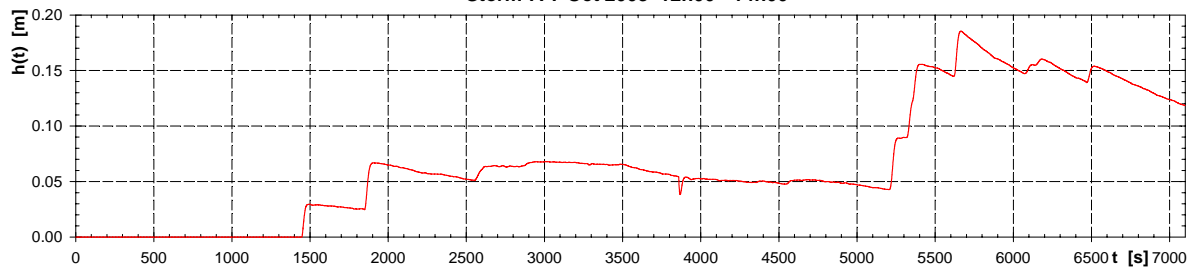
Fig. 58: *H(t) in the overtopping tank for storm 7 of Oct. 7, 2003 (12.00 – 14.00)*
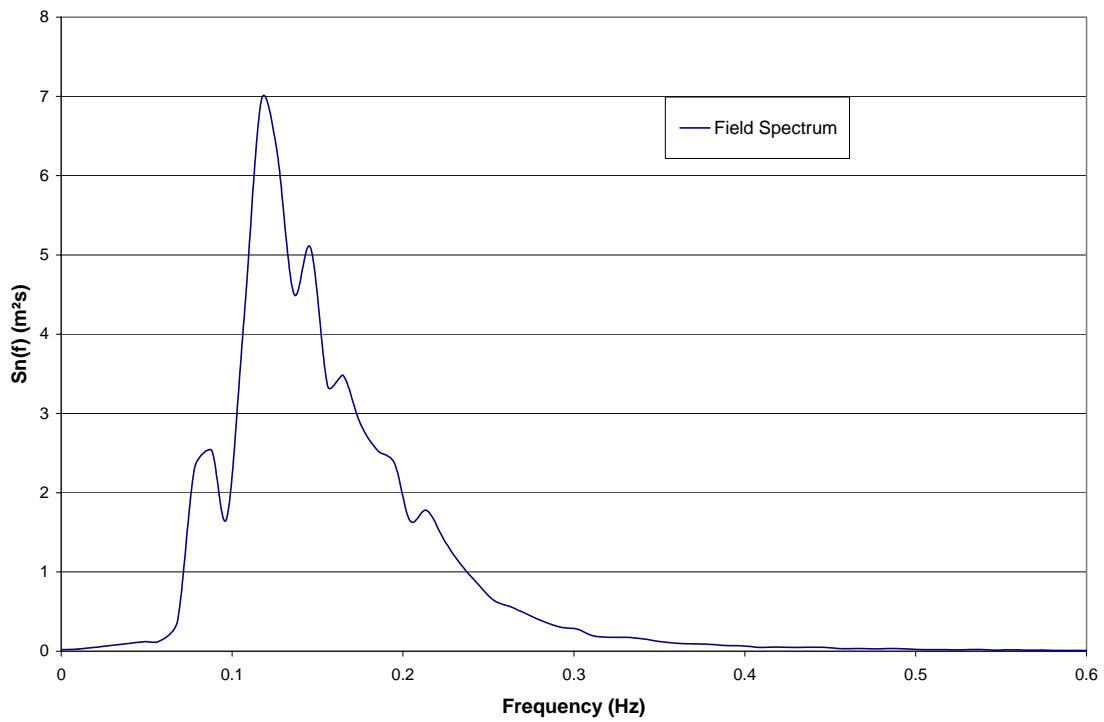
Fig. 59: *Field Spectrum for storm 8 of Dec. 22, 2003 (00.00 – 02.00)*
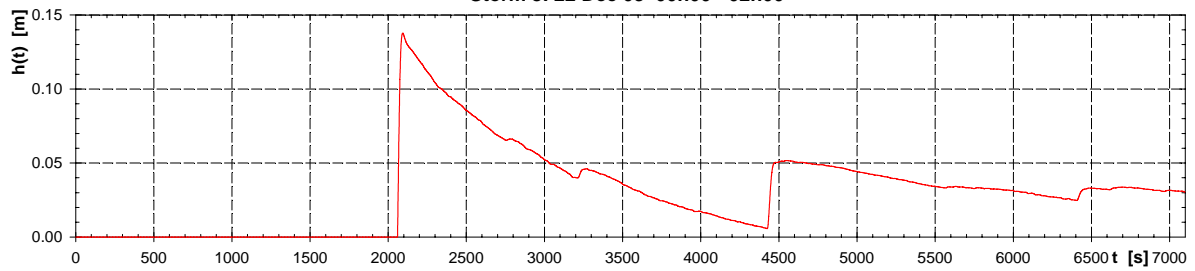
Fig. 60: *H(t) in the overtopping tank for storm 8 of Dec. 22, 2003 (00.00 – 02.00)*
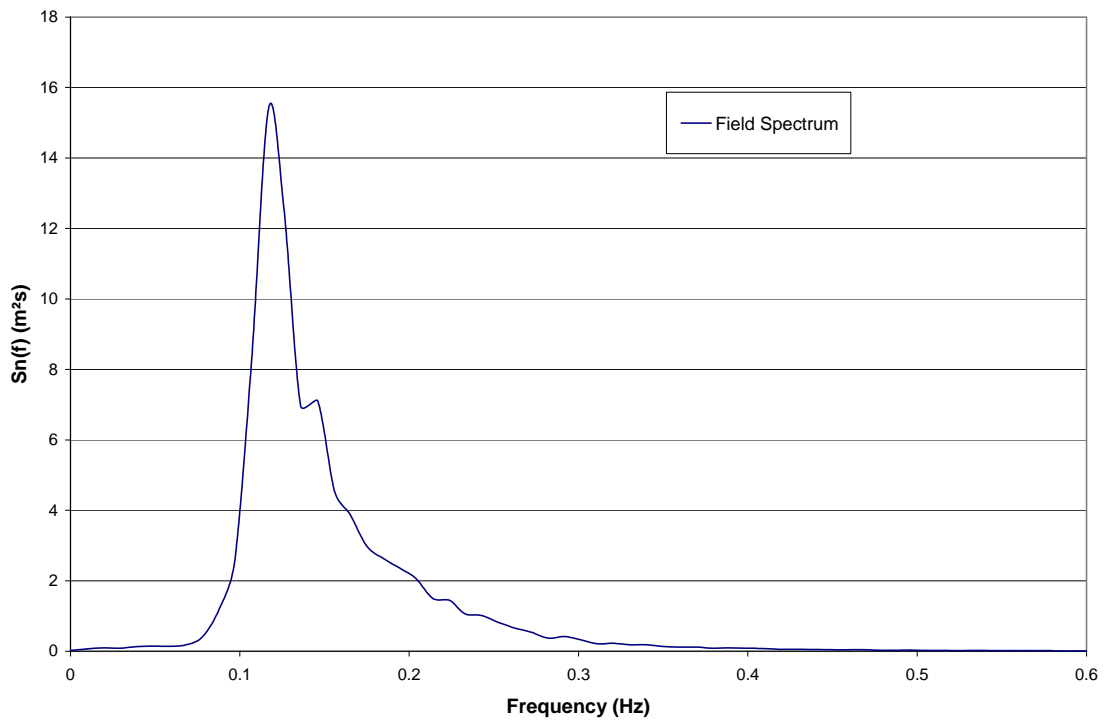
Fig. 61: *Field Spectrum for storm 9 of Feb. 8, 2004 (14.45 – 16.45)*
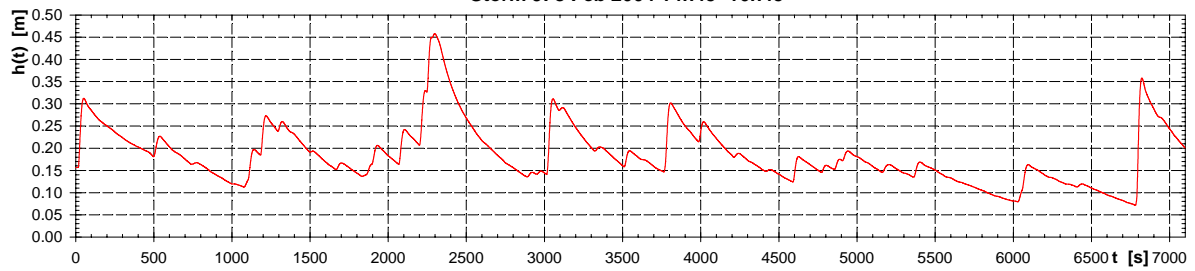
Fig. 62: *H(t) in the overtopping tank for storm 9 of Feb. 8, 2003 (14.45 – 16.45)*

4.2 DIRECTIONAL WAVEDATA

As mentioned above, from storm 6 on, data from the directional waverider buoy are available. The directional wave data is gathered from the buoy in separate files every 30 min. Consequently information is grouped in intervals of 30 min each time. Since for storms 6 to 8 every time 2 hour periods have been considered, for each of these storms 4 intervals of 30 min have to be considered. Fig. 63 gives the spectral density as a function of frequency and direction for 4 different 30 min intervals for storm 7 dd Oct. 7, 2003.

(a)   12h06 – 12h36   **(b)**   12h37 – 13h06

(c)   13h07 – 13h36   **(d)**   13h37 – 14h07
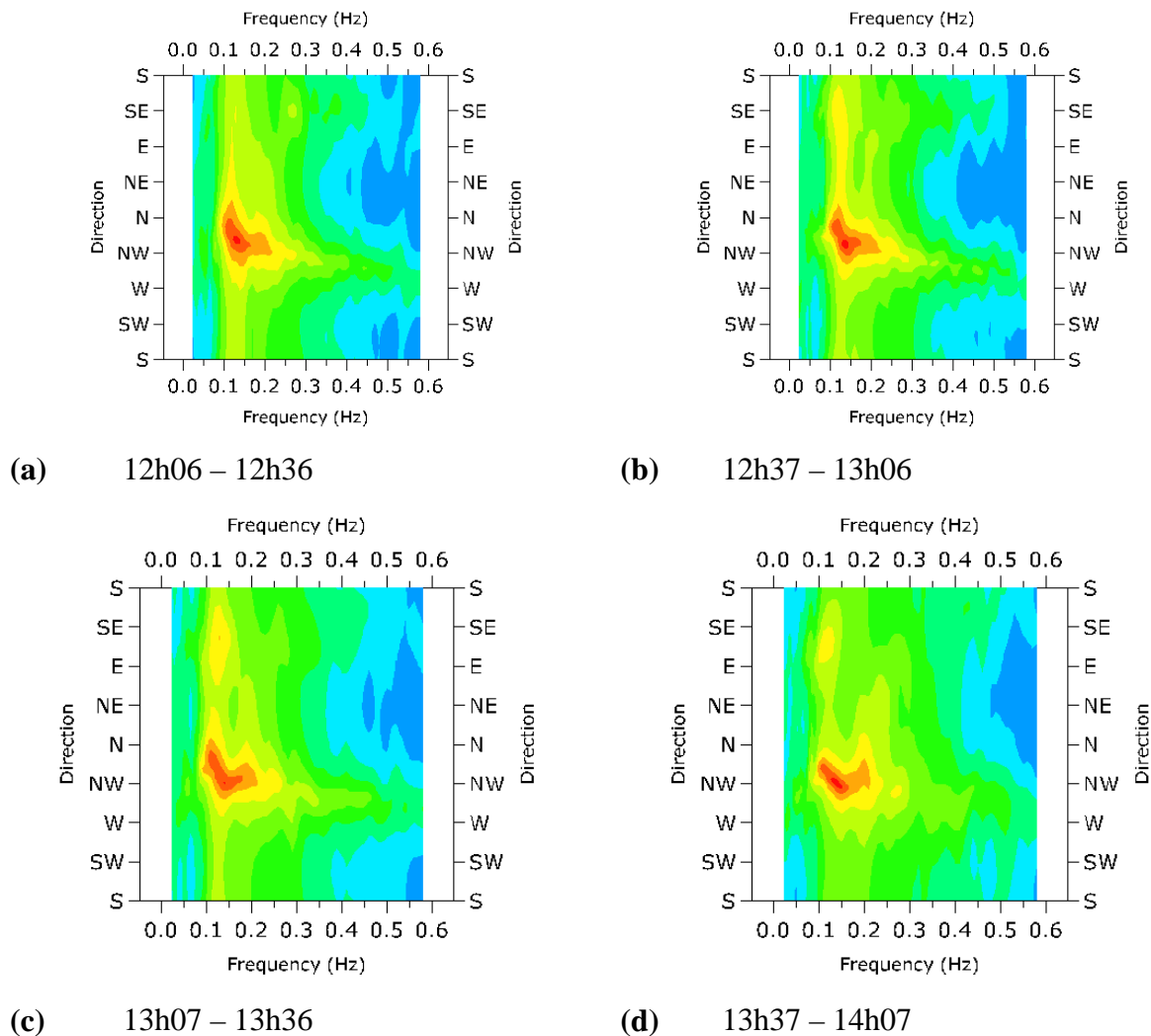
Fig. 63: *Spectral density as function of frequency and direction for storm 7 of Oct 7, 2003.*

From the 4 plots in Fig. 63 it is clear that the directionality of the waves is nearly constant during the complete 2 hour duration of the storm, namely NW to N but predominantly Northwest. Moreover the wave direction NW is more or less perpendicular to the instrumented part of the Zeebrugge breakwater.

(a)   00h01 – 00h30   **(b)**   00h31 – 01h00

(c)   01h01 – 01h30   **(d)**   01h31 – 02h01
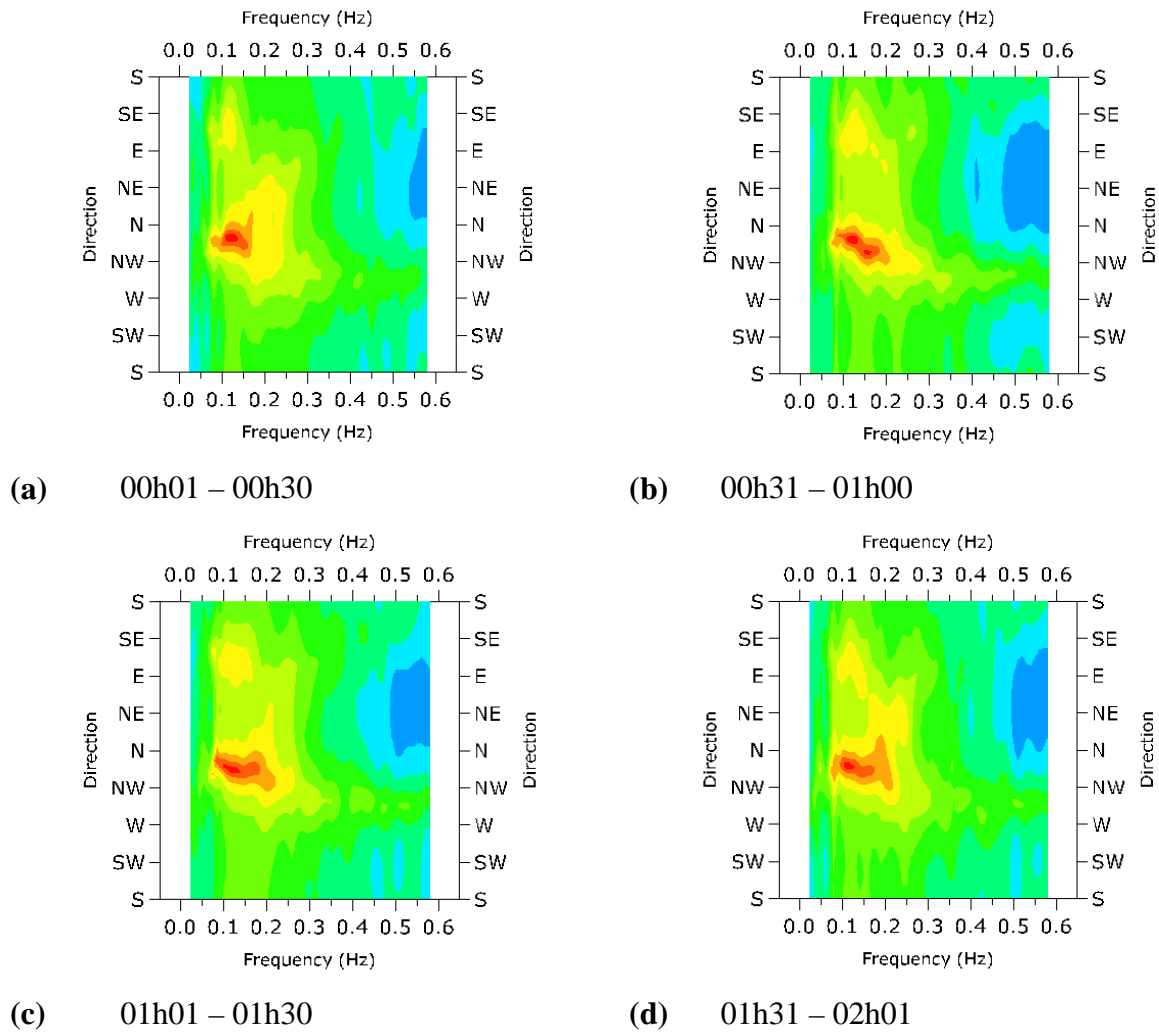
Fig. 64: *Spectral density as function of frequency and direction for storm 8 of Dec 8, 2003.*

From the 4 plots in Fig. 64 it is clear that the directionality of the waves is nearly constant during the complete 2 hour duration of the storm. The waves are mainly perpendicular to the breakwater.

(a)   14h26 – 14h55   **(b)**   14h56 – 15h25

(c)   15h26 – 15h55   **(d)**   15h56 – 16h25
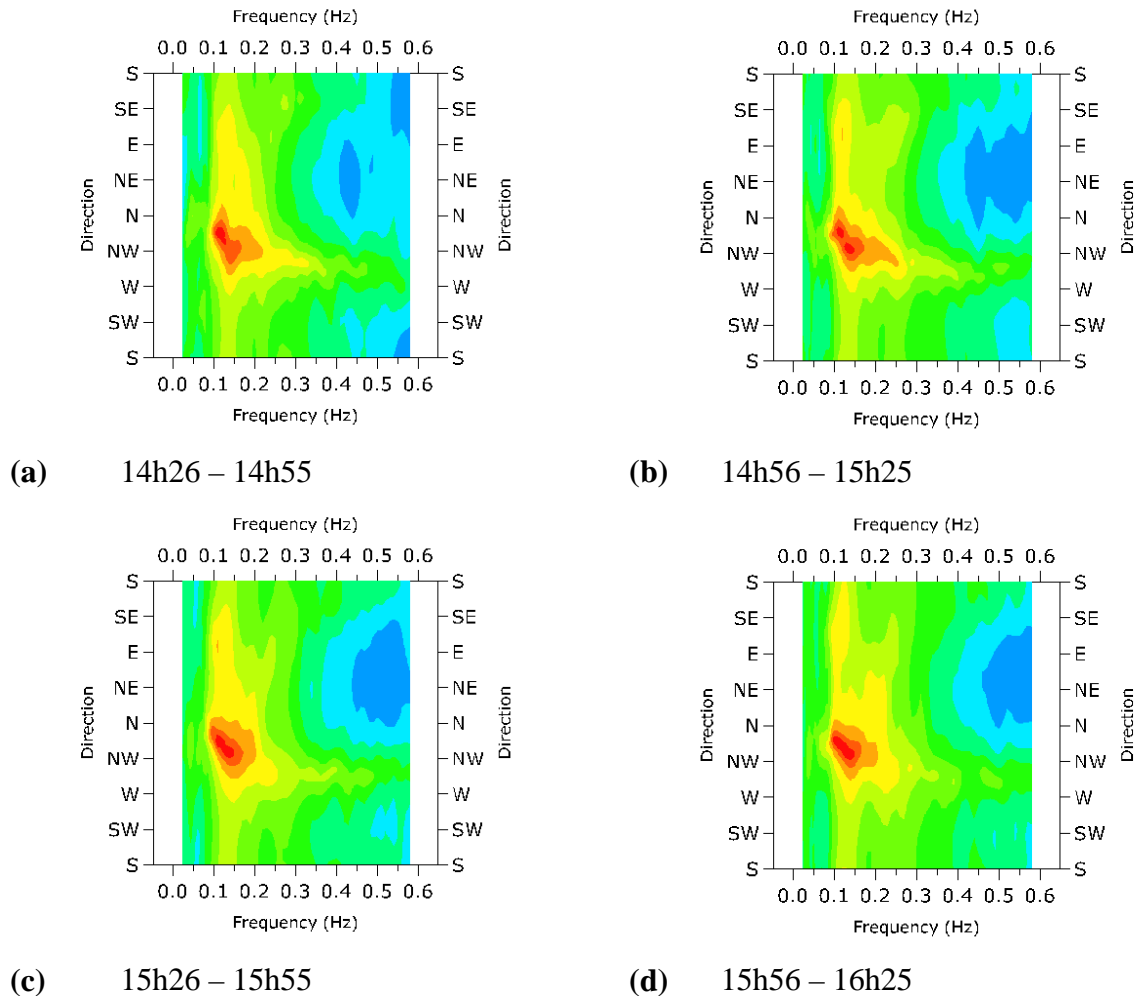
Fig. 65: *Spectral density as function of frequency and direction for storm 9 of Feb 8, 2004.*

The 4 plots in Fig. 65 also show a wave direction which is nearly constant during the whole 2 hour storm duration. Again, a wave attack more or less perpendicular to the breakwater is observed in these plots.

4.3 DISCUSSION

The obtained results as given in Table 3 are discussed in more detail.

In Fig. 66 the average overtopping rates from Table 3 are presented graphically. From both Table 3 and Fig. 66 a number of observations are made.
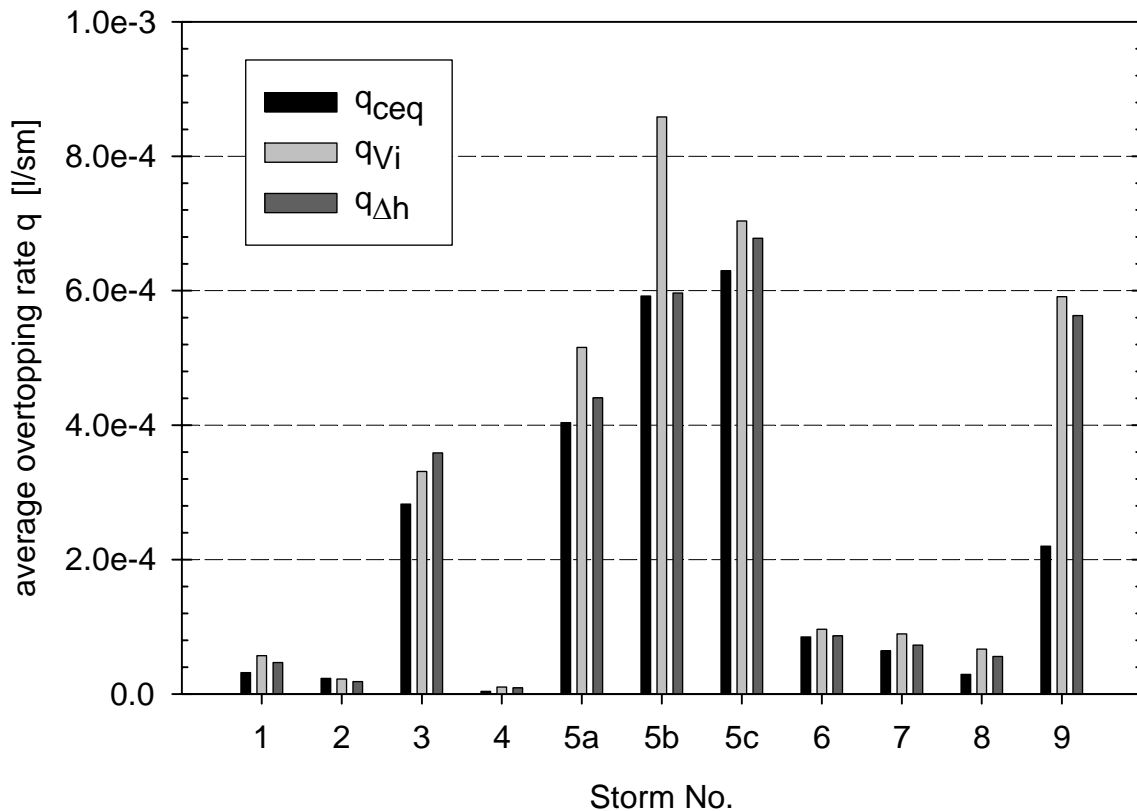
Fig. 66: *Graphical presentation of the average overtopping rates for three different calculation methods, based on table 2*

Storms 1, 2, 4, 6, 7 and 8 have q-values lower than 0.1 l/sm, showing that there has been very little wave overtopping during these storms. Storms 3, 5a, 5b, 5c and 9 have q-values ranging between 0.3 (for storm 3) and 0.9 l/sm (for storm 5b), indicating more severe wave overtopping. The storms with small overtopping rates have a smaller number of overtopping events N_{ov}, whereas the storms with larger overtopping rates have a larger N_{ov}.

In general, the average overtopping rate q_{ceq}, calculated using the first method based on the continuity equation, is smaller than the two other overtopping rates q_{Vi} and $q_{\Delta h}$ (except for storm 2). On average for the storms 1, 2, 4, 6, 7 and 8 with small overtopping rates the deviation between q_{ceq} and q_{Vi} is 33 %, and for storms 3 and 5 with large overtopping rates the deviation is 19 %, while this deviation is 34 % for storm 9 where this difference is comparable to the storms with smaller overtopping. The deviation between q_{ceq} and $q_{\Delta h}$ is 17 % and 9 % for the storms with small overtopping rates and large overtopping rates respectively. In general, q_{Vi} is larger than $q_{\Delta h}$ (except storm 3). The deviation between q_{Vi} and $q_{\Delta h}$ is 13 % and 10 % for the storms with small overtopping rates and large overtopping rates respectively. From these observations, the following relationship is obtained:

$$q_{ceq} < q_{\Delta h} < q_{Vi} \tag{12}$$

with

$$q_{ceq} \approx 0.69 q_{Vi} \tag{13.a}$$

and

$$q_{\Delta h} \approx 0.88 q_{Vi} \qquad (13.b)$$

Equations above give a kind of confidence interval for the measured overtopping ratios.

4.4 COMPARISON TO LITERATURE

The formulae presented by Owen (1980) and van der Meer et al. (1998) are well-known and widely used for breakwater crest level design. These formulae originally are based on extensive datasets from model tests with smooth impermeable sloping structures. By applying a reduction factor for the slope roughness, the formulae are applicable to rock slopes. These two formulae will be used here for comparison with the field data, and are presented hereafter.

4.4.1 LITERATURE FORMULAE

The wave overtopping formula presented in van der Meer et al. (1998) is:

$$\frac{q}{\sqrt{gH_{m0}^3}} = \frac{a_v}{\sqrt{\tan\alpha}} \gamma_b \xi_0 \exp\left(-b_v \frac{R_c}{H_{m0}} \frac{1}{\xi_{0,p}\gamma_b\gamma_f\gamma_\beta\gamma_v}\right) \qquad (14.a)$$

with a maximum of:

$$\frac{q}{\sqrt{gH_{m0}^3}} = 0.2\exp\left(-2.6\frac{R_c}{H_{m0}} \frac{1}{\gamma_f\gamma_\beta}\right) \qquad (14.b)$$

where R_c is the crest freeboard, defined as the vertical distance between SWL and crest level of the breakwater. The coefficients $a_v = 0.06$ and $b_v = 5.2$ are mean values based on the average of all test data. Reduction factors γ_b, γ_f, γ_β and γ_v include effects of a berm, surface roughness, oblique wave attack, and a vertical wall on top of the slope, respectively. The breaker parameter $\xi_{0,p}$ used by van der Meer et al. (1998) is calculated using the peak wave period T_p:

$$\xi_{0,p} = \frac{\tan\alpha}{\sqrt{\dfrac{2\pi H_{m0}}{gT_p^2}}} \qquad (15)$$

$$\xi_{m-1,0} = \frac{\tan\alpha}{\sqrt{\dfrac{2\pi H_{m0}}{gT_{m-1,0}^2}}} \qquad (16)$$

The Dutch guideline on wave run-up and overtopping on dikes (TAW, 2002) suggests to replace T_p by $T_{m-1,0}$ (in eq. 15, resulting in eq. 16) at the toe of the structure to account for

the effects of double-peaked wave spectra related to wave transformation and breaking in shallow foreshores (based on results presented by Van Gent, 2001). In this case, the values for the coefficients in eq. (14.a) are replaced by $a_v = 0.067$ and $b_v = 4.75$.

The wave overtopping formula by Owen (1980) reads:

$$\frac{q}{gH_s T_m} = a_o \exp\left(-b_o \frac{R_c}{T_m \sqrt{gH_s}} \frac{1}{\gamma_r}\right) \qquad (17)$$

with validity range $0.05 < \dfrac{R_c}{T_m \sqrt{gH_s}} < 0.30$, where a_o and b_o are dimensionless empirically derived coefficients, whose values depend on the breakwater slope, and γ_r is a surface roughness reduction factor.

Both overtopping formulae (eq. 14 and eq. 17) have been derived originally for smooth impermeable slopes. A surface roughness coefficient has been introduced effectively into the formulae to take into account the effect of increased slope roughness on the overtopping. Nowadays it is common use to apply both formulae to predict overtopping at permeable rubble mound slopes. In this case the surface roughness reduction coefficient takes into account the combined effect of slope roughness and permeability.

4.4.2 CREST FREEBOARD FOR ZEEBRUGGE BREAKWATER

Both empirical formulae, eq. (14) and eq. (17), include the crest freeboard parameter R_c, defined as the vertical distance between SWL and crest level. For the actual Zeebrugge breakwater case the crest level of the breakwater is not straightforward, and has to be defined here. Fig. 67 shows the geometry of the breakwater crest at the location of the overtopping tank. The photo is taken from the land ward side before the overtopping tank has been constructed. The actual crest level is located between Z + 10.20 m (top of crest wall on service road), assumed as minimum crest level; and Z + 12.40 m (theoretical design crest level for upper layer of armour units), assumed as theoretical maximum crest level.
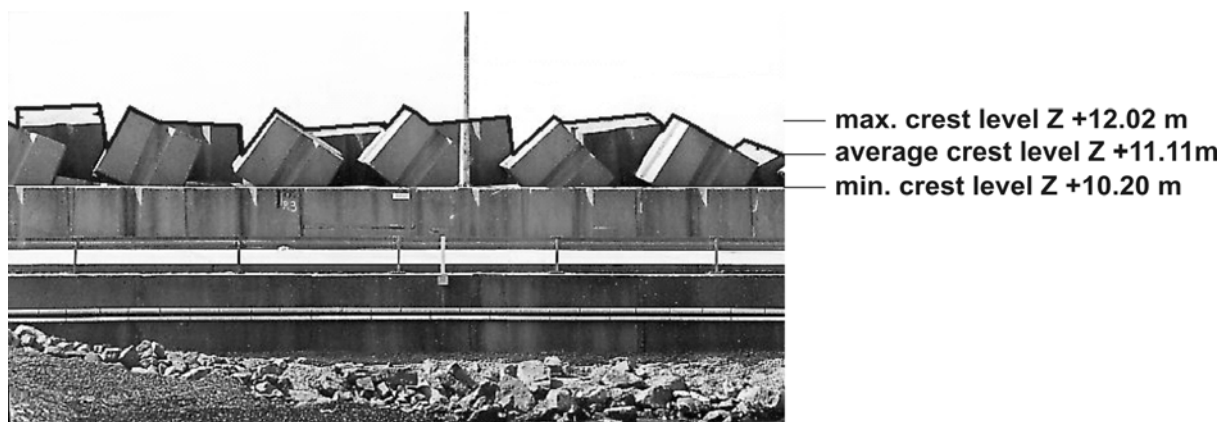
Fig. 67: *Definition figure of three different crest levels taken into account.*

The theoretical maximum crest level is not realistic and a more practical maximum crest level is proposed. The maximum crest level used in the wave overtopping prediction formulae is Z + 12.02 m, determined by calculating the average value of the crest level of all points from the bold line in Fig. 67, representing the local level of the armour unit faces in front of the overtopping tank.

Since the armour units of the crest do not have an idealized wall profile with the same wall height along the crest, the actual crest level experienced by the waves is somewhere in between the minimum level Z + 10.20 m and maximum level Z + 12.02 m. For the calculations, the average level between minimum and maximum level is taken as the best representation of the actual crest level for wave overtopping: Z + 11.11 m. The crest freeboard is denoted R_{c1} for the maximum crest level Z + 12.02 m, R_{c2} for the minimum crest level Z + 10.20 m, and R_{c3} for the actual average crest level Z + 11.11 m. The crest freeboard R_{c3} is considered to be the most accurate estimation among these three with upper limit R_{c1} and lower limit R_{c2}.

4.4.3 VAN DER MEER ET AL. (1998) FORMULA

For the application of eq. (14) to the Zeebrugge breakwater, the reduction factors γ_b, γ_β and γ_v are set to unity. There is no berm present ($\gamma_b = 1$), for the reported storms in Table 3 perpendicular wave attack is assumed ($\gamma_\beta = 1$), and there is no vertical wall on the breakwater slope ($\gamma_v = 1$). The reduction factor for surface roughness, γ_f, for the case of the Zeebrugge breakwater with an armour layer with grooved cubes, is determined using the following methodology, for lack of more appropriate values for γ_f for this armour layer. For rock slopes with a double layer of rock, van der Meer & Stam (1992) suggest to calculate γ_f as the ratio of the wave run-up level exceeded by two percent of the incoming waves $R_{u2\%}$ on a rough slope to $R_{u2\%}$ on a smooth slope for the same ξ_0. The general prediction formula used for the calculation of the run-up level exceeded by two percent of the incident waves $R_{u2\%}$ is (TAW, 2002):

$$\frac{R_{u2\%}}{H_{m0}} = 1.75 \gamma_b \gamma_f \gamma_\beta \xi_{m-1,0} \qquad (18.a)$$

with a maximum of:

$$\frac{R_{u2\%}}{H_{m0}} = \gamma_f \gamma_\beta \left(4.3 - \frac{1.6}{\sqrt{\xi_{m-1,0}}} \right) \qquad (18.b)$$

Eq. (18) is valid for the range $0.5 < \gamma_b \xi_{m-1,0} < 8$ to 10. In case of the Zeebrugge breakwater, again $\gamma_b = 1$, and $\gamma_\beta = 1$. The average breaker parameter $\xi_{m-1,0}$ for the field data, calculated from the values for all storms in Table 3, is $\xi_{m-1,0} = 3.67$. For this value, the maximum (eq.

(18.b)) is applicable, resulting in $\dfrac{R_{u2\%}}{H_{m0}} = 3.46$ for a smooth slope with $\gamma_f = 1$. Using the average value for $\xi_{m-1,0}$ is justified since $\xi_{m-1,0}$ varies only in a very small range for the field storms ($3.46 < \xi_{m-1,0} < 4.03$). The dimensionless two percent run-up level for the Zeebrugge breakwater with a rough slope has been determined based on extensive full scale measurements of wave run-up, resulting in $\dfrac{R_{u2\%}}{H_{m0}} = 1.76$ for $\xi_m = 3.59$ (Van de Walle et al., 2002). The reduction factor γ_f is calculated using the wave run-up level ratio: $\gamma_f = 1.76/3.46 = 0.51$.

This calculated value is compared with other suggested values from literature. De Waal and van der Meer (1992) suggest to use γ_f in the range 0.55 – 0.60 for two or more layers of rock. Owen suggests to use γ_f in the range 0.5 – 0.6 for two or more layers of rubble. Updated values provided in CEM (2003) estimate γ_f in the range 0.50 – 0.55 for two or more layers of rock. Good agreement is obtained between the calculated reduction factor $\gamma_f = 0.51$ and the reduction factors indicated in literature. Consequently, $\gamma_f = 0.51$ is used for the determination of the predicted average overtopping rates.

4.4.4 OWEN (1980) FORMULA

The application of the Owen formula, eq. (17), to the Zeebrugge breakwater requires the determination of the coefficients a_o and b_o for the slope $\tan \alpha = 1/1.4$. Interpolation between values given by Besley (1999) yields $a_o = 0.00866$ and $b_o = 19.96$. Owen suggests to use a value in the range 0.50 – 0.55 for the surface roughness reduction factor γ_r for the case of rough rock slopes. The range is very similar to the range proposed by De Waal and van der Meer (1992), and therefore the same value for the reduction factor $\gamma_r = 0.51$ for use in the Owen formula is maintained.

4.4.5 CORRECTION FOR PERMEABLE CREST BERM: BESLEY (1999) FORMULA

To take account of a permeable crest, Besley (1999) suggests to multiply the predicted overtopping rate from the Owen (1980) formula, eq. (17), with a reduction factor:

$$C_r = 3.06 \exp\left(-1.5 \frac{C_w}{H_s}\right) \tag{19}$$

valid for $\dfrac{C_w}{H_s} > 0.75$, or $C_r = 1.0$ for $\dfrac{C_w}{H_s} < 0.75$, where C_w is the crest berm width. For the Zeebrugge breakwater, the permeable crest berm width is located in front of the access road, and is estimated around $C_w = 5.0$ m.

4.4.6 COMPARISON AND DISCUSSION

A comparison between predicted average overtopping rates by Owen (1980) or Besley (1999) and van der Meer et al. (1998) formulae for all storms is given for the three crest freeboard values R_{c1}, R_{c2} and R_{c3} in Fig. 68(a), 68 (b) and 68(c) respectively, on a linear scale. For the Zeebrugge field data, Owen (1980) consistently predicts higher average overtopping rates than van der Meer et al. (1998). Application of the reduction factor C_r due to the presence of a permeable crest berm reduces the over prediction significantly and much better agreement is observed between Besley and van der Meer et al. (1998), especially for the actual average crest level (denoted R_{c3}) and for the minimum crest level (R_{c2}) with best agreement.

comparison prediction formulae [R_{c1}]

a)

comparison prediction formulae [R_{c2}]

b)

comparison prediction formulae [R_{c3}]

c)
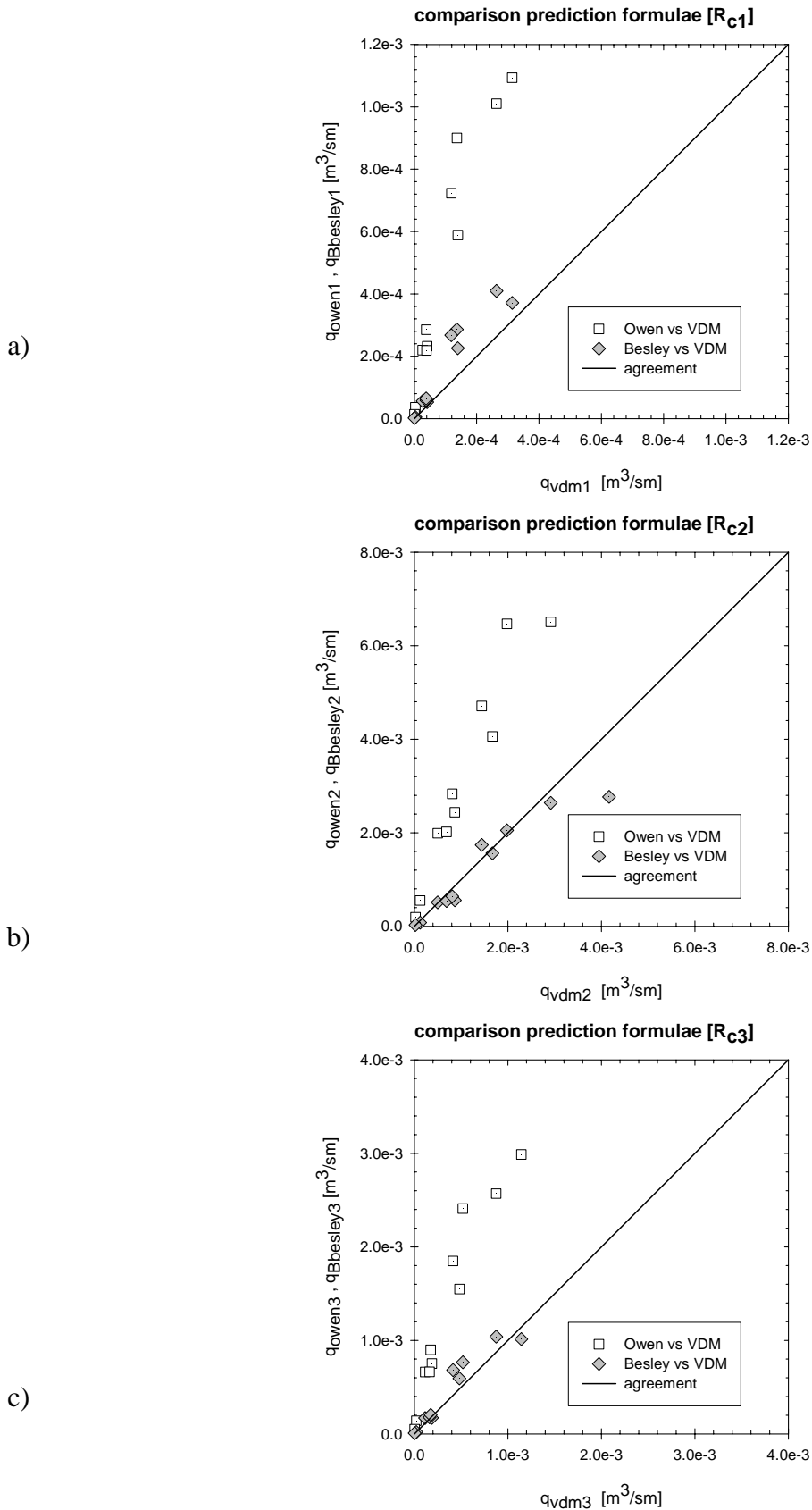
Fig. 68: *Comparison between predicted average overtopping rates by Owen (1980),* q_{owen}, *or Besley (1999),* q_{besley}, *and van der Meer et al. (1998),* q_{vdm}, *for the Zeebrugge field data, for crest freeboards* R_{c1} *(a),* R_{c2} *(b) and* R_{c3} *(c).*

The measured average overtopping rates have been compared to the predicted average overtopping rates from van der Meer et al., Owen and Besley, in Fig. 69, for the three crest levels and associated crest freeboards. The range of the measured q -values obtained using the three methods is indicated in Fig. 69 using a vertical bar. Linear scales have been used in the graphs.
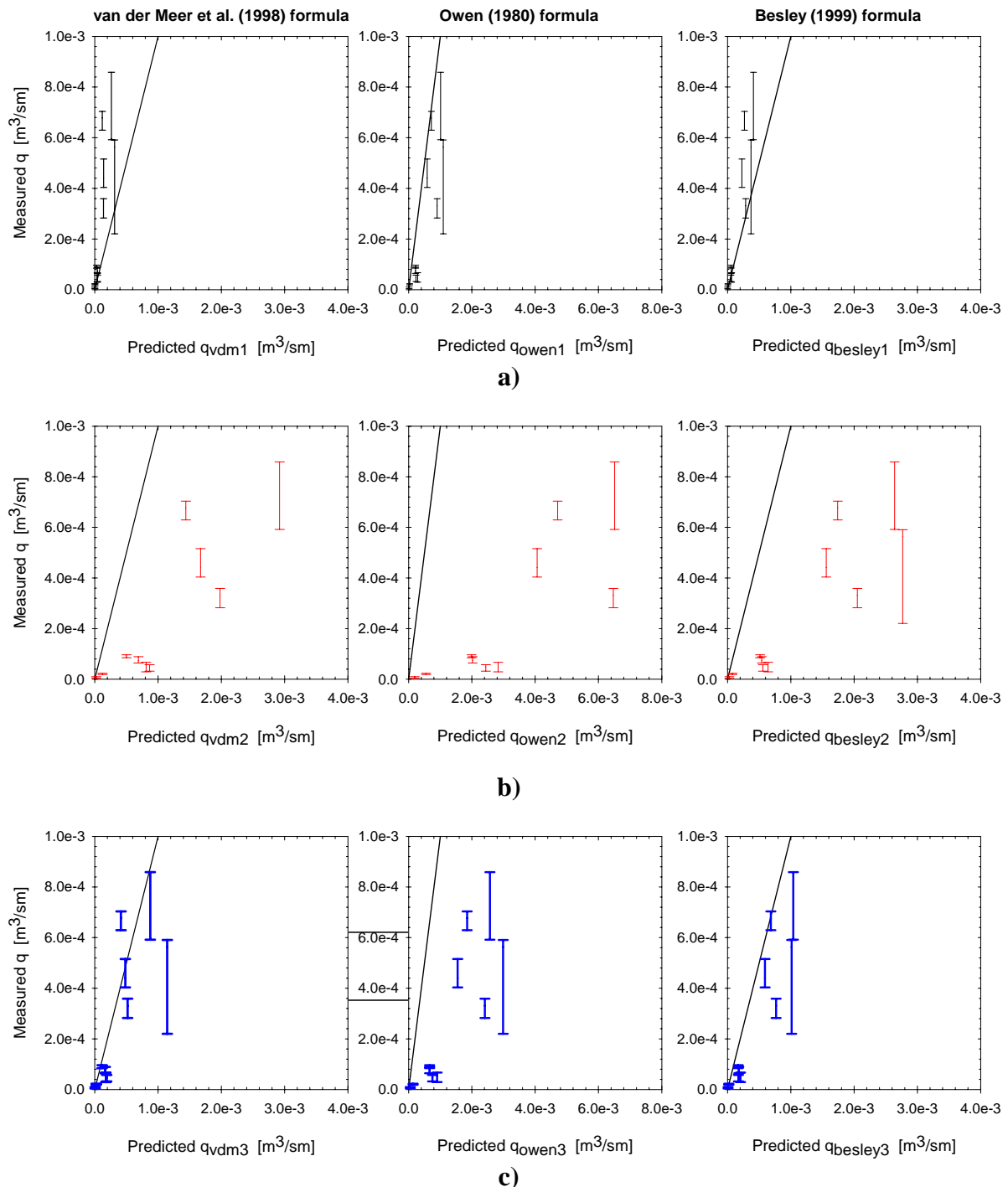
Fig. 69: *Comparison between measured and predicted average overtopping rates, using van der Meer et al. (1998, left column), Owen (1980, middle column) and Besley (1999, right column) prediction formulae; for crest freeboards* R_{c1} *(a),* R_{c2} *(b) and* R_{c3} *(c).*

For the maximum crest level at $Z + 12.02$ m (using R_{c1}, cf. Fig. 69(a)), the van der Meer et al. prediction underestimates the measured average overtopping rates by a factor up to about 6 (e.g. storm 5c), especially for higher q-values. Owen's prediction however slightly overestimates the measured overtopping rates, and the reduction of Besley shows good agreement for smaller q-values and underestimates larger q-values.

Using the minimum crest level at $Z + 10.20$ m (using R_{c2}, cf. Fig. 69(b)), the predicted average overtopping rates from all formulae considerably overestimate the measured q-values. The van der Meer et al. and Besley predictions have the same magnitude, and the Owen prediction is about three times as large for the large overtopping rates. Finally, using the actual average crest level at $Z + 11.11$ m (using R_{c3}, cf. Fig. 69(c)), the predicted q-values by van der Meer et al. and Besley are in relatively good agreement with the measured q-values, and the Owen prediction overestimates the measured average overtopping rates by a factor up to about 7 (for storm 3). In general best agreement between measured and predicted overtopping rates is observed using van der Meer et al.'s and Besley's prediction formulae for the actual average crest level $Z + 11.11$ m and R_{c3}. Moreover Besley's prediction using R_{c3} is always on the safe (conservative) side.

A more traditional presentation of the prediction formulae is given in Fig. 70, where a dimensionless overtopping discharge (using a logarithmic scale) is plotted versus a dimensionless crest freeboard. The thick solid line is the prediction formula itself, the thin solid lines are the 95 % confidence intervals of the formula (based on variation coefficients provided by the author of the formula). The measured field data have been plotted in the same graph using vertical bars to indicate the scatter from using the three calculation methods. Fig. 70(a) and 70(b) show the resulting graphs for van der Meer et al. and Besley, respectively, for R_{c3} ($Z + 11.11$ m).

The measured overtopping rates are within the 95 % confidence intervals of both prediction formulae (except one storm, for Besley's prediction, in Fig. 70(b)), and therefore good agreement is found between measured and predicted values. Also indicated in Fig. 70 are the prediction formulae using the recommended values for the surface roughness reduction factor $\gamma_f = 0.50$ and $\gamma_f = 0.55$ (applicable for designing a structure). For the case of the Zeebrugge breakwater, the value $\gamma_f = 0.50$ shows best agreement with the measured overtopping rates.
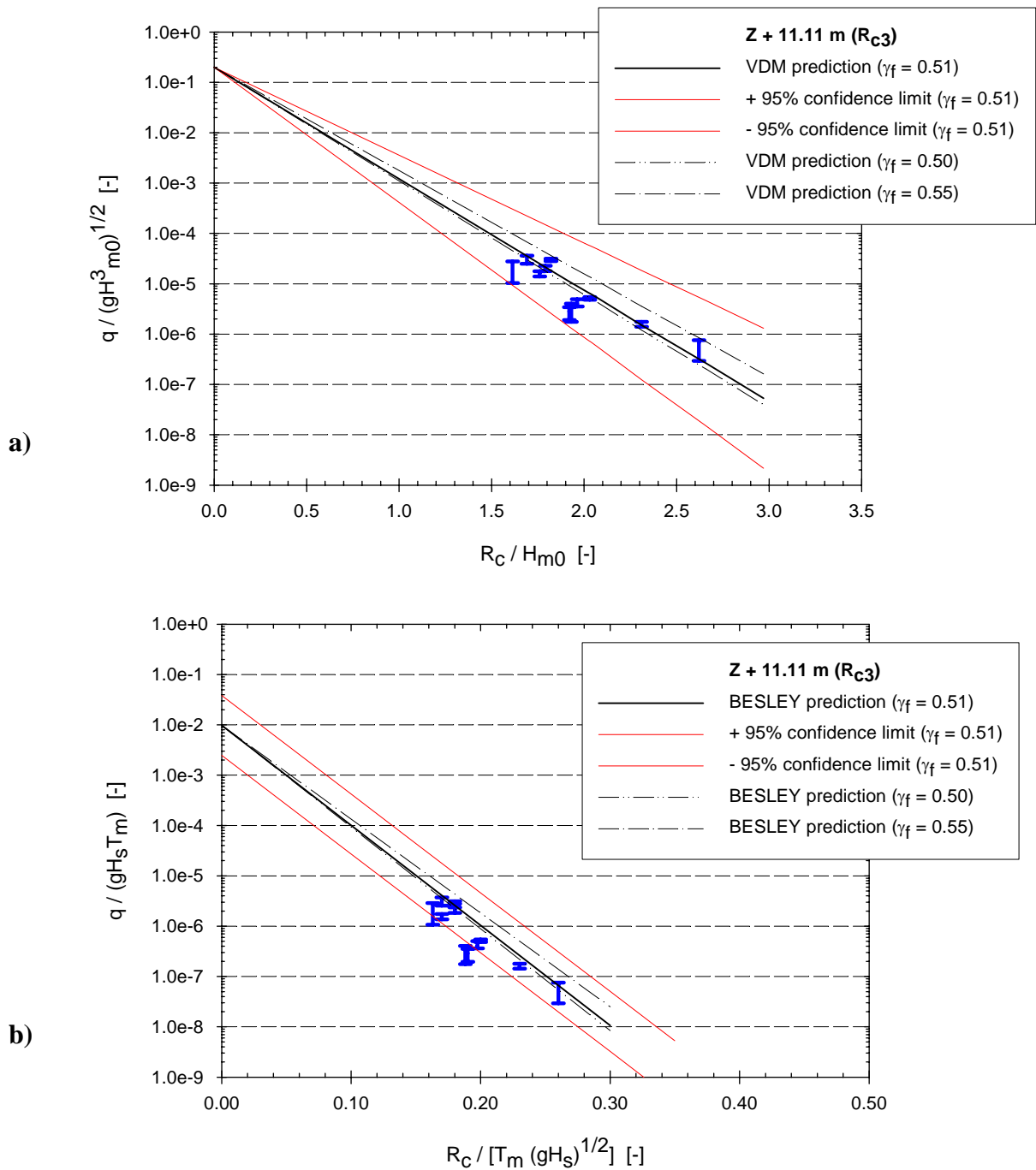
Fig. 70: *Measured and predicted (top (a): van der Meer et al., 1998; bottom (b): Besley (1999)) non-dimensional average overtopping rates and 95 % confidence limits as a function of the non-dimensional crest freeboard for the crest freeboard R_{c3}, using surface roughness reduction factor $\gamma_f = 0.51$. Also indicated are predicted overtopping rates for $\gamma_f = 0.50$ and $\gamma_f = 0.55$.*

5   RESULTS FROM HAZARD MEASUREMENTS

Wave impacts have been measured at the Zeebrugge breakwater since January 16th, 2003. From that moment on 3 storms have occurred: Oct. 7th, 2003, Dec. 22th, 2003 and Febr. 8th, 2004. The wave characteristics are given in Table 5.

Table 5:   *Wave characteristics on Oct. 7th, 2003, Dec. 22th, 2003 and Febr. 8th, 2004.*

Storm No.	Date	Time	MWL (Z+ …m)	H_{m0} (m)	T_p (s)
7	Oct. 7th, 2003	12.00 - 14.00	4.77	3.23	7.91
8	Dec. 22th, 2003	00.00 – 02.00	5.26	3.03	8.57
9	Febr. 8th, 2004	14.45 – 16.45	5.32	3.59	8.57

5.1 FIELD MEASUREMENTS OF HAZARDS

5.1.1 SMALL 'CHILD' DUMMY (D1)

The smallest dummy, placed at the landward side of the access road, is foreseen with 3 load cells (LC1, LC2 and LC3 as given in Fig. 71).

The maximum impact measured on the dummy during the storms 7 and 8 is 50 N. On Febr. 8th, 2004 (storm 9) no impacts are calculated as one of the loads cells was broken.

Fig. 72 gives an overview of the measurements on Dec. 22th, 2003, for a duration of 15 min. All measured loads are near the offset value of the devices: resp. loads of ca. 190 N, -120 N and -10 N for LC1, 2 and 3. This graph shows the impact on the dummy is very low (ca. 25 N for LC1, ca. 15 N for LC2 and ca. 15 N for LC3).

Fig. 71: *Load cells installed at the little dummy*
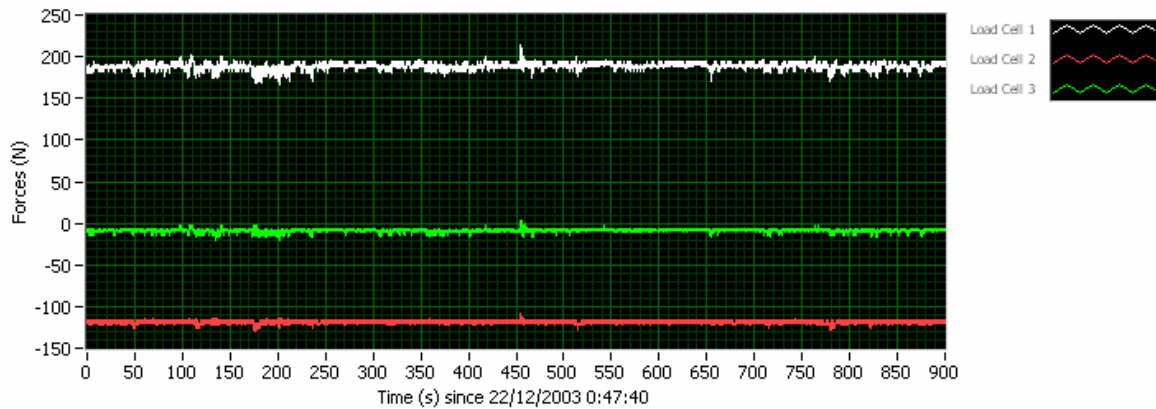
Dec. 22th, 2003, 15 min

Fig. 72: *Field measurements by the load cells on the little dummy (Dec. 22th, 2003, 15 min)*

5.1.2 LARGE 'ADULT' DUMMY (D2)

Dummy D2 is one of the large dummies that is installed on the crest wall behind the armour units. This dummy contains 3 load cells LC4, LC5 and LC6 as given in Fig. 73.

Measurements are carried out during the three given storms. Fig. 74 gives an overview of the forces measured by the load cells. The signals in Fig. 74(a) originate from storm 8 (Dec. 22th, 2003) taking a period of 2 s. All these load cells measure positive forces. The signals in Fig. 74(b) originate from storm 9 (Febr. 8th, 2004) taking a period of 1 s.

Fig. 73: *Load cells installed at the large dummy D2*

(a)

Dec. 22th, 2003 (2 s duration)

(b)

Febr. 8th, 2004 (1 s duration)
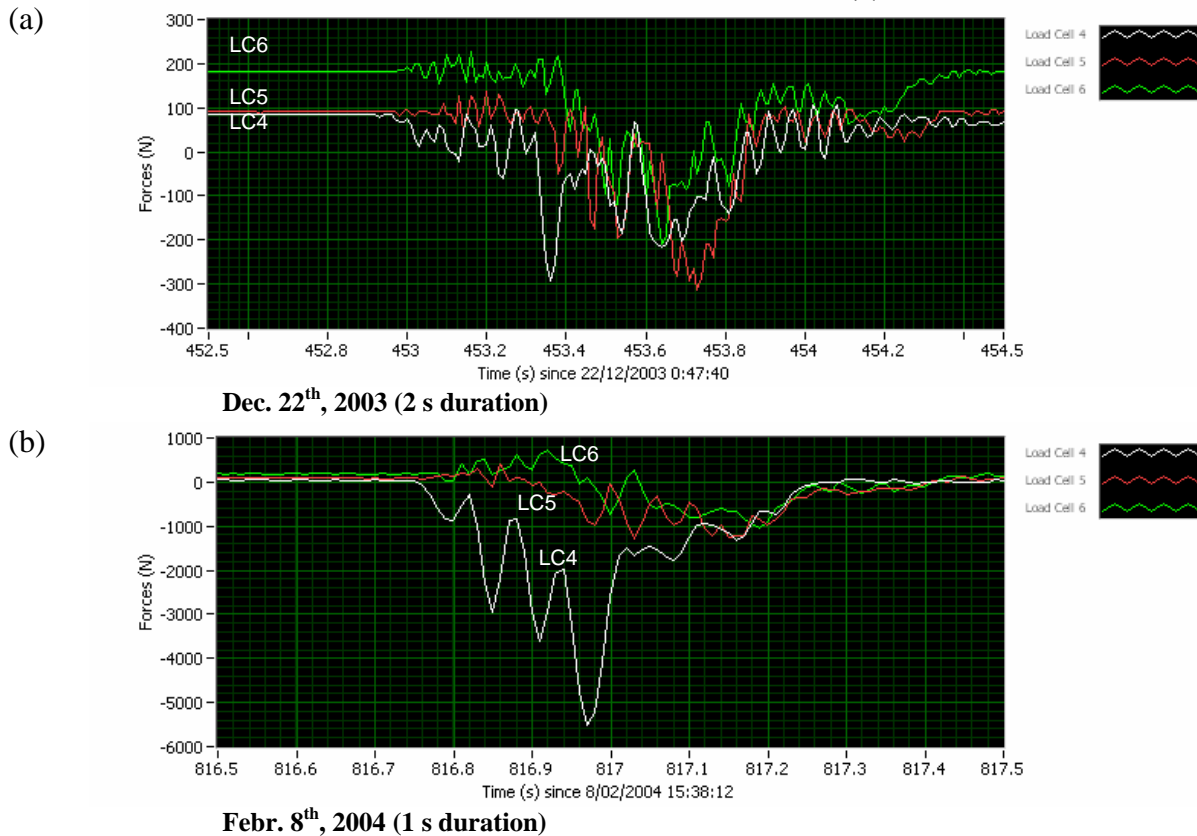
Fig. 74: *Field measurements by the load cells on the large dummy D2 on (a) Dec. 22th, 2003 (2 s duration) and on (b) Febr. 8th, 2004 (1 s duration)*

5.1.3 LARGE 'ADULT' DUMMY (D3)

Dummy D3 is the second large dummy that is installed on the crest wall behind the armour units near the measurement jetty. This dummy contains 3 load cells LC7, LC8 and LC9 as given in Fig. 75. In front of the dummy at the seaward side, a velocity meter is installed.
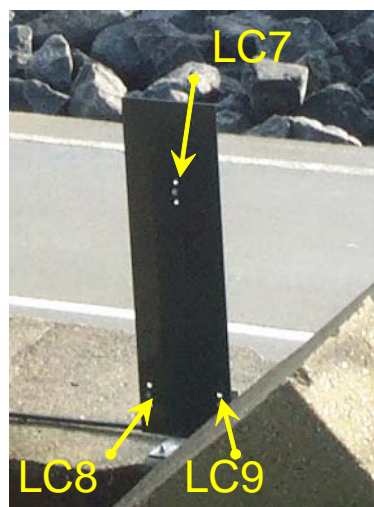
Fig. 75: *Load cells installed at the large dummy D3*

Measurements are carried out during the three given storms. Fig. 76 gives an overview of the forces and velocities measured by the load cells and the velocity meter. The signals in Fig.

76(a) originate from storm 7 (Oct. 7th, 2003) taking a period of 1.5 s. Fig. 76(b) and (c) show 2 different impacts on the dummy during storm 9 (Febr. 8th, 2004) resp. at 15:49:45 and 16:23:23 and taking each a period of 1.5 s. On Fig. 76(b) a clear impact can be distinguished: at 693.6 s all load cells measure a compression (loads become negative).

In Fig. 76 (b) and (c), the velocities near the dummy are given (blue horizontal line near zero value).

(a)

Oct. 7th, 2003 (1.5 s duration)

(b)

Febr. 8th, 2004 (1.5 s duration)

(c)

Febr. 8th, 2004 (1.5 s duration)
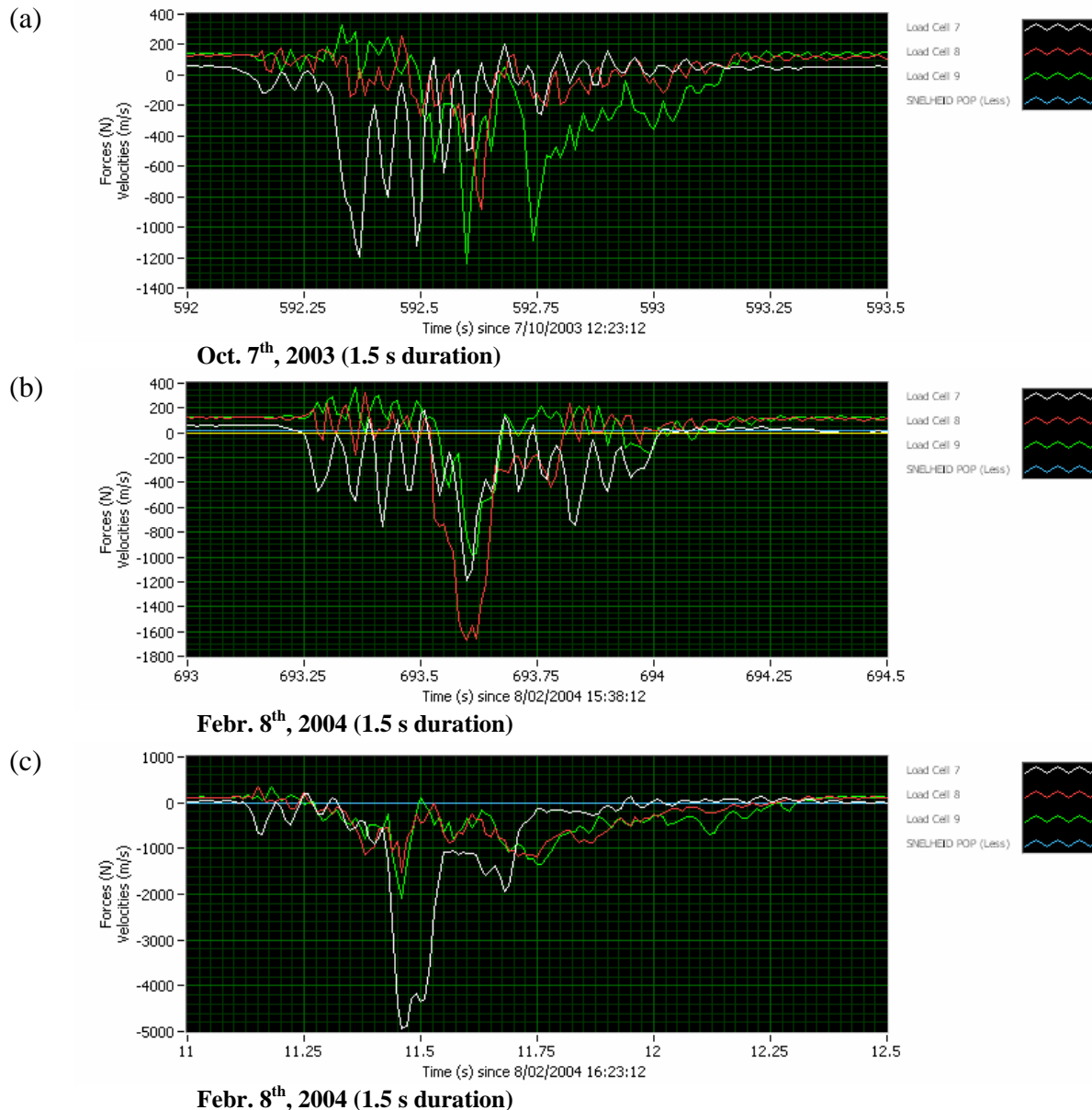
Fig. 76: *Field measurements by the load cells on the large dummy D3 and the velocity meter near the large dummy D3, on (a) Oct. 7th, 2003 (1.5 s duration), on (b) Febr. 8th, 2004 (1.5 s duration) and on (c) Febr. 8th, 2004 (1.5 s duration)*

5.1.4 PIPELINE

The pipeline, installed on the crest wall behind the armour units, contains 4 load cells LC13, LC14, LC15 and LC16 as given in Fig. 77. In front of the pipeline, at the seaward side, the small velocity meter is installed.

Measurements are carried out during the three given storms. Fig. 78 gives an overview of the forces and velocities measured by the load cells and the velocity meter.

The signals in Fig. 78(a) originate from storm 9 (Febr. 8th, 2004) taking a period of 7 s. The impact only takes 1 second. The time signals in Fig. 78(a) show that the overtopping wave smashed the pipeline with a large impact at the bottom side. The two lower load cells (LC13 and LC14) indicate a positive load (a tension) while the two upper load cells (LC15 and LC16) indicate a negative load (a pressure). Fig. 78(b) show a smaller impact on the pipeline during storm 8 (*Dec. 22th, 2003*).

The velocities near the pipeline at the moment of the impact in Fig. 78(b) are given in Fig. 79. The velocities at 8 locations and directions (see Fig. 79(b)) are calculated (v1 to v8). The maximum velocity during this overtopping is 15 m/s and is located at v4.

Fig. 77: *Load cells installed at the pipeline*

(a)

Febr. 8th, 2004 (7 s duration)

(b)

Dec. 22th, 2003 (7 s duration)
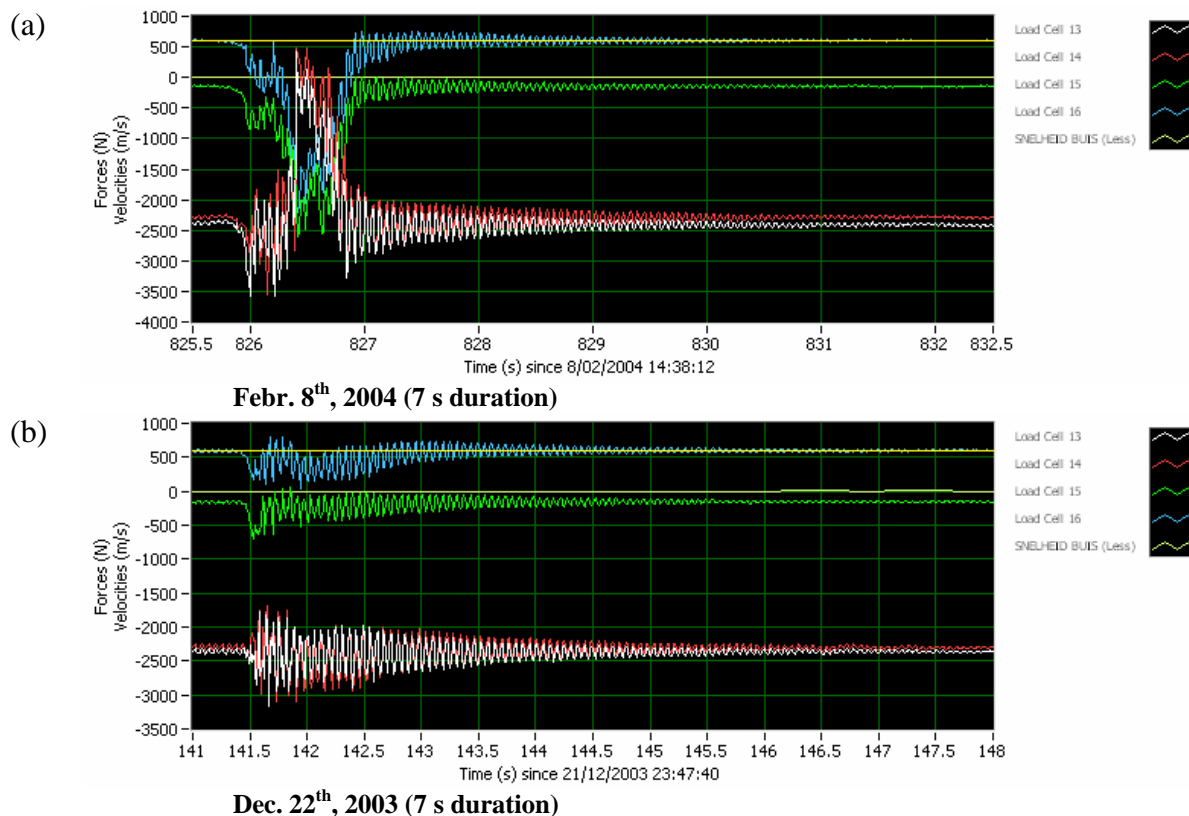
Fig. 78: *Field measurements by the load cells on the pipeline and the velocity meter near the pipeline, on (a) Febr. 8th, 2004 (1.5 s duration) and (b) Dec. 22th, 2003 (7 s duration)*

(a)

Dec. 22ᵗʰ, 2003

(b)
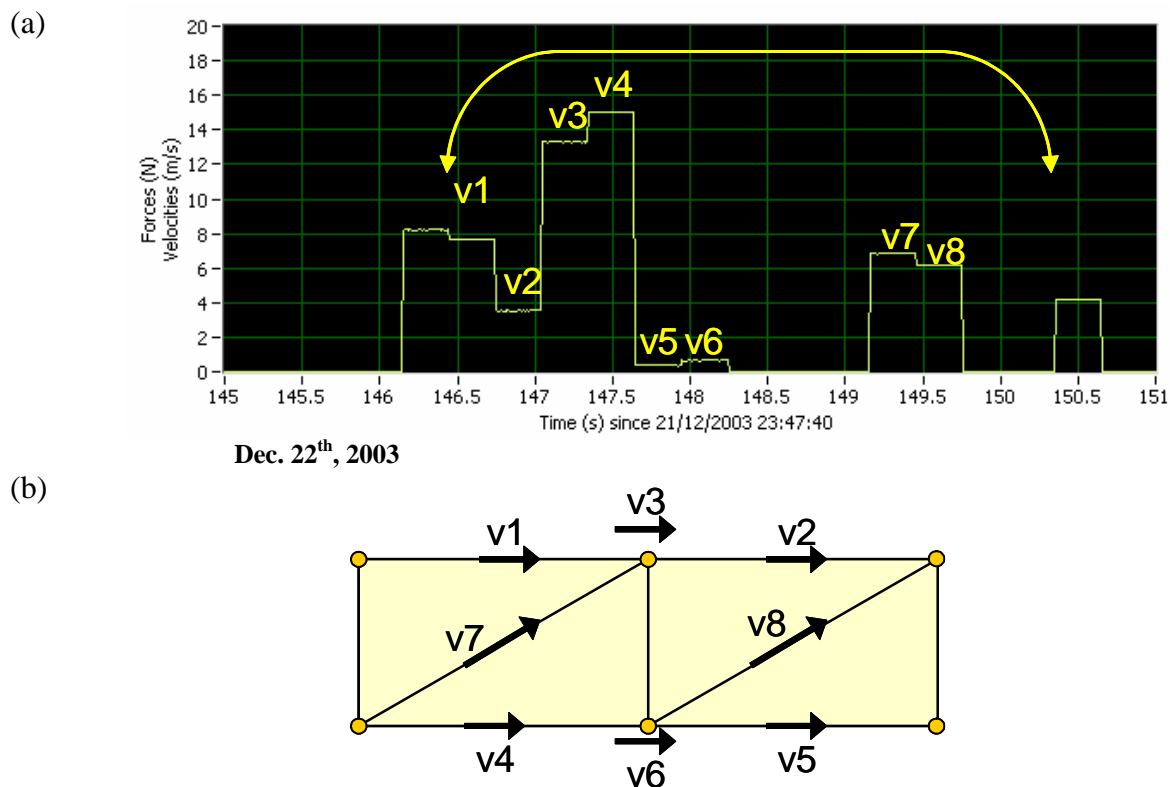
Fig. 79: *Velocities near the pipeline on Dec. 22ᵗʰ, 2003: (a) measured values and (b) location*

5.1.5 VERTICAL WALL

The vertical wall is installed on the crest wall under the measurement jetty, and contains 3 load cells LC10, LC11 and LC12 as given in Fig. 80.

Measurements are carried out during the three given storms. Fig. 81 and 82 give an overview of the forces and pressures measured by the load cells and the pressure sensors. Part (a) of the graphs show the signals measured by the load cells and part (b) of the graphs shows the measurements of the pressure sensors. The relation between the numbering used in Fig. 81 and 82 and the numbering used in the graphs is given in Table 6.

The signals in Fig. 81 originate from storm 9 (Febr. 8ᵗʰ, 2004) taking a period of 1.5 s. This graph shows that an impact on the lower part of the wall has been measured by the load cells (LC10 and LC11) as well as by the pressure sensors (especially by PS1 and PS2).
Another example of wave impact on the vertical wall measured during storm 7 (Oct. 7ᵗʰ, 2003) is given in Fig. 82. The wave impact is located at the lower part of the wall (see signal of LC10, LC11 and PS1) and is less than the one given in Fig. 81.

Fig. 80: *Load cells(LC) and pressure sensors (PS) installed at the vertical wall*
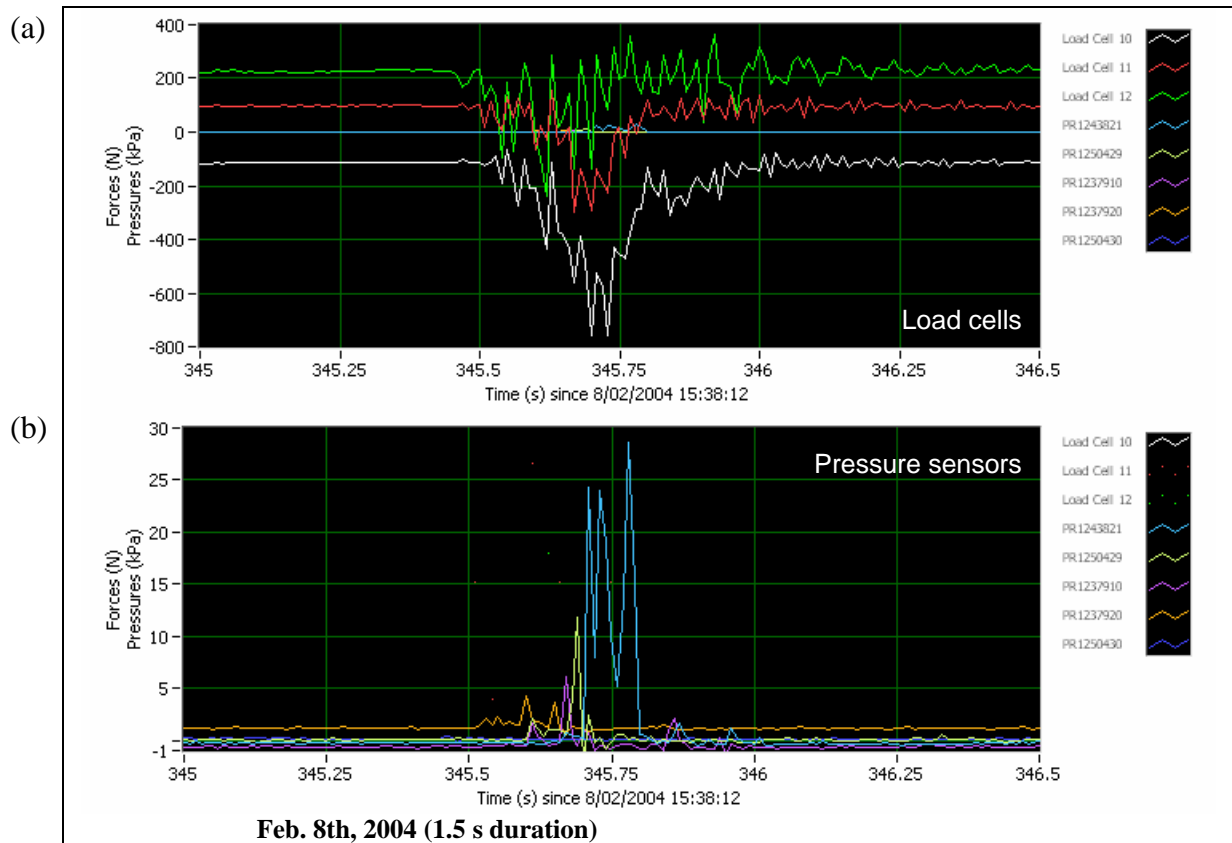
Fig. 81: *Field measurements by (a) the load cells and (b) the pressure sensors on the vertical wall on Febr. 8th, 2004 (1.5 s duration)*
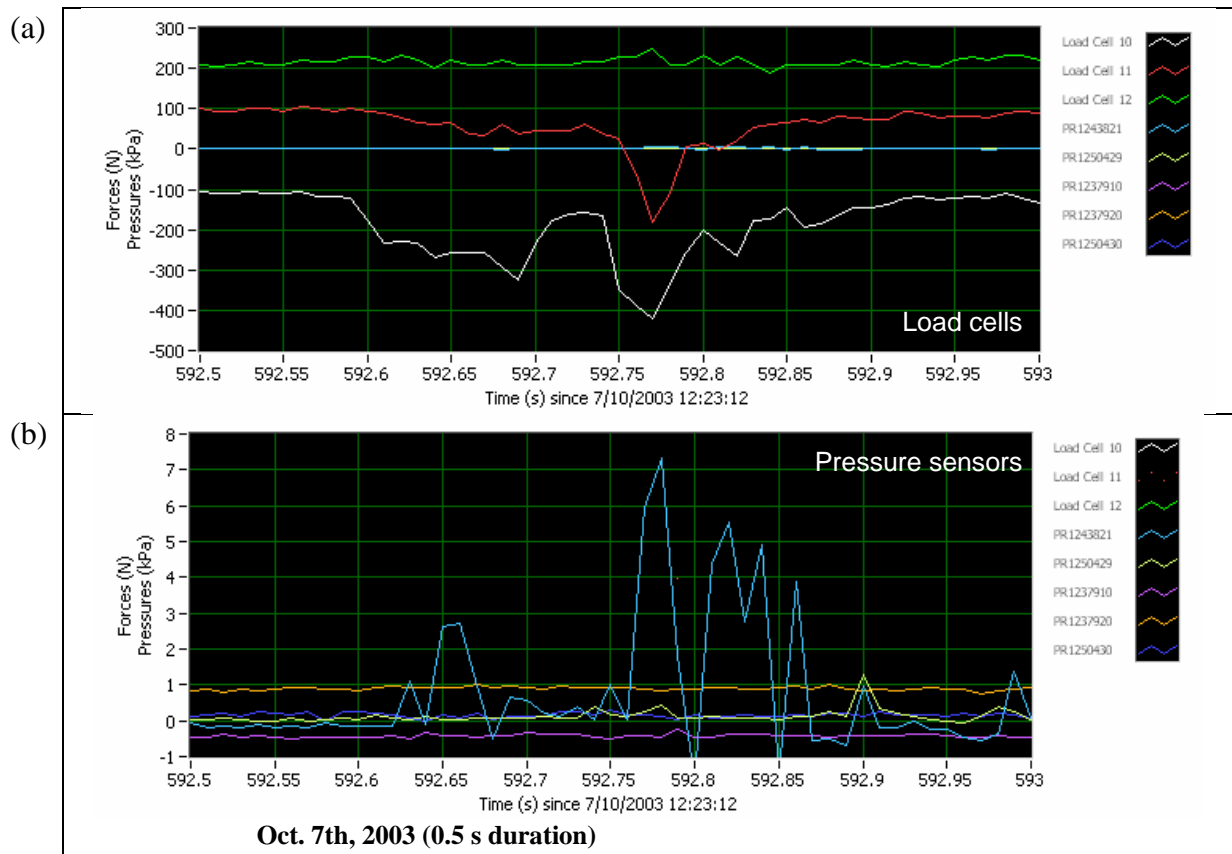
Fig. 82: *Field measurements by (a) the load cells and (b) the pressure sensors on the vertical wall on Oct. 7th, 2003 (0.5 s duration)*

Table 6:   *Relation between pressure sensor numbers in Fig. 80 and in graphs.*

N° in Fig. 80	N° in graphs
PS1	PR1243821
PS2	PR1250429
PS3	PR1237910
PS4	PR1237920
PS5	PR1250430

5.2 ANALYSIS AND RESULTS FROM HAZARD MEASUREMENTS

5.2.1 DUMMIES

For each storm, the two highest impact loads per load cell are determined. For these impacts the total impact on the dummy is calculated.

In Table 7 the most relevant total impacts (2 per storm) on dummy2 during the given storms are shown. For each impact, the loads per load cell are given. The maximum load (8110 N) on dummy2 is measured on Febr. 8th, 2004. The impact of the maximum load is located on the upper part of the dummy (LC1 > LC2 + LC3).
A similar table is made for dummy3, located near the measurement jetty (Table 8).The maximum load on dummy3 is also measured on Febr. 8th, 2004.

Impacts on the smallest dummy are nihil.

Table 7: *Total and individual impacts measured by load cells (LC) on dummy2 during resp. storms*

Date	LC1 (N)	LC2 (N)	LC3 (N)	Total impact (N)
Oct. 7th, 2003	2520	120	655	3295
	610	800	590	2000
Dec. 22th, 2003	375	405	390	1170
	315	430	155	900
Febr. 8th, 2004	5590	1335	1185	**8110**
	2405	1790	1235	**5430**

Table 8: *Total and individual impacts measured by load cells (LC) on dummy3 during resp. storms*

Date	LC1 (N)	LC2 (N)	LC3 (N)	Total impact (N)
Oct. 7th, 2003	1245	1005	1375	3625
	665	995	1050	2710
Dec. 22th, 2003	970	250	490	1710
	270	385	740	1395
Febr. 8th, 2004	4970	1640	2225	**8835**
	1950	1015	1340	**4305**

From these tables it can be concluded that the highest impacts on the dummies - ca. 8100 N for dummy2 and ca. 8800 N for dummy3 - are measured during the storm of Febr. 8th, 2004.

Different pressure distributions are made for dummy2 (Fig. 83) and dummy3 (Fig. 84) for the three highest total impacts on Febr. 8th, 2004. Following distributions are considered (but not all are applicable for one impact):

- rectangular distribution starting from upper border of dummy;
- rectangular distribution starting from lower border of dummy;
- triangular distribution starting from upper border of dummy;
- triangular distribution starting from lower border of dummy;
- trapezoidal distribution over whole height of dummy;
- point load.

The mentioned loads in Fig. 83 and 84 are considered to be uniformly distributed over the width of the dummy (0.5 m). The highest impacts (drawing (a) in both figures) on the dummies are located at the upper part of the dummy.
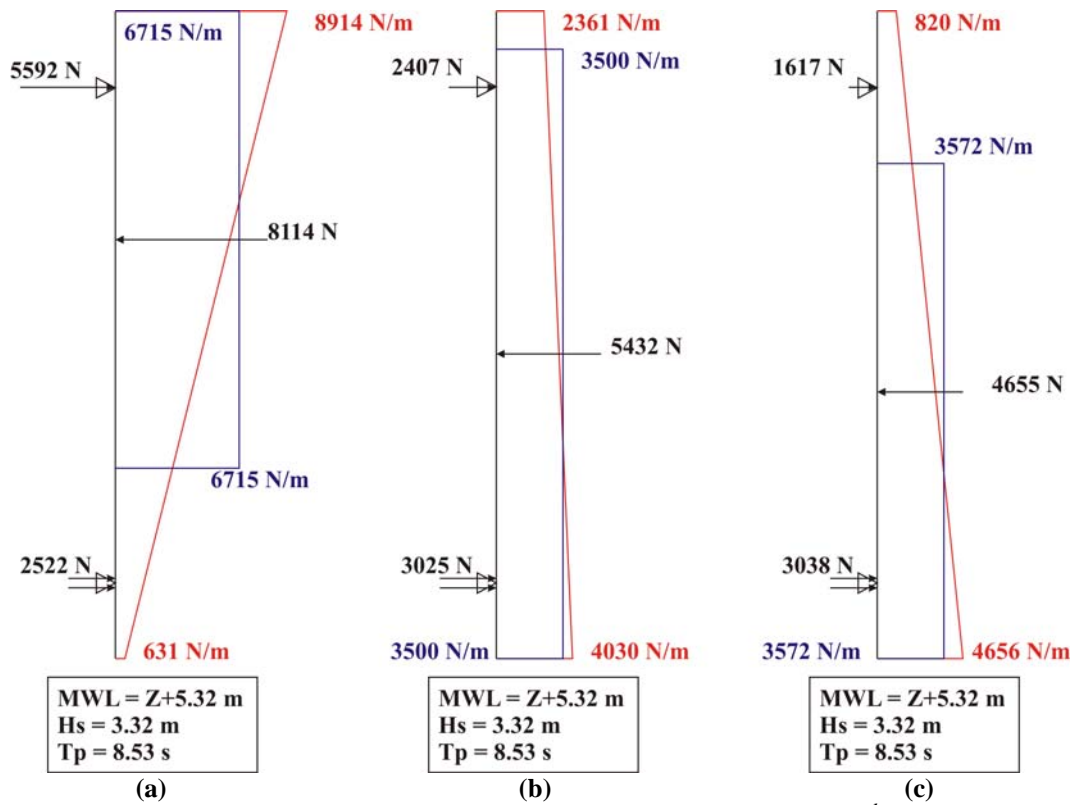
Fig. 83: *Pressure distributions for the three highest impacts on Febr. 8th, 2004 on dummy2: (a) 8114 N, (b) 5432 N and (c) 4655 N.*
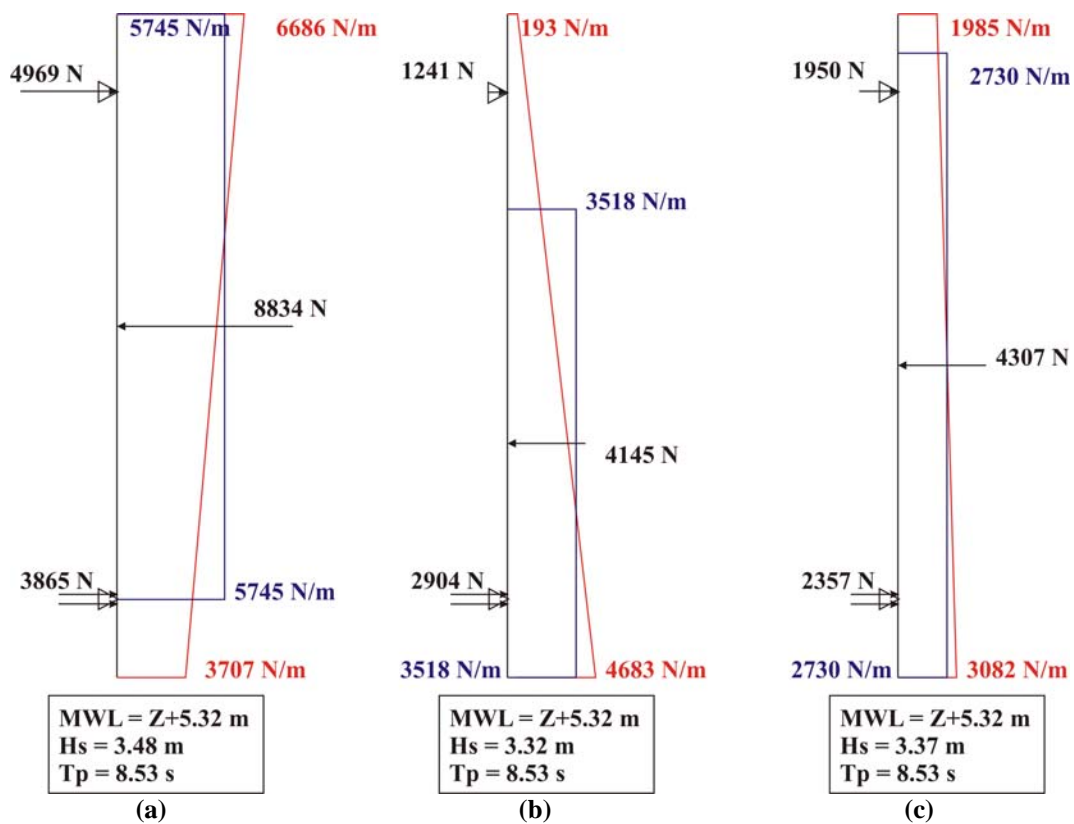

Fig. 84: *Pressure distributions for the three highest impacts on Febr. 8th, 2004 on dummy3: (a) 8834 N, (b) 4145 N and (c) 4307 N.*

5.2.2 VERTICAL WALL

Analogue as for the dummies the two highest impact loads during three storms are determined for each load cell on the vertical wall and for each storm. For these impacts the total impact on the vertical wall is calculated.

In Table 9 the most relevant total impacts (2 per storm) on the vertical wall during the given storms are shown. For each impact, the loads per load cell are given. The maximum load (1425 N) on the vertical wall is measured on Febr. 8th, 2004. The impact of the maximum load is located near load cell 2 (LC2 > LC1, LC3).

The pressures measured at the same moments are given in Table 10. The numbering used for the load cells (LC) and the pressure sensors (PS) in Table 10 is given in Figure 85.
The maximum impact measured at Febr. 8th, 2004 is, as registered by the pressure sensors, located at the bottom side of the vertical wall.
On Febr. 8th, 2004 also an impact of 730 N is measured and is located at the upper side of the vertical wall (pressures of 0.6 and 0.9 kPa resp. measured by PS4 and PS5).

Table 9: *Total and individual impacts measured by load cells (LC) on the vertical wall during resp. storms*

Date	LC1 (N)	LC2 (N)	LC3 (N)	Total impact (N)
Oct. 7th, 2003	45	305	275	625
	135	55	105	295
Dec. 22th, 2003	10	115	135	260
	205	50	-10	245
Febr. 8th, 2004	411	630	386	**1427**
	505	115	110	**730**

Table 10: *Total and individual impacts measured by load cells (LC) and pressure sensors (PS) on the vertical wall during resp. storms*

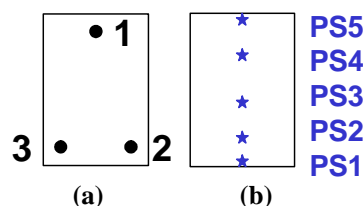| Date	LC1 (N)	LC2 (N)	LC3 (N)	Total impact (N)	PS1 (kPa)	PS2 (kPa)	PS3 (kPa)	PS4 (kPa)	PS5 (kPa)
Oct. 7th, 2003	45	305	275	625	7.5	1.0	0	0	0
	135	55	105	295	1.2	2.0	0	0	0
Dec. 22th, 2003	10	115	135	260	3.9	3.0	0.8	0	0
	205	50	-10	245	0	0	0	0	0
Febr. 8th, 2004	411	630	386	**1427**	2.9	1.2	0.7	0.3	0
	505	115	110	**730**	0	0	0	0.6	0.9

Fig. 85: *Localisation of the load cells (a) and the pressure sensors (b) on the vertical wall.*

Different pressure distributions are also investigated for the vertical wall (Fig. 86) for the three highest total impacts on Febr. 8th, 2004. The mentioned loads in Fig. 83 and 84 are considered to be uniformly distributed over the width of the wall (0.5 m). The pressures measured at the same moment of the given impacts are indicated in italic in the figures.

The highest impacts (drawing (a) and (b)) on the wall are located at the lower part of the dummy. Pressure sensors are installed in the middle of the wall. When no pressures are measured (see Fig. 86 (b)), the overtopping water has hit the plate at the border of the plate.

The impacts are clearly lower than the impacts on the dummies. This is probably because the wall is located higher than the dummies.
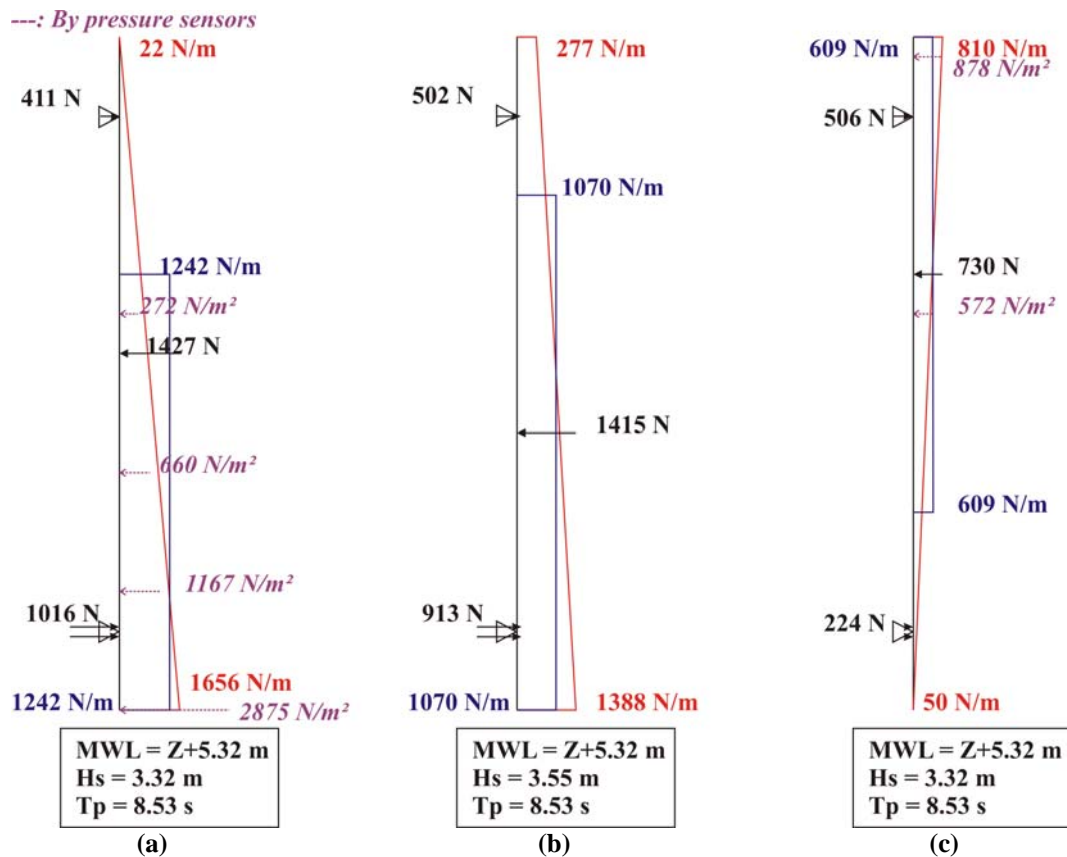
Fig. 86: *Pressure distributions for the three highest impacts on Febr. 8th, 2004   on the vertical wall: (a) 1427 N, (b) 1415 N and (c) 730 N.*

5.2.3 PIPELINE

Analogue as for the dummies and the vertical wall, the two highest impact loads during three storms are determined for each load cell on the pipeline and for each storm (Table 11). For these impacts the total impact on the pipeline and the direction of the total impact is calculated. Figure 87 explains the direction (angle α) of the impact and the numbering of the load cells (looking from above the pipeline).

Fig. 87: *Direction of the impact load (a) and localisation of the load cells (b) on the pipeline.*

Table 11: *Total and individual impacts measured by load cells (LC) on the pipeline during resp. storms*

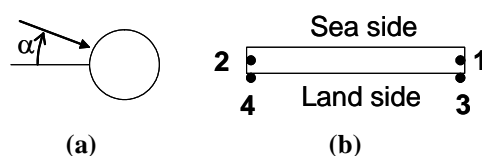| Date	LC1 (N)	LC2 (N)	LC3 (N)	LC4 (N)	Total impact (N)	α (°)
Oct. 7th, 2003	-450	-450	410	600	1350	-41.6
	465	525	285	215	1110	63.3
Dec. 22th, 2003	805	815	645	565	2020	53.3
	725	890	645	1310	2535	39.5
Febr. 8th, 2004	-2820	-2755	2460	2790	**7660**	-46.7
	1095	2830	1265	2705	**5585**	44.6

Comparable to the measurements of the dummies and the vertical wall, the highest total impact appears at Febr. 8th 2004. Impacts up to 5585 N and 7660 N are calculated over the whole length of the pipeline. These values correspond to line loads of resp. 930 N/m and 1300 N/m. The highest impact is located at the lower part of the pipeline (ca. 45° below the horizontal), while the lower impact is located at the upper part of the pipeline (ca. 45° above the horizontal) (Figure 88).
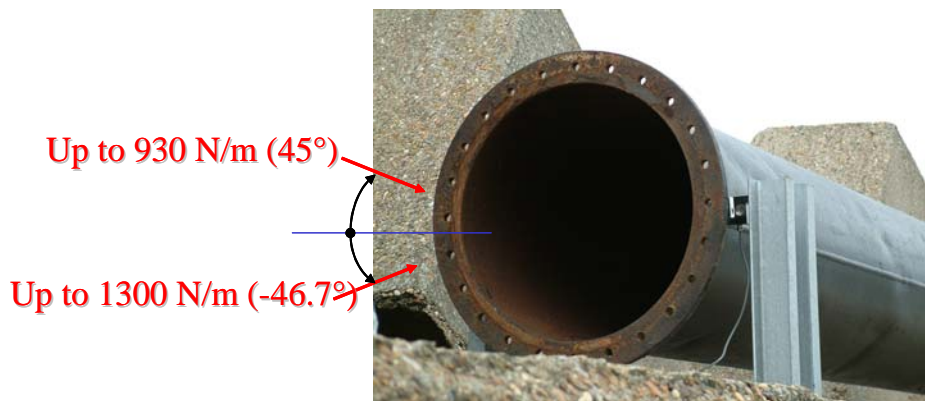
Fig. 88: *Direction of the highest impact loads measured on Febr. 8th 2004 on the pipeline.*

At the moment of maximum impact at the pipeline (Febr. 8th 2004 – 7660 N) velocities are measured in front of the structure. Figure 89 gives an overview of the measured velocities at this specific moment.

v1:	3.4 m/s	v5:	0.23 m/s
v2:	14.45 m/s	v6:	0.35 m/s
v3:	5.45 m/s	v7:	3.77 m/s
v4:	1.75 m/s	v8:	0 m/s
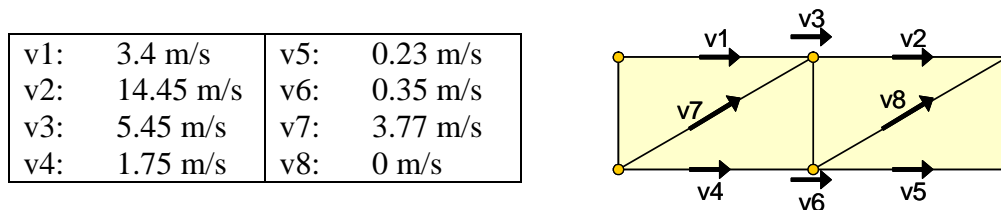
Fig. 89: *Velocities measured in front of the pipeline on Febr. 8th 2004.*

5.2.4 GLASS WINDOWS

During the abovementioned storms no breaking of window glass has occurred.

6   CONCLUSIONS

The full scale overtopping measurements reported in this report are partly incorporated in the journal paper Troch et al. (2004). A description of the infrastructure to identify / measure hazards from wave overtopping are found in Geeraerts et al. (2003).
Conclusions can be formulated as follows:

6.1 OVERTOPPING MEASUREMENTS

In this paper, full scale wave overtopping measurements carried out at the Zeebrugge rubble mound breakwater during 1999 – 2003 have been presented and analysed. The measurement set-up, using a waverider buoy to measure incident waves and an overtopping tank to catch the volumes of overtopping water, and equipped with an outflow weir on a short side and water depth measurements, has been used successful in obtaining reliable field data.

Eleven storm records have been used in the analysis of the field data, with duration between 1 and 2 hours, with significant wave heights ranging between 2.6 m and 3.9 m and peak periods ranging between 7 and 10 s. Although the measured storm conditions are considerably lower than the design storm conditions (with $H_s = 6.20$ m and $T_p = 9.0$ s), average overtopping rates close to 1 l/s.m (and $\dfrac{q}{\sqrt{gH_s^3}} = O\left(10^{-5}\right)$) have occurred.

Three methods for deriving the average overtopping rate inside the overtopping tank have been used, based on measurements of outflow discharge over the weir and instantaneous water depth inside the overtopping tank.

Average overtopping rates from the field data have been compared with predicted values from the widely used prediction formulae from van der Meer et al. (1998), Owen (1980) and Besley (1999). For application of these formulae to the case of a rubble mound breakwater, the value of the reduction factor for the surface roughness of the armour layer used is 0.51. The actual value for the crest freeboard parameter R_c for the case of the Zeebrugge breakwater is not obvious, and therefore a sensitivity analysis has been carried out, varying the crest freeboard between a maximum value R_{c1} (with crest level at Z + 12.02 m), and a minimum value R_{c2} (with crest level at Z + 10.20 m), and the average value R_{c3} (with crest level Z + 11.11 m) between maximum and minimum values. Best agreement between measured and predicted values is observed using the average crest level (with R_{c3}) and van der Meer et al's and Besley's prediction formulae.

For average overtopping rates up to 1 l/s.m very good agreement between the prototype average overtopping rates and the prediction formulae of van der Meer and Besley is achieved, taking into account the precise choice of surface roughness and crest freeboard parameters.

6.2 FIELD MEASUREMENTS OF HAZARDS

Concerning the field measurements of hazards, the following can be concluded:

- A fully operational measurement system to identify and measure hazards from overtopping waves is available
- The highest impacts are measured on Febr. 8th, 2004, during a storm characterised by $H_{m0} = 3.23$ m, $T_p = 7.91$ s and MWL = Z+4.77 m:
    - Little dummy: no measurements available
    - Large dummy2: 8100 N
    - Large dummy3: 8800 N
    - Vertical wall: 1425 N
    - Pipeline: 7660 N (α = -47°) or 5585 N (α = 45°)
        i.e. 1300 N/m (α = -47°) or 930 N/m (α = 45°)
- The link to the wave characteristics and overtopping volumes/rates is available
- Analysis and results show that the system works and is stand-by

Acknowledgements

7   REFERENCES

Besley, P., 1999. Wave overtopping of Seawalls. Design and Assessment Manual. Hydraulics Research Wallingford. R&D Technical Report W178, ISBN 1 85705 069 X.

Geeraerts, J., Troch, P., De Rouck, J., Van Damme, L., Pullen, T., 2003. Hazards resulting from wave overtopping – Full scale measurements. Proc. Conf. Coastal Structures, Portland, Oregon, USA.

Pedersen J., 1996. Wave forces and overtopping on crown walls of rubble mound breakwaters. PhD-thesis, Hydraulics and Coastal Engineering Laboratory, Department of Civil Engineering, Aalborg University.

Owen M.W. (1982) "The hydraulic design of sea-wall profiles" Proc. ICE Conf. on Shoreline Protection, September 1982, pp 185-192, publn Thomas Telford, London

TAW, 2002. [Dutch Technical Advisory Committee on Water Defence] Technisch Rapport Golfoploop en Golfoverslag bij Dijken [Technical Report on Wave Run-up and Wave overtopping at dikes]. In Dutch. 44pp, Delft, The Netherlands.

Troch P., De Rouck J., Van Damme L., 1998. Instrumentation and prototype measurements at the Zeebrugge rubble mound breakwater, Coastal Engineering 35, pp. 141 – 166.

Troch, P., Geeraerts, J., Van de Walle, B., De Rouck, J., Van Damme, L., Franco, L., Allsop, W. Full scale wave overtopping measurements on the Zeebrugge rubble mound breakwater. Coastal Engineering, Elsevier. Vol. 51 / 7 pp. 609-628.

van der Meer, J.W., Tönjes, P., de Waal, H., 1998. A code for dike height design and examination, Proceedings International Conference on Coastlines, Structures and Breakwaters, Institution of Civil Engineers, London, Thomas Telford, London, pp. 5 - 19.

Van de Walle, B., De Rouck, J., Van Damme, L., Frigaard, P., Willems, M., 2002. Parameters influencing wave run-up on a rubble mound breakwater. Proc. 28th ICCE, Cardiff, UK. ASCE. pp. 2008 – 2018.